HOLOGRAPHIC DETERMINATION OF MECHANICAL PROPERTIES AND BEHAVIOUR OF MATERIALS

by

Arnold Sher

B.Sc. (Eng)(Mech) U.C.T.

A thesis submitted in partial fulfilment of the requirements for the degree of Master of Science in Engineering.

Department of Mechanical Engineering

University of Cape Town

September 1991

DECLARATION

This is to certify that the results, calculations and any other work presented in this thesis are essentially my own work, and that no part of it has been submitted for a degree at any other university.

Signed by candidate

A. Sher

September 1991

ABSTRACT

This study, which was primarily experimental, was aimed at investigating the feasibility and development of experimental procedures using holographic interferometry to determine different material properties such as: i) Modulus of Elasticity (E) ii) Poisson's ratio (ν) (which included a study into the Modulus of Rigidity (G)) iii) creep behaviour at room temperature.

The Elastic Modulus (E) was determined from the relationship $E=v^2\rho$, where v is the velocity of a longitudinal wave propagating in a long rod and ρ is the density of the rod. The technique of double-exposure holographic interferometry was used to record longitudinal waves propagating in long brass and steel rods. The waves were initiated by striking the end of the rod with a pendulum. From the pulsed laser interferograms obtained, the distance travelled by the wave in a known time could be measured and thereby the velocity (v) could be calculated.

Experimental results indicate that it is feasible to use holographic interferometry when dynamically determining the Elastic Modulus. The values produced for brass and steel compared favourably with the ones obtained from the ultrasonic velocity technique.

The second part of the study investigated the possibility of employing time-average holograms of resonant vibrating cantilever beams to determine dynamically the Poisson's ratio. Poisson's ratio can be related to the anticlastic curvature displayed by bending beams. Various widths and

thicknesses of mild steel were tested to determine if there are any specific geometric constraints which affect the Poisson's ratios obtained.

It was shown that both width and thickness affect the anticlastic behaviour of the cantilever beams and thus the obtained Poisson's ratio. Reliable values of Poisson's ratio were only obtained for limited beam thickness.

The holographic determination of Poisson's ratio was further investigated in a second study. In this study Poisson's ratio was related to the Elastic Modulus determined previously and the Modulus of Rigidity obtained from a holographic experimental technique developed for this purpose.

Finally the possibility of using holographic interferometry in the study of the creep behaviour of metals was investigated.

An experimental procedure was developed which predicts the exponent of the time function during the primary stage of creep when it takes the form of a power law. Double-exposure holograms of a lead cantilever beam creeping under the action of an end load were used for this purpose. The obtained time exponent compares favourably with that obtained under constant stress conditions.

ACKNOWLEDGEMENTS

I wish to express my sincere thanks to:

Associate Professor **J. GRYZAGORIDIS** for initially suggesting and supervising this study. His guidance, encouragement, supervision, corrections, advice and help throughout this project was invaluable.

Professor **R. PENNY** for his encouragement, advice and guidance.

Mr **J. MEYER** for his enthusiasm and electronic expertise.

Mr **V. APPLETON** for photographic assistance.

Mr **M. BATHO and the Mechanical Engineering Workshop, U.C.T** for their technical assistance.

My family **JACK, SALLY, CARRON & MARTIN** for their encouragement, support and belief in me.

DEDICATION

This thesis is dedicated to **BARRY BLECHMAN** (17/11/67 - 17/3/91). Your friendship, support and sincerity will always be cherished. The glimpse you showed me of your immense intellectual and artistic ability will always inspire me to strive for that which is beyond the mundane.

TABLE OF CONTENTS

LIST OF FIGURES

LIST OF TABLES

NOMENCLATURE

E	Elastic Modulus
G	Modulus of Rigidity
ν	Poisson's ratio
ρ	Density
v	Velocity
CW	Continuous Wave Laser
HeNe	Helium Neon Laser
λ	Wavelength
J	Joules
nsec	nanosecond
μsec	microsecond
msec	millisecond
sec	second
nm	nanometers
mm	millimeters
cm	centimeters
m	meters
mW	Milliwatts
ml	milliliter
g	gram
Kg	Kilogram
Pa	Pascal
θ,γ,α	Geometrical angles
N,m	Number of fringes
ω	Frequency in rad/sec

f	Frequency in cycles/sec
z	Amplitude
T	Period of vibration
J_o	Bessel Function
σ	Stress
τ	Shear Stress
ε	Strain
γ	Shear Strain
L,l	Length
V	Volts
Ω	Ohms
F	Farads
K	Degrees Kelvin
V_l	Longitudinal velocity
V_s	Shear Velocity
δ,d,X,u	Displacement
x,y,z	Co-ordinate system
R	Radius
K	Radius of curvature
w	Width
t	Thickness
T	Torque
J	Polar area moment of inertia
L_{Tr}	Transducer length
L_{LA}	Lever Arm
l_{rod}	Rod length

t	time
T	Temperature
Q	Activation Energy
R	Boltzmann's constant

CHAPTER 1

1.1 HOLOGRAPHY:- A METHOD FOR FORMING OPTICAL IMAGES

> "The highly coherent light produced by the laser is used in a novel photographic process, in which the light-sensitive film, instead of recording an image, in effect records the light waves themselves."
>
> Emmett N.Leith and Juris Upatnieks
>
> Scientific American, 1965

Leith and Upatnieks were referring to an image recording technique which they called 'photography by wave-front reconstruction'. This technique is now commonly referred to as *holography*, and Dennis Gabor is credited with its discovery in 1948.

The term *holography* is derived from the Greek words *holos* meaning 'the whole' or 'entire' and *gramma* which means 'message' or 'record'.

Unlike photography which provides a method of recording the two-dimensional intensity distribution of a scene, while neglecting all phase information, holography captures the intensity as well as phase distribution of the light reflected by the scene. It is this phase distribution of the scattered light which is responsible for the depth of focus and perspective of the object.

In photography each scene consists of a large number of reflecting or radiating points of light. The waves from each of these points all contribute to a complete wave. This wave is transformed by the optical lens in such a way that it collapses into an image of the radiating object. It is this image which is recorded on the photographic emulsion, as levels of intensity.

Holography records the object wave in such a way (without optical elements) that a subsequent illumination of this record serves to reconstruct the original object wave. A visual observation of this reconstructed wavefront yields a view of the object which is practically indiscernible from the original object. Thus the recording of the object wave itself, rather than an image of the object, constitutes the basic difference between photography and holography.

1.2 THE AIMS OF THIS THESIS

Applications for holography have been found in such diverse fields as art, advertising and security. Since 1965 engineering and scientific research has applied holography to a new branch of interferometry, namely holographic interferometry.

Holographic interferometry permits the principles of interferometry to be extended and applied to any object, regardless of its shape or surface condition. The published applications of holographic interferometry are numerous. They extend from the nondestructive testing of materials and components through to the verification of finite element models.

Nondestructive testing refers to the field of material or object testing, where the test specimen is not physically destroyed whilst either its material properties, or compliance to a set standard are determined.

The aim of this thesis was to investigate the feasibility of applying holographic interferometry to the determination of material properties or behaviour. The specific material properties and behaviour for which holographic interferometric experimental techniques were developed were Modulus of Elasticity, Poisson's ratio, Modulus of Rigidity and the behaviour of Creep.

1.3 PLAN OF THESIS DEVELOPMENT

The dissertation begins by outlining the historical development and principles of holography. This is followed by a detailed description of Leith-Upatnieks off-axis transmission holograms and the effect thereon due to the type of laser chosen i.e. continuous wave or pulsed laser. Relevant holographic interferometric techniques and methods for the quantification of resulting fringe patterns are presented. This chapter is concluded with a general description of the equipment and processing made available for this thesis by the University of Cape Town's holographic laboratory.

Chapters 3, 4 and 5 report on the specific investigation into Modulus of Elasticity, Poisson's Ratio (which included an investigation into the Modulus of Rigidity) and the behaviour of Creep respectively. The general format of each of these chapters is as follows:- an introduction to the

material property or behaviour and the motivation for using holographic interferometry to investigate it, is followed by a literature survey of:- i) standard tests to determine this property and ii) previous holographic interferometric studies, if any, which have been applied to this property or behaviour. The final experimental set-up is described along with any problems encountered. Results obtained are presented and analysed. Each chapter concludes with conclusions which were drawn based on the specific study.

The thesis concludes with recommendations based on this investigation into the holographic determination of mechanical properties and behaviour of materials.

CHAPTER 2

2.1 A HISTORICAL INTRODUCTION

In 1948, when Gabor proposed the idea of holography (2.1) his primary objective was to increase the resolution of the electron microscope. Gabor suggested placing the object in the electron beam, just in front of a reduced image of the electron source. A hologram formed by the electrons diffracted from the object would be recorded on a photographic plate some distance beyond the object (Fig. 2.1). Gabor reasoned that when reconstructing the hologram with coherent light, the hologram would act as a diffraction grid and produce a three dimensional image of the recorded object.

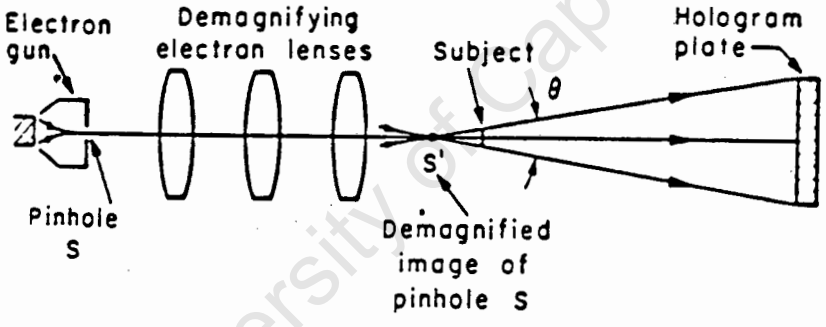

The projection method of forming an electron-wave hologram.

Figure 2.1 (Collier et al,1971)

Gabor experimented (2.2) with the use of visible light in both the recording and reconstruction stages. The necessary monochromaticity of the light was obtained by filtering the radiation from a mercury arc; the required spatial coherence was obtained by illuminating pinholes.

This 'in-line' holographic technique was unsuccessful because of certain technical difficulties, such as mechanical and electrical stability and the lack of a light source of adequate coherence length.

Research into holography lay dormant for many years until in 1962 Leith and Upatnieks (2.3) demonstrated a new method for the creation of holograms. By allowing the wave diffracted from the object to interfere with a reference wave which was off-axis, rather than in-line, the hologram created had a grating-like structure which during the reconstruction stage behaved as a diffraction grid. The reconstruction yielded two waves representing the two first orders of the grating. One of these waves was the same as the original wave from the object, the other was the twin wave.

While interest was being revived in holography, largely due to the advances of Leith and Upatnieks, the continuous wave laser was invented (2.4), which was capable of producing very intense monochromatic radiation in regions of the spectrum that could be recorded photographically.

Leith and Upatnieks in 1964 also introduced the concept of diffuse illumination holography (2.5). Before this the only holograms that had been made were of thin transparent objects. Now with the advent of the gas laser it was possible, by using a diffuser, to illuminate the whole object. The implications of this development are twofold.

Firstly, the light scattered from each point of the object spreads out so as to cover the entire holographic plate. Thus the information about any single object point is recorded over the whole holographic plate and therefore only a small portion of the hologram is required to form an image

of the entire object.

Secondly, a technique exists to record holograms of diffusely reflecting, three dimensional objects. Since the object is diffusely illuminated or diffusely reflecting, light from a large range of perspectives reaches the photographic plate. An observer viewing the image formed by this hologram can move his head and see around foreground objects, and must even refocus his eyes, depending on whether he is viewing a near or far object point.

It was during this period of revived interest in holography that several different types of holography were developed. These different techniques may be distinguished by the following: the way in which they are constructed; the type of object which can be formed; and/or the method of reconstructing the stored image. The most common types of holograms are Gabor, Leith-Upatnieks off-axis transmission, image plane, white light (2.6) and Fourier transform. Each type of hologram has characteristics clearly distinguishing it from another and each has certain advantages over others for a given application.

2.2 THE LEITH-UPATNIEKS OFF-AXIS TRANSMISSION HOLOGRAM

As the Leith-Upatnieks off-axis transmission hologram is the basis of the holographic interferometric techniques used in this study, a detailed description of the set-up for this method is presented.

Figure 2.2 illustrates a typical experimental set-up to construct an off-axis transmission hologram (2.7). The coherent monochromatic light from the laser source is split into two beams by means of the

beamsplitter *BS*. One of the beams (known as the object beam) is expanded and used to illuminate the object *O* to be recorded, while the other beam (known as the reference beam), is expanded and directed by means of mirrors towards a high-resolution photographic film *H*. The latter beam provides a reference beam against which the phase of the scattered light from the object is compared when they are combined at the photographic film plate. Since the object and reference waves are mutually coherent, they will form a stable interference pattern when they meet at the recording medium. The microscopic details of the interference pattern are unique to the object wave; different object waves (objects) will produce different interference patterns.

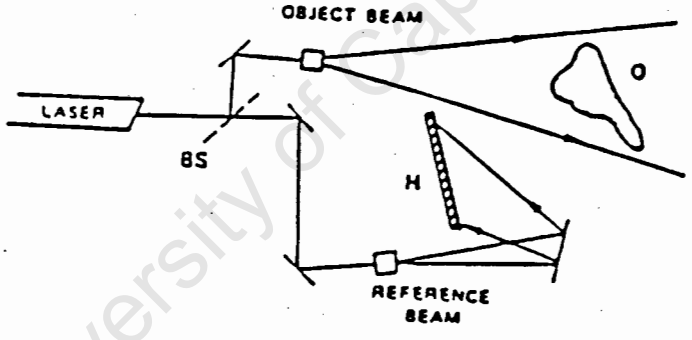

Figure 2.2 A typical experimental arrangement for constructing an off-axis transmission hologram (Walters in Erf ed., 1974).

The detailed permanent record of this interference pattern on the photographic emulsion is called the 'hologram'. The hologram bears no

resemblance to a conventional photograph in that an image is not recorded. The interferometric fringes which are recorded on the film are not visible to the unaided eye because of the extremely fine interfringe spacing ($\pm$ $5x10^{-4}$mm). The fringes which are visible on the hologram are the result of dust particles in the optical system which produced the hologram.

The processed hologram can be used to reconstruct a three-dimensional image of the original object. This will occur when it is illuminated with a beam of light which is similar to the original reference wave used to record the hologram. One of the reconstructed images (Fig. 2.3a) will appear as the virtual image located behind the hologram in the position the original object had occupied, the other image (Fig. 2.3b) when reconstructed with a conjugate wavefront, will appear as a real image located in front of the plate.

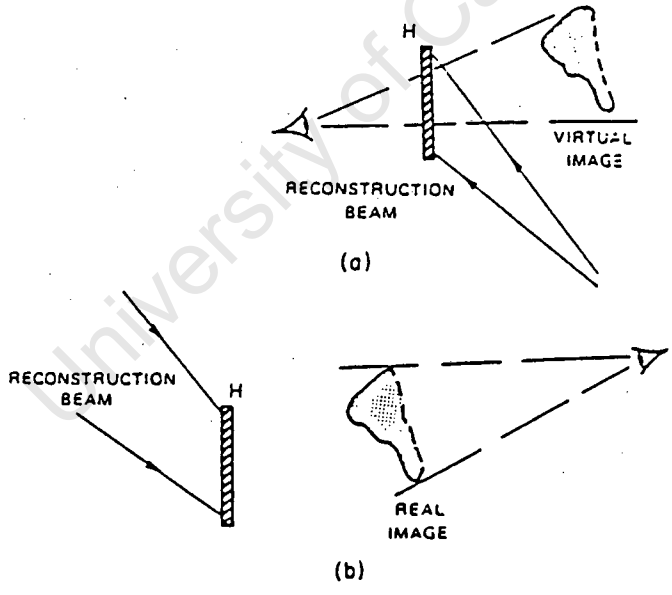

Schematic diagrams illustrating holographic reconstruction of (a) the virtual image and (b) the real image.

Figure 2.3a,b (Walters in Erf ed., 1974)

Thus Leith-Upatnieks off-axis transmission holography is a two-step process by which images can be formed. In the first step a complex interference pattern is recorded and becomes the hologram. In the second step the hologram is illuminated in such a way that part of the transmitted light is an exact replica of the original object wave.

2.3 CONTINUOUS WAVE AND PULSED LASER HOLOGRAPHY

Although the basic set-up may be the same, the type of laser chosen as the source of light in transmission holography has a direct effect on parameters such as stability, duration of exposure, types of mirrors and beam expanders, image magnification and coherence. The types of lasers used in holography may be classified into two categories (1) Continuous Wave (CW) and (2) Pulsed Lasers.

2.3.1 CONTINUOUS WAVE LASER HOLOGRAPHY

In a continuous wave laser (2.8) an atomic or molecular gas at low pressure is contained in a long discharge tube. The axis of the discharge tube defines the optical axis of the system. Centered on this axis, at each end of the tube, is a high-reflectivity mirror, aligned so that light travelling along the axis reflects back and forth many times through the gas which acts as an amplifying medium.

The gas is excited by means of an electrical discharge, either at radio frequencies, dc, or pulsed. Under certain conditions a population inversion (i.e. more atoms in a higher lying level than in a lower level) may be made to exist. Under these conditions the gas discharge becomes a

light amplifier for the transition for which there is an inversion. A spontaneous emission causes stimulated emission and the process cascades as the light travels along the tube. Because of the inversion, amplification of the spontaneous emission results. As the light reflects back and forth between the mirrors, the random nature of the spontaneous emissions is swamped by the in-phase, coherent nature of the stimulated emissions. The temporal coherence of the light output is quite high, but because of the nature of the amplifying transition, most laser beams do not have a single, but rather a multiple frequency.

The temporal coherence referred to above, although usually expressed in units of length, is a measure in time of the phase consistency of successive wavefronts (2.7). The temporal coherence length of a light source is entirely dependent upon the number of different light frequencies radiated by the light source, or, more precisely, the temporal coherence is inversely proportional to the frequency bandwidth of the source. The laser which is usually thought of as monochromatic (single frequency) has a characteristic frequency spread. However, the frequency bandwidth is usually quite narrow, and thus long temporal coherence lengths are attainable with this type of light source.

The Helium-Neon (HeNe) laser has unwanted frequency bands, but the number of such bands is quite small and can be overlooked. The Argon ion laser requires an etalon in the laser cavity, to remove unwanted frequency bands, in order to make it suitable for holographic work.

Transmission holograms require a source having an extended coherence length. Since the reference beam is separated from the object beam,

maintaining equal path lengths for both beams using a standard light source would be extremely difficult, since it would require matching them to within a few microns. When recording three-dimensional objects the distance travelled by the two beams is not equal, therefore coherence lengths of the order of centimeters is required.

Another term used to describe a coherent source of radiation is its spatial coherence, which is a measure of the uniformity in the phase of the wavelength.

The spatial coherence requirements of the light source used for making transmission holograms is not critical. It is during the reconstruction of the hologram that the spatial coherence of the reference beam has to be matched. This is almost impossible if the reference beam has random spatial coherence. Therefore, reference beams having good spatial coherence are desired, for they can be easily duplicated in the reconstruction process. Changes in the radius of curvature or wavelength of the source between reference beam wavefront and the reconstruction beam wavefront result in changes of the image magnification, while changes other than in radius or wavelength will result in distortion of the reconstructed image.

The spatial coherence requirements for holography are not significant when using continuous wave lasers as the same laser (i.e. the same wavelength) can be used for both making and reconstructing the hologram.

Since holography involves the recording of interferometric fringes on a photographic emulsion, the equipment must be stable to within a fractional

wavelength of the illuminating light being used. As transmission holograms require two separate beams, random changes in length between the two beams greater than a fractional part of a wave would tend to reduce the fringe contrast in the holographic recording.

Because of the relatively low output power of continuous wave lasers, exposure times of the order of seconds are required when recording holograms. Care must thus be taken to ensure that objects as well as all mounts for the optical components and the film holder are rigid. Typically transmission holography requires a stable platform which has a resonant frequency below 1 Hz. Methods used to isolate the holographic table from vibrations include mounting all of the optical components on a rigid platform such as a block of granite with the optical mounts securely fastened to the surface. A steel plate supported by inner tubes of tyres can also be used. The use of a steel table also allows the securing via magnets of the various components used in the making of a hologram. Other methods for vibration isolation include using an acoustically damped honeycomb material for the optical table supported by a pneumatic isolation arrangement. Finally, the choice of location for a holographic laboratory is important. It must be as far away as possible from all mechanical and acoustical activity so as to ensure further vibration isolation.

Besides the laser and film holder essential components for the production of an off-axis transmission hologram are as follows:

The beamsplitter reflects a portion of the light impinging on it and transmits the rest (2.7), thereby generating the two required beams (object and reference). Various methods are used to split the beams so as to

eliminate secondary reflection which occurs at the second surface of the beamsplitter.

The expander-spatial filter which is used to expand and spatially filter the object and reference beams, consists of a microscopic objective to focus the radiation through a small pinhole aperture (Fig. 2.4). The microscopic objectives permit expansion of the beams to large diameters in short distances. A pinhole aperture, located at the beam focus, eliminates the undesirable diffraction rings caused by any dust in the system prior to expansion, since the scattered light rays do not focus on the same spot as the well collimated laser beam. In addition, any aberrations introduced into the wavefront by the microscopic objective, or optical elements prior to it, which would tend to increase the focus spot size will be substantially reduced by the insertion of the pinhole.

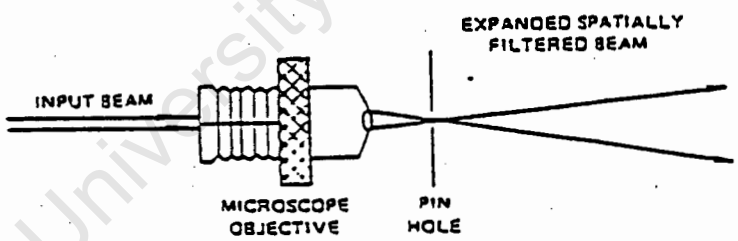

Microscope objective and aperture used as an optical beam expander-spatial filter.

Figure 2.4 (Walters in Erf ed., 1974)

When required, mirrors which are front-surfaced, aluminized and flat to within ± λ/2 are quite sufficient.

2.3.2 PULSED LASER HOLOGRAPHY

Since 1965, pulsed lasers have been applied to holographic investigations where the phenomena under study are inherently transient or where it is difficult to isolate the experimental apparatus from ambient vibrations (2.9). Pulsed lasers are able to deliver pulses with energies up to ten of joules in extremely short pulse widths (5-50nsec). To date, the two most popular pulsed laser used in holography are the ruby and frequency-doubled Nd:YAG lasers. Of late, Alexandrite and CO_2 lasers have also been used to make pulsed holograms.

The major differences between ruby and frequency-doubled Nd:YAG lasers for holographic applications stem from the pulse energies and repetition rates that can be delivered from these two types of lasers (Table 2.1). In terms of pulse energy, the higher energy storage capacity of ruby makes these lasers clearly superior. Ruby lasers are commercially available that deliver holographic quality pulses containing up to 10J, while frequency-doubled Nd:YAG systems deliver less than 1J. The difference in repetition rates between the two pulsed lasers is inherent in the characteristics of the lasing media. Ruby lasers operate by means of a three-level energy exchange that requires that more than half of the atoms in the ground state be raised to an excited state before lasing can occur. Frequency-doubled Nd:YAG lasers, operate as four-level systems without such a requirement and as a result, the threshold pumping energy for laser action is much lower and the system needs to dissipate less heat.

Table 2.1 (Pitlak et al, 1985)

Typical Pulse Energies Available from Pulsed Ruby and Frequency-Doubled Nd:YAG Lasers†

Pulse energy (J)	Laser	Repetition rate (Hz)
0.03	YAG	10
0.05*	Ruby	1
0.07	YAG	30
0.1	YAG	40
0.15*	Ruby	1
0.26	YAG	30
0.36	YAG	20
0.65	YAG	10
0.70*	Ruby	1/15
1.2*	Ruby	1/15
4.0*	Ruby	1/15
10.0*	Ruby	1/30

*Ruby lasers are also commonly available in double- and triple-pulse arrangements, with each pulse in the output train carrying approximately 50% and 30% of the quoted single-pulse energy, respectively.

Both ruby and Nd:YAG lasers operate by optically pumping a flashlamp that is fired by discharging an energy storage capacitor. For ruby lasers this optical pumping typically takes 0.8-1.25 milliseconds, resulting in a delay between the 'firing' of the laser and the laser actually emitting light.

A Q-switch, which generally consists of a Pockels cell and one or more polarizers, is included in the laser optical train (Fig. 2.5). The Q-switch is used to generate a single high intensity pulse from the laser. The rod is pumped while the Q-switch is low, thus allowing the rod to store a large amount of heat. The Q-switch is then switched to a very high level, allowing light to oscillate in the cavity, building up very rapidly (50 to 400 nanoseconds) and emitting a single short pulse.

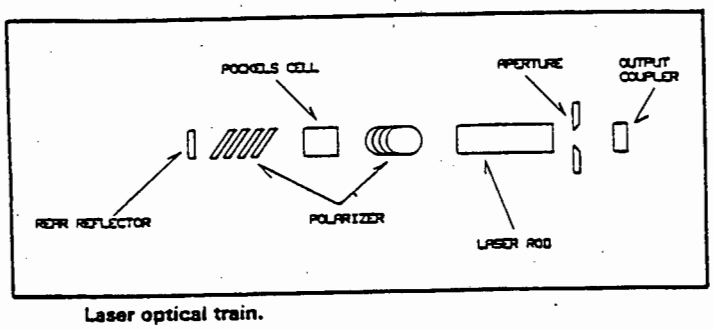

Laser optical train.

Figure 2.5 (Pitlak et al, 1985)

The holographic set-up used to make pulsed laser holograms is similar to that used to make continuous wave holograms, but concave (negative) lenses must be used to expand the laser beams, since the high energy pulsed beams if brought to a focus by a convex lens will cause an explosion to occur at the point of focus due to the ionization of the air. This will spoil the laser beam shape and the hologram will not be recorded (2.10).

As the pulse duration is of the order of 20 nanoseconds, the need for optical tables isolated from surrounding vibrations is largely eliminated. Pulsed holography may be used to study objects both in a static or dynamic state.

When reconstructing a pulsed hologram, some magnification will occur as a different wavelength of light is being used to reconstruct the image,

usually that of a continuous wave laser.

2.4 HOLOGRAPHIC INTERFEROMETRY

Holographic interferometry, first reported by Powell and Stetson in 1965 (2.11), is similar to conventional holography except that two exposures, hence two holograms of the object, are recorded on the same photographic plate; the object being deformed between the two exposures. Upon reconstruction of the hologram, two three-dimensional images of the object will be formed. Since both reconstructed images are formed in coherent light and exist at approximately the same location in space, they will interfere with each other and produce a set of bright and dark interference fringes normally visible on the reconstructed image. The fringes represent contours of equal displacement of the object's surface, along the viewing axis (2.12).

There are three variations of the basic holographic interferometric technique:

1. Double-exposure holographic interferometry :- Two holographic recordings of the object in two energy states (e.g. before and after the application of a stress) are made on the same film prior to processing. When the hologram is reconstructed it will produce an interference pattern which is indicative of the object's surface displacement.

2. Real-time holographic interferometry :- This technique consists of taking a single holographic exposure of an object in an unstressed

state, processing the film, and replacing it in exactly the same position in which it was recorded. The hologram is reconstructed using the identical coherent reference beam used in the construction process. The reconstructed image is superimposed onto the original object, which is also illuminated with the same light as when the hologram was recorded. Interference fringes will be seen if the object is stressed slightly. This interferometric comparison between the original state of the object (holographic reconstructed virtual image) and the new state of the object (stressed) is made at the instant it occurs; thus, real-time holographic interferometry.

3. Time-average holographic interferometry :- A single holographic recording is made of an object undergoing cyclic vibratory motion, and assumes that the exposure time in recording the hologram is long compared to one period of the vibration cycle. Upon reconstruction of the hologram, the interference among the ensemble of the images, or the vector sum of the individual wavefronts, produces an interference pattern which is weighted towards the deformation extremes of the test piece, i.e. the images recorded near zero velocity contribute most strongly to the holographic recording.

2.4.1 QUANTITATIVE INTERPRETATION OF DOUBLE-EXPOSURE AND REAL-TIME HOLOGRAPHIC INTERFEROMETRY FRINGE PATTERNS

In January 1966 Haines and Hildebrand published the first paper (2.12) which dealt with the interpretation of fringe patterns arising from the translation or rotation of an object such which would be observed in real-time and double-exposure holographic interferometry. Since the

publication of this paper, many researchers have proposed various methods for the interpretation of fringe patterns caused by the displacement of an object.

The need for various methods to interpret the fringe patterns has arisen since the early days of holographic interferometry when it was observed that fringe localization depends on the type of motion undergone by the object. Haines and Hildebrand (2.14) reported that in-plane translation gives rise to fringes localized some distance from the image, while rotation (tilt i.e. out-of-plane motion) of the object about an axis in its own plane produces fringes localized at the image.

An understanding of techniques used in the two cases is thus required in order that a researcher using holographic interferometry may set up the experiment in such away as to maximise the effectiveness of the chosen method.

The following two interpretation techniques discussed by Briers in his review paper (2.13) are presented:-

(1) Fringe counting (FC)

(2) Zero-order fringe (ZF)

2.4.1.1 THE FRINGE COUNTING (FC) TECHNIQUE

This technique was first proposed by Aleksandrov and Bonch-Bruevich (Fig. 2.6)(2.14). This method makes use of the fact that the fringes are, in general, localized some distance from the surface of the reconstructed image and employs the parallax between the fringes and the image. The eye

is focused on the reconstructed image and is stopped down until the fringes have good visibility. The direction of view is then changed progressively by scanning the line of sight linearly across the hologram. The number of fringes which pass across the image point under consideration is counted as the viewing direction is changed by a known amount. This method gives the component of translation of the point in a direction perpendicular to the bisector of the two extreme lines of sight and in the plane containing these lines of sight. The magnitude of the component is calculated as follows:

$$d_x = \frac{N\lambda L}{x} \tag{2.1}$$

where d_x is the component of the translation as defined above; N the number of fringes passing the point of observation; λ the wavelength of light; L the distance from the hologram to the reconstructed image; and x the distance scanned across the hologram.

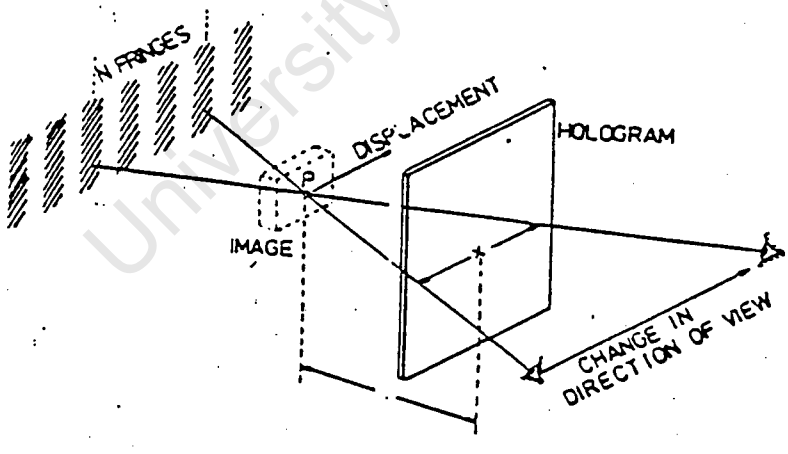

Figure 2.6 Parameters used in the fringe counting (FC) technique (Briers, 1976)

2.4.1.2 THE ZERO-ORDER FRINGE (ZF) METHOD

This technique was first described by Ennos (2.15). It is based on the argument that the change in optical path from the source to the observer is related to the fringe order by the equation:

$$\Delta = m\lambda \tag{2.2}$$

where Δ is the change in optical path; m is the fringe order; and λ the wavelength of the light. When using this technique care must be taken in identifying the zero-order fringe as the fringe order, m, can only be determined absolutely if a known zero-order fringe is in the field of view. Normally a point which is known not to have moved between the two exposures is taken as the point from which the fringes are counted.

Referring to Figure 2.7, the displacement of an object at an angle γ to the bisector of the angle (θ) between the illumination and viewing directions is given by:

$$d = \frac{m\lambda}{2\cos(\theta/2)\cos\gamma} \tag{2.3}$$

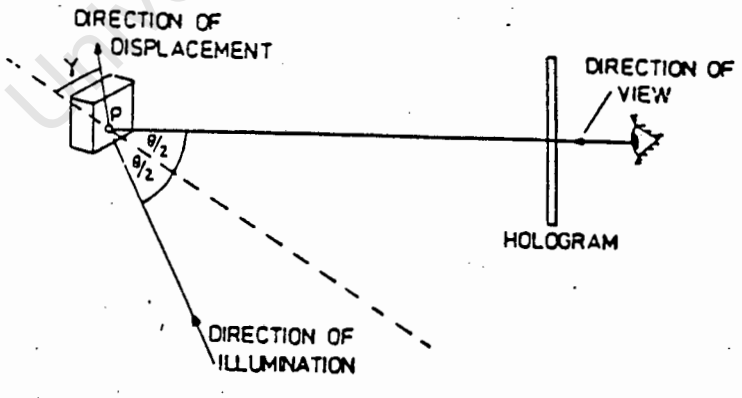

Figure 2.7 General geometry for the ZF technique (Briers, 1976)

The main advantages of the zero-order fringe technique are that it can be used on photographs of the reconstructions of the holographic images instead of the actual holograms and that the physical interpretation is simple.

The zero order fringe technique can be used for any type of displacement of an object, though it is most useful when the fringes are localized on the image. Thus this technique complements the fringe counting technique which can only be used when the fringes are localized at some distance from the image, i.e. indicating the in-plane components of the displacements.

2.4.2 QUANTITATIVE INTERPRETATION OF TIME-AVERAGE HOLOGRAPHIC INTERFEROMETRY

If a vibrating object (2.16) is moving with a frequency ω and amplitude z, then the object field can be mathematically represented as

$$U_o = A_o \exp(ik\gamma z\cos\omega t) \tag{2.4}$$

where γ is a function of the incident illumination angle and observation angle. A_o and k are the amplitude and phase of the illuminating light field respectively. This equation expresses the form of the object field for any instant in time (t), and, since the hologram records every position of the object over one period of vibratory cycle T, it is necessary to take the time-average of this equation over one period of the vibratory cycle to obtain the correct form of the image which will be reconstructed:

$$U \propto (1/T) \int_0^T U_o dt = (A_o/T) \int_0^T \exp(ik\gamma z\cos\omega t)dt \tag{2.5}$$

The corresponding intensity in the image is given by

$$I = |U|^2 \propto |A_o|^2 \left| (1/T) \int_0^T \exp(ik\gamma z\cos\omega t)dt \right|^2 \tag{2.6}$$

This equation can be further simplified, knowing that the integral representation of the Bessel function $J_n(x)$ is of the form

$$J_n(x) = (i^{-n}/2\pi) \int_0^{2\pi} \exp(ix\cos t)\exp(int)dt \tag{2.7}$$

For the case when $n = 0$ equation 2.7 can be written

$$I \propto |A_o|^2 J_o^2[k\gamma z] \tag{2.8}$$

where J_0 is the zero-order Bessel function.

It can be seen from equation 2.8 that the intensity varies as a square of the Bessel function. This variation is characterized by being a maximum when the argument of the Bessel function is equal to zero, and having succeeding maxima which decrease in value. A plot of this function is presented in Figure 2.8.

From Figure 2.8 and equation 2.8 it is observed that when the displacement is zero, the reconstructed image intensity is the brightest. Therefore, regions having no motion, or nodes in the vibratory pattern, exhibit the greatest intensity and can readily be detected upon inspection of the reconstructed image as a bright white fringe.

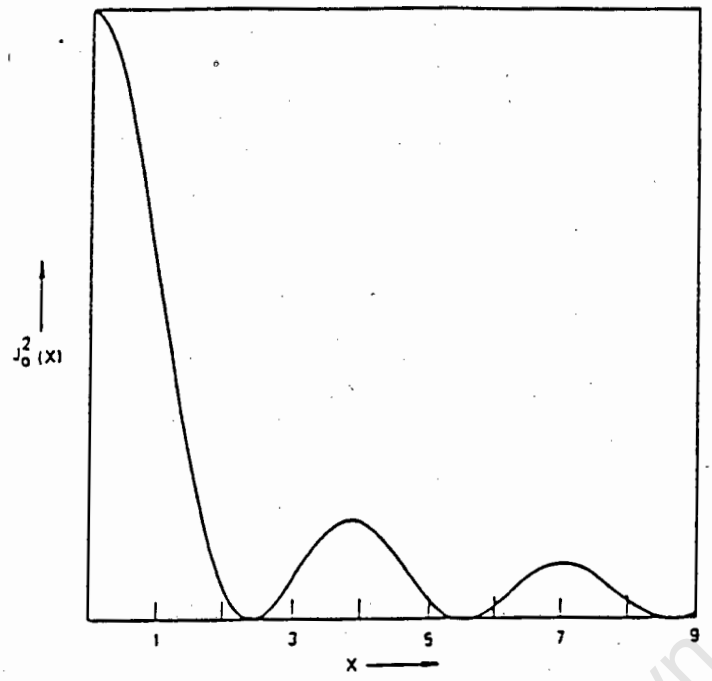

Interferometric fringe intensity variation along a beam as a result of a cyclic vibratory motion.

Figure 2.8 (Walters in Erf ed., 1974)

Pryputniewicz (2.17), and more recently Gryzagoridis (2.18), quantitatively compared the results obtained from time-average holograms of a vibrating beam to those predicted by beam theory. The results from the time-average holograms compared to beam theory values reported by Pryputniewicz are shown in Figure 2.9 and 2.10 for the first and second bending modes respectively.

Note the bright white fringes indicating nodes and the saddle-like fringes indicating anti-nodes (i.e. a point of inflection).

Thus time-average holographic interferometry can provide information about amplitude of vibration and the location of the vibratory nodes and anti-nodes.

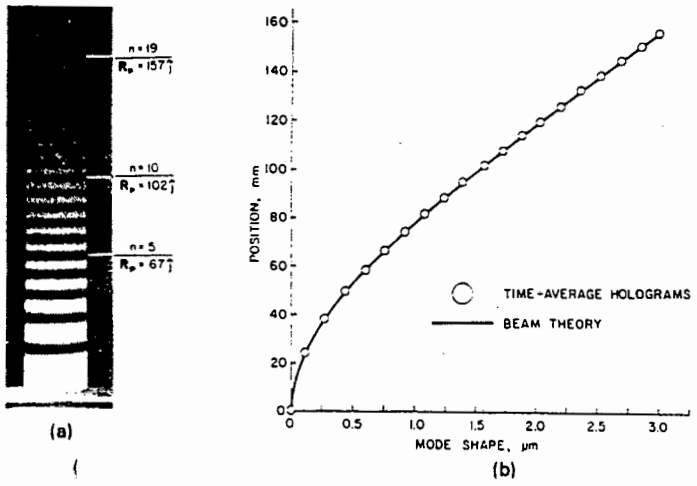

Shape of the first bending mode of the vibrating cantilever beam: (a) image reconstructed from the time-average hologram; n is the fringe order, and R_p is the position vector; (b) comparison between the experimental results obtained from the time-average hologram and the results based on the beam theory.

Figure 2.9 (Pryputniewicz, 1985)

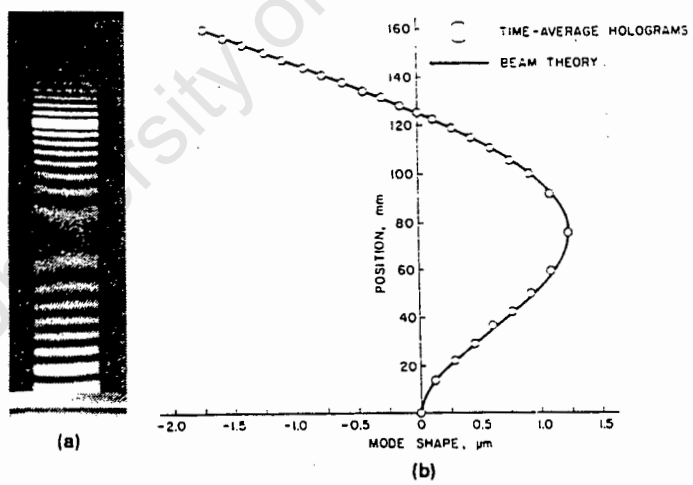

Shape of the second bending mode of the vibrating cantilever beam: (a) image reconstructed from the time-average hologram, (b) comparison between the experimental results obtained from the time-average hologram and the results based on the beam theory.

Figure 2.10 (Pryputniewicz, 1985)

2.5 OPTICAL EQUIPMENT AND CHEMICALS

The following is a brief description of the optical equipment and chemicals which were used in this investigation:-

1) LASER

a) A Spectra Physics 35 mW Helium-Neon continuous wave laser with an output wavelength of 633 nm.

b) A Pulsed ruby laser which delivers an energy of 1J in single mode. The wavelength of light emitted is 694 nm.

When performing continuous wave holographic experiments upon the holographic table, which was a steel plate supported by air cushions, the following were used (Fig. 2.11).

2) BEAMSPLITTER

The beamsplitter was a circular wedge variable beamsplitter. One side of which is aluminum coated, the density of which varies with angle of rotation.

3) BEAM EXPANDER

The beam expander consisted of a 40x microscope objective, a 5 micron pinhole and a focusing mechanism.

Figure 2.11 (left to right):- Adjustable mirror, Emulsion film/plate holder, Collimating lens, Beam expander and Beamsplitter.

4) **EMULSION FILM/PLATE HOLDER**

The precision plate holder consisted of a base and film/plate holding frame. The plate holding frame locates on the base by knife-edges. Spring clips secure the film or glass plates on the holder.

5) **ADJUSTABLE MIRROR**

The adjustable mirrors which were used to direct the laser beam were aluminized on the front surface and included a fine adjusting mechanism, for lateral and vertical movement.

6) **COLLIMATING LENS**

The collimating lenses were used to collimate the expanded laser beam.

7) **CHEMICALS**

The holographic film used was Agfa Holotest Film 8E75 and all holograms were processed using the following developer:-

Solution A	
Distilled water	700 ml
Pyrogallol	15 g
Metol	5 g
Distilled water to make	1000 ml

Solution B	
Distilled water	700 ml
Sodium carbonate	60 g
Potassium hydroxide	20 g
Distilled water to make	1000 ml

Immediately prior to being used, Solution A and B were mixed in equal parts.

CHAPTER 3

3.1 INTRODUCTION TO ELASTIC MODULUS

In engineering, a material's Elastic Modulus (also referred to as Young's Modulus) is of fundamental technological importance. It has applications in areas such as load-deflection, buckling, creep and fracture mechanics.

The importance of Elastic Modulus is reflected by the number of Standards organizations which have formulated procedures for the determination of static and dynamic modulus of certain types of materials.

The standard test for determining the Elastic Modulus of metallic specimens is set out in ASTM E 111 - 82 (3.1). In view of the above stated importance of the Elastic Modulus it is surprising that "there is no recognized testing method for the determination of dynamic elastic modulus in metallic materials" (3.2).

With regard to the dynamic determination of the Elastic Modulus and the fact that no standard test exists for the determination of this mechanical property, a study was undertaken to investigate the applicability of holographic interferometry to the determination of the aforementioned mechanical property.

3.2 DEFINITION OF ELASTIC MODULUS

When a specimen is subjected to a tensile load, the ratio of the resulting elongation (δ) to the length of the specimen (L) is referred to as the

total strain (ε)

$$\varepsilon = \frac{\delta}{L} \tag{3.1}$$

Elasticity is that property of a material which enables it to regain its original shape and dimensions when the load is removed. Hooke's law states that, within certain limits, the stress (σ) in a material is proportional to the strain which produced it. A material which obeys Hooke's law is said to be elastic.

$$\sigma = E\varepsilon \tag{3.2}$$

E, the Modulus of Elasticity, is the constant of proportionality and has the units of stress (force/area) (3.3).

3.3 THE DETERMINATION OF THE ELASTIC MODULUS

As mentioned above a detailed procedure for the determination of the Elastic Modulus is given in ASTM E 111-82 (3.1). In summary a test specimen is loaded uniaxially and load and strain are measured, either incrementally or continuously. The axial stress is determined by dividing the load value by the specimen's original cross-sectional area. The appropriate slope is calculated from the stress-strain curve, which may be derived under conditions of either increasing or decreasing load.

3.4 THE DYNAMIC DETERMINATION OF THE ELASTIC MODULUS

The techniques currently employed to dynamically determine the Elastic Modulus can be classified into three categories:-

1. Wave propagation methods.
2. Resonance methods.
3. Ultrasonic pulsed spectroscopy.

3.4.1 WAVE PROPAGATION METHODS

The equation of motion of longitudinal elastic waves in a rod can be derived in the following manner.

Consider a small element PQ of length δx and let the cross-sectional area of the rod be A (Fig. 3.1). If each plane-section of a rod is assumed to remain plane during the motion and the stress over it to be uniform, the stress on the face P is σ_{xx}, the stress on face Q will be give by $\sigma_{xx} + (\partial\sigma_{xx}/\partial x)\delta x$

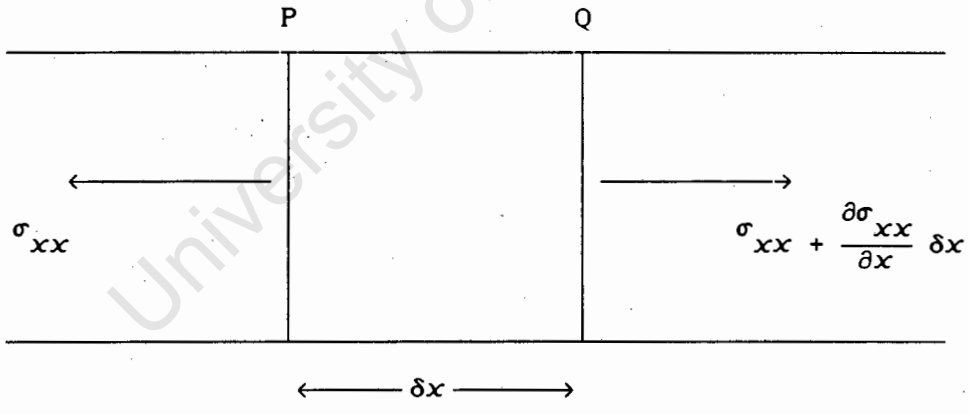

Figure 3.1 Forces acting on element of bar in longitudinal motion.

If the displacement of the element is given by u, then from Newton's second

law of motion:

$$\rho A \delta x \frac{\partial^2 u}{\partial t^2} = A \frac{\partial \sigma_{xx}}{\partial x} \delta x \qquad (3.3)$$

where ρ is the density of the rod.

Since the ratio between the stress σ_{xx} and the strain $\partial u/\partial x$ in the element is the Elastic Modulus E, equation 3.3 may be written:

$$\rho \frac{\partial^2 u}{\partial t^2} = E \frac{\partial^2 u}{\partial x^2} \qquad (3.4)$$

A possible solution of the differential equation 3.4 may be written as:

$$u = f(vt-x) + F(vt+x) \qquad (3.5)$$

where

$$v = \sqrt{E/\rho} \qquad (3.6)$$

F and f are arbitrary functions depending on the initial conditions. The function f corresponds to a wave travelling in the direction of increasing x, whilst the function F corresponds to a wave travelling in the opposite direction.

The above treatment is only approximate since the longitudinal contraction and expansion of the section will necessarily result in lateral contraction and expansion of the section. This lateral motion will result in a non-uniform distribution of stress across the sections of the rod, and the plane transverse sections will become distorted. This effect becomes of importance when the operative wavelengths are of the same order as the diameter of the rod (3.4).

The "Velocity of Ultrasonic Wave Pulses", which falls in this category, is one of the better known techniques for dynamically measuring the Elastic Modulus of materials (3.2). In this technique the wave speed V in the specimen is determined by measuring the transit time t of an ultrasonic pulse over a known length L in a specimen ($V = L/t$). From this the Elastic Modulus can be calculated from equation 3.6 (i.e. $E = V^2\rho$)

For ultrasonic wavelengths less than the dimensions of the specimens, two normal modes of wave propagation in isotropic media occur i.e. a longitudinal and a shear mode with velocities V_l and V_s respectively. The Elastic Modulus is then given by equation 3.7.

$$E = \rho V_s^2 \frac{(3V_l^2 - 4V_s^2)}{(V_l^2 - V_s^2)} \qquad (3.7)$$

Figure 3.2 is a schematic layout of a typical ultrasonic velocity measurement scheme. The transducer converts the excitation signal, received from pulser in the form of a spike voltage, into a mechanical oscillation or sound wave which is coupled into the specimen to propagate at the sound velocity. After entering the specimen, the ultrasonic pulse echoes back and forth between the specimen faces, constantly decaying in amplitude due to scattering, absorption, and boundary interface losses. Each time the wave pulse is incident on the transducer/specimen interface, a portion of the elastic wave energy is converted into an electrical signal by the transducer. This received signal is then amplified and displayed on an oscilloscope so that the transit time measurements can be made. The accuracy of these measurements depends on the dimensions of the specimen

(path length, end-face parallelism, etc), the particular ultrasonic coupling technique, and the signal to noise ratio. Typically the accuracy of these transit time measurements is ± 0.1% or better (3.2).

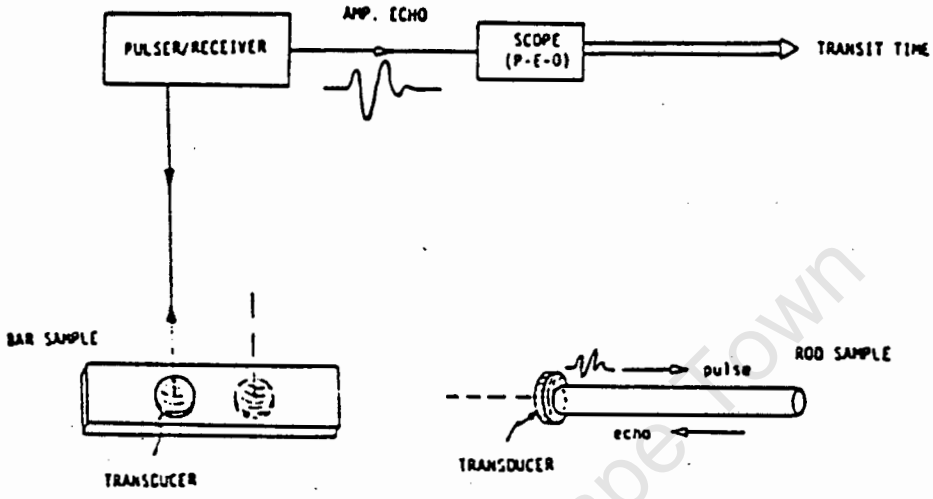

Figure 3.2 Ultrasonic velocity measurement system with direct contact of transducer on specimen (Wolfenden et al, 1989).

3.4.2 RESONANCE METHODS

Equation 3.6 may be shown in a different form:

$$E = \rho(f\lambda)^2 \qquad (3.8)$$

where f is the resonant frequency and λ is the wavelength which is usually determined by the specific geometrical details of the specimen. For

example, for a uniform beam resonating in its fundamental longitudinal mode the wavelength is twice the length of the beam i.e. $E = 4\rho L^2 f^2$.

It is therefore possible to determine the Elastic Modulus by measuring the resonant frequency of standing or decaying elastic waves. Techniques which fall into this category are the 'Free-Free Beam Technique', 'Impulse Excitation Technique', 'Magnetically Excited Resonance', 'Piezoelectric Ultrasonic Composite Oscillator Technique (PUCOT)' and 'Cantilever Beam Method'.

Whilst the apparatus may vary amongst experimenters, the basic principle of operation is the same for all the Free-Free beam techniques (Fig. 3.3).

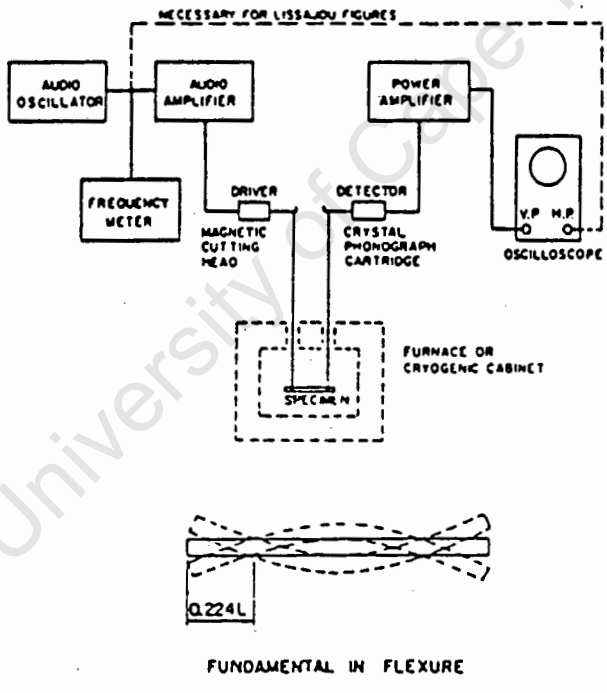

Figure 3.3 Schematic diagram of the instrumentation used in the Free-Free beam test method and the test configuration (Wolfenden et al, 1989).

The specimen is suspended near its nodal points by pure silk or cotton-covered polyester thread. The sine wave signal from a function generator is fed to a power amplifier and then to the driver transducer. The signal from the pickup transducer is analysed on a suitable analyser, which is configured in a peak averaging mode using exponential averaging. The function generator is swept manually through the frequency range of interest while the output signal is examined. The fundamental frequency is quite easily determined in this manner (3.2).

The Impulse Excitation technique entails:- (a) the excitation of the test specimen by means of a light mechanical impulse and (b) the analysis of the resultant transient vibration. An electronic circuit is used to isolate the harmonics and the fundamental resonant frequency from the spectrum of noise, and to measure the period corresponding to the fundamental frequency. The specimen is supported preferably at the nodes of the desired vibrational mode. By positioning correctly the location of the exciting impulse, each mode can be induced easily. Very little exciting energy is required, even for large specimens, because the measurement is performed at low strain amplitudes. Hence only a very light tap is sufficient to initiate the measurement. The most versatile means of detecting the vibrational motion is provided by a hand held piezoelectric probe which is used to analyse signals from about 20 Hz to 80 kHz in frequency (3.2).

The "Magnetically Excited Resonance technique" involves the use of an instrument known as the Modul-R which measures the longitudinal resonant frequency of a specimen of ferromagnetic material near 25 kHz. The specimen must be ferromagnetic because both the specimen drive and pickup

Table 3.1 (Wolfenden et al, 1989)

PUCOT equations for the three-component system.

$$L = (1/2f)(E/\rho)^{1/2} = \lambda/2$$
$$\tau(S) = m(S)^{1/4}\,\tau(DG)\,\tau(DGS)/A$$
$$A = \{\tau(DG)^2 m(DGS) - \tau(DGS)^2 m(DG)\}^{1/2}$$
$$E = 4\rho L^2/\tau(S)^2$$

L = specimen length
f = frequency
E = Young's modulus
ρ = density
λ = wavelength
τ = resonant period
S = specimen
D = drive crystal
G = gage crystal
m = mass

The fifth alternative is to clamp the beam as a cantilever. The cantilever arrangement is attractive from an experimental point of view since the bar can be driven via the clamping device and the vibrations detected by a noncontacting optical transducer. Rosinger and Ritchie (3.5) concluded that for accurate Elastic Modulus calculations from the measured resonant frequencies of cantilever beams, the tests must be restricted to long slender beams. The weakness of the cantilever resonant beam method is associated with the clamping arrangement, which will not realize the ideal boundary conditions assumed by the various theories i.e. Bernoulli-Euler, Timoshenko etc.

3.4.3 ULTRASONIC PULSED SPECTROSCOPY

For completeness a newly developed technique is mentioned, namely Ultrasonic Pulsed Spectroscopy for the Measurement of Phase Velocity and Attenuation. This method can be used both on thin and thick specimens,

where as the previous mentioned methods are suitable only for thick specimens. This technique has been reported by Dayal and Kinra (3.6).

The above mentioned techniques , excluding the cantilever beam method, were compared in an interlaboratory testing program (six different organizations took part). Two nickel-based alloys were tested and all techniques yielded values of Elastic Modulus that agreed to within 1.6% of each other (3.2).

3.4.4 CONCLUSIONS OF REVIEW OF TECHNIQUES TO DYNAMICALLY DETERMINE THE ELASTIC MODULUS

Conclusions which were drawn from current dynamic techniques for determining the Elastic Modulus with regard to an investigation into the use of holographic interferometry as a means for determining this mechanical property were as follows:

1. The route followed by the techniques in the categories 2 and 3 (i.e. the determining of resonant frequency) is not suitable for holographic interferometry. As stated in the previous chapter on holographic interferometry, the fringes obtained are related to the displacement of the object. Since first it would be necessary to excite the test specimen into resonance in either a Free-Free beam or cantilever type situation, the resonant frequency can be determined directly from the driving transducer. The subsequent double exposure or time-average holograms obtained may be compared to the mode shape expected at that frequency, however the frequency required to determine the Elastic Modulus cannot be calculated from these holograms.

2. Pulsed ruby holographic interferometry will be ideally suited to a variation of the methods in the first category. Instead of determining the transit time t for the ultrasonic pulse to cover a known distance, it would be possible with holographic interferometry to observe a disturbance travelling through the test specimen. The disturbance would give rise to an elongation, and therefore a fringe, in the section of the specimen through which it was travelling. From the double-exposure hologram obtained, it would be possible to measure the distance covered by the disturbance in the known time between the two exposures. The velocity of the longitudinal wave can then be calculated and the Elastic Modulus determined.

3. A light tap similar to that used by the Impulse Excitation Technique would be sufficient to initiate a disturbance to be used to determine the Elastic Modulus of the specimen being examined.

4. A review is necessary of previous applications of holographic interferometry to the detection of shock waves in materials.

3.5 HOLOGRAPHIC INTERFEROMETRY APPLIED TO SHOCK WAVES IN MATERIALS

In 1971 Aprahamian et al reported studies of a plate or beam being struck transversely by a pendulum (3.7,3.8). From the double exposure holograms obtained whilst the shock wave travelled through the specimen, the transverse displacement of the specimen after a specific time could be calculated. This displacement was then compared to the theoretically

expected displacement. Figures 3.5a and 3.5b are typical double-exposure holograms obtained of the propagating transverse wave in the beam 25 μsec and 50 μsec after impact respectively.

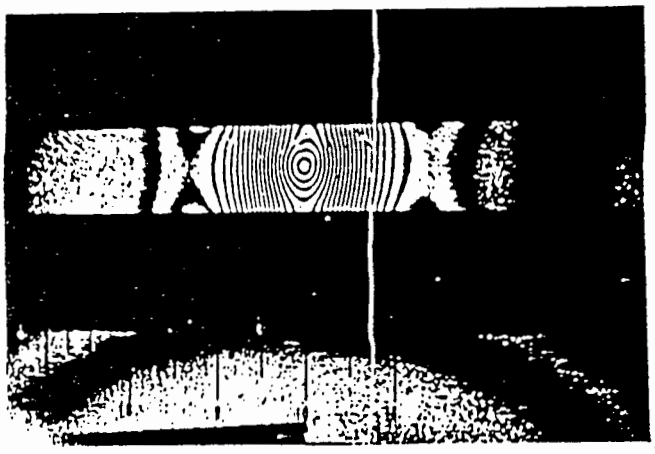

Pulsed holographic interferogram showing the propagating transverse wave in the beam 25 μsec after impact

Figure 3.5a (Aprahamian et al, 1971)

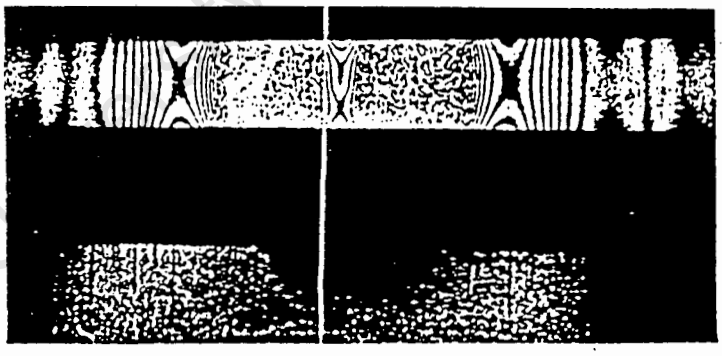

Pulsed holographic interferogram showing the propagating transverse wave in the beam 50 μsec after impact

Figure 3.5b (Aprahamian et al, 1971)

Aprahamian reported (3.7) that "the arrangement of the optics was fairly straightforward and readily accomplished; however, a more difficult problem was to time the pulse of the laser to occur at a particular time delay after initiation of the wave"

In section 2.3.2 the need was explained for flashlamps to "pump up" the ruby rod prior to the laser firing. This delay while the ruby rod is being "pumped up" is unavoidable. The time-event sequence (pre-firing technique) used by Aprahamian to correct for this delay so as to ensure the laser pulsed a particular time Δ_2 after the initiation of the wave was as follows (Fig. 3.6):

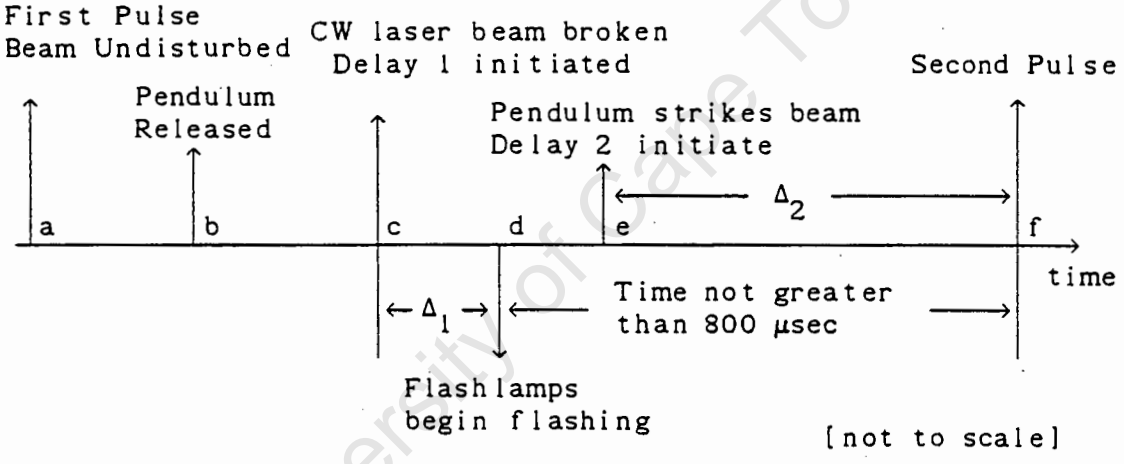

Figure 3.6 Aprahamian's time-event sequence for pre-firing pulsed laser

a) The specimen in its undisturbed state was holographed so as to serve as the first of the two exposures.

b) The pendulum was released and started on its way to impact the specimen.

c) The hammer end of the pendulum interrupted the light beam of the

CW laser. This breaking of the light beam generated a signal via the photocell. The signal entered the time-delay circuit of oscilloscope 1 and, after a suitable delay Δ_1 (point d), the oscilloscope put out a signal to flash the flashlamps.

e) The pendulum continued to travel until it made contact with the specimen. Upon striking the specimen it initiated a transverse wave from the center of the specimen outwards. When the pendulum contacted the beam, it also completed an electrical circuit which sent a signal to oscilloscope 2. After an appropriate time delay Δ_2 (the desired time for the wave to have travelled since initiation) the oscilloscope 2 generated a voltage which triggered the Pockels cell and allowed the laser to lase (point f).

Once the electronics had been established, care had to be taken to ensure that the period of the pendulum was consistent. If for example, the pendulum took either a 100 μsec quicker or longer to strike the specimen, the flashlamps would either not have charged the ruby rod sufficiently or the flashlamps after 900 μsecs would have begun to lose their intensity and consequently the ruby rod would have lost its energy.

Holloway et al in 1977 (3.9,3.10) investigated wave propagation in pink westerly granite, by explosive charges detonated at various depths within pink granite specimens (30.5 cm x 30.5 cm x 15.2 cm). Through the use of a pulsed ruby laser, holograms depicting the ground motion were taken and the vertical, radial and transverse components of the displacement were determined. This was done for several time intervals after the detonation of the explosive. The time-event sequence is shown in Figure 3.7.

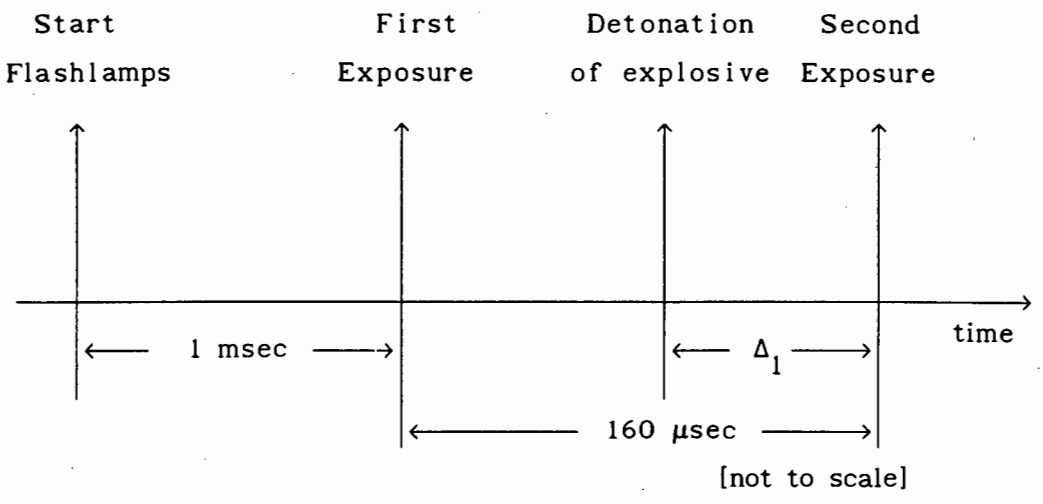

Figure 3.7 Holloway's time-event sequence for pre-firing pulsed laser

By adjusting the electronic control circuit it was possible to detonate the explosive at various times after the first exposure and thereby control the effective time the wave had travelled between the two exposures (Δ_1).

This type of electronic control over the events is possible only because an electrical charge is used to detonate the explosive, so there is no need to correct for the time it takes for the "impulse" to arrive at the specimen as is the case when using an impactor, e.g. a pendulum.

Holloway et al identified and determined the speeds of the primary (dilational, P), secondary (distortional, S) and Rayleigh waves. Knowing the wave velocities it was possible to determine the elastic constants for the rock sample. Holloway reported that his results agreed with the work of Birch (3.11).

It is interesting to note that in a subsequent study in 1988 Holloway et al (3.12) used a similar timing-event sequence. In this study the measurement

of surface displacements resulting from the detonation of an explosive charge on the surface of three rock models was studied. The full field information offered by holographic interferometry overcame the drawbacks normally associated with such a study. Photoelasticity and other photomechanical methods place limitations on the material and geometry of the object, whilst other experimental methods using conventional detectors, e.g. accelerometers, are restricted to pointwise measurement.

3.5.1 CONCLUSIONS OF REVIEW OF HOLOGRAPHIC INTERFEROMETRY AS APPLIED TO SHOCK WAVES IN MATERIALS

From the above review the following conclusions were drawn:-

1. Holographic interferometry has been successfully applied by investigators as a means for observing stress wave propagation through a material.

2. The high energy of the pulsed laser was required in an investigation of this type so as to freeze the propagation of the shock wave.

3. Aprahamian's time-sequence required the first exposure to be made before the release of the pendulum. This can lower the quality of the final hologram obtained since fringes would inevitably arise from even small changes in ambient conditions and more importantly from the rigid body motion of the specimen due to the swing of the pendulum.

4. The source of impulse employed by Holloway (detonation of an explosive) removed many of the problems associated with pre-triggering

the laser. Unfortunately it resulted in damage to the test specimen and therefore it is not classed as a non-destructive test.

5. A light tap such as that used by Aprahamian (i.e. from a pendulum) was adequate to initiate a large enough disturbance which was detected by holographic interferometry. This is consistent with the impulse excitation technique mentioned previously which utilizes a light tap as its source of disturbance. In addition if care was taken in the design of the pendulum, it would give consistent periods of swing which is necessary for a pre-firing device.

3.6 THE DETERMINATION OF THE EXPERIMENTAL PROTOCOL

3.6.1 THE PULSED LASER (HOLOCAMERA)

The pulsed laser which was made available and used in this study was of the ruby-type. The pulsed laser came in a package called the Holocamera. The Holocamera contains all the laser and optical components required to make Leith-Upatnieks off-axis transmission holograms. Appendix I is a schematic of the component layout of the Holocamera.

The active medium is the ruby rod; a sapphire crystal, Al_2O_3, doped with a small concentration of Cr_2O_3. Optical pumping is accomplished by the absorption of energy from flashlamps to raise the trivalent chromium from the ground state to a higher electronic energy level from which they subsequently decay by spontaneous emission to the upper laser level. If the optical pumping rate is fast enough to achieve an overpopulation of the upper laser level, with respect to the lower laser level (the ground state

in this three-level system), the system will oscillate. Once in oscillation, the output will be emitted as a random sequence of laser pulses with a spectral content over the entire fluorescent bandwidth.

For holographic applications, the pulsed laser must be suitably operated so that the laser output will be restricted to a single, or at least a few axial modes, and to the fundamental transverse mode. In this regime, long coherence lengths (greater than one meter) can be obtained. The modifications required include the use of an auxiliary etalon (resonant reflector) to reduce the number of axial resonant modes, a concave mirror and aperture to control the transverse mode structure, and a Q switch. The purpose of the Q switch is to derive a short-duration pulse (±20ns) to minimize the frequency shifting due to the thermal variations during the relatively long (1-2 msec) pumping cycle (3.13).

The basic optical resonator in the Holocamera is provided by a plane partially reflecting wedged output mirror and a 5m curvature concave fully reflecting rear mirror. Operation in single transverse mode is assured by the inclusion of a small aperture, mounted in the end plate of the pumping chamber. The oscillator is pumped by four Xenon-filled flashtubes driven by a high stability power supply (3.14).

Q-switching is achieved by a Pockels cell and polariser and the drive circuit is designed so that either one or two Q-switched pulses are emitted as required. The configuration of laser rod, polarizer, Pockels cell and rear reflector is referred to as pulse-off Q-switch. The Pockels cell is placed between a high reflector and reference polarizer. Quarter-wave voltage is placed on the cell, causing linearly polarized light to be

circularly polarized after one pass. The light reflects from the 100% reflector back through the cell with linear polarization that is orthogonal to the input. The returning light is then rejected by the polarizer. When no voltage is present on the cell, light is not affected and passes back through the polarizer. This is referred to as pulse-off Q-switching, since the quarter-wave voltage is applied to lower the Q of the cavity and is then turned off to cause the laser pulse to be emitted (2.9).

Finally, etalons are also included. Their purpose is to act as additional wavelength selecting elements so as to reduce the number of modes operating and hence increase the coherence length of the holographic oscillator. The etalons are used in transmission and are therefore coated with high reflectivity dielectric coatings to increase their finesse and reduce further the bandwidth of the laser.

Upon lasing, the pulse is steered via mirrors to the ruby amplifier. Here the relatively low energy emitting from the oscillator ruby is pumped up to the required energy level.

Thereafter it is split into the two beams. The object beam being directed towards the object, while the reference beam is manipulated via a series of prisms and mirrors onto the holographic plate. The prisms are used to increase the distance travelled by the reference beam so that it can match that of the object beam.

The Holocamera is controlled by a control unit, the settings of which are chosen by the operator. Appendix II is a schematic of the control panel.

The laser can be fired either internally or externally. The Pockels cell may be on or off during lasing. The operator also has the option of firing the Pockels cell externally. When the laser (i.e. the flashlamps) by itself, or the laser and the Pockels cell are triggered externally a 8-15 V signal must be applied to the appropriate connection on the rear of the control unit.

The Holocamera can also be made to emit in either a single pulse or in double pulse mode. The setting of the desired delay between the pulses (1-800μsec) is keyed into Delay 2. The values for Delay 1, Capacitor Voltage, Delay and Amplifier Capacitor Voltage are obtained from Appendix III. Fine tuning is allowed in order to obtain the optimum energy balance for the two pulses (Appendix IV).

If the external trigger is used for the Pockels cell, then the Pockels cell must be triggered at a time approximately equal to Delay 1 since the time that the flashlamps began pumping. This is to ensure maximum energy from the pulsed laser.

Between lasings (except if the internally controlled double pulse feature is being used) there is a fifteen second delay.

The ruby pulsed laser emits a red light at a wavelength of 694 nm.

3.6.2 THE TIME-EVENT SEQUENCE

In view of the conclusions of the review into previous studies of shock waves in materials using holographic interferometry and the performance

characteristics of the Holocamera, the following time-event sequence was proposed:

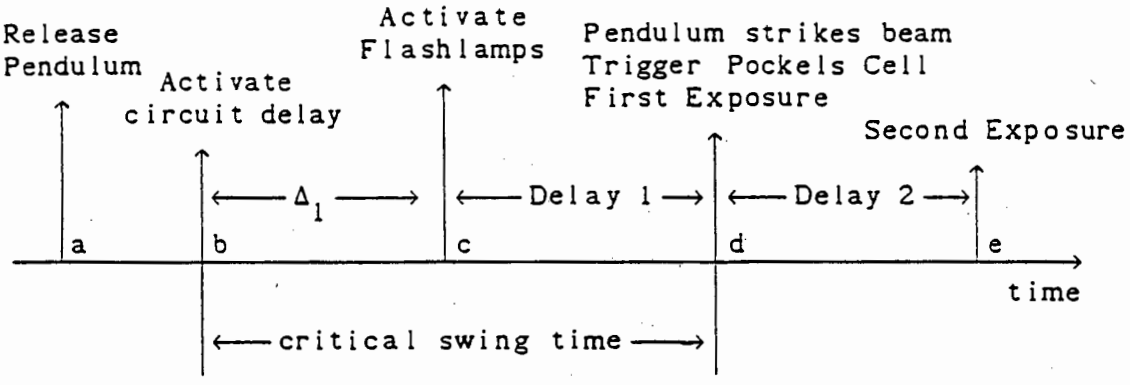

[not to scale]

Figure 3.8 Proposed time-event sequence for pre-firing pulsed laser

a) The pendulum is released and starts travelling toward the rod.

b-d) The critical swing time is determined by test runs prior to the experiment. It is the time that the pendulum takes to travel from the trigger of the laser firing control circuit to the rod.

b) A laser firing control circuit is activated. The circuit must be able to after a required delay (adjustable = Δ_1) put out 8-15 V to activate the flashlamps. The adjustable delay must be set equal to the difference between the critical swing time and Delay 1. This is to ensure that the flashlamps are prefired at a time equal to Delay 1 before the pendulum strikes the rod.

c) Flashlamps are activated at a time approximately equal to Delay 1 before the pendulum strikes the beam. Delay 1 is dependent upon the desired time between the two exposures (Delay 2). Values for Delay 1 are obtained from Appendix III.

d) The pendulum strikes the beam. This completes an electrical

circuit which puts out an 8-15 V signal to the Pockels cell external trigger. Thus the laser is fired for the first exposure.

e) The Holocamera automatically fires the laser at a time equal to Delay 2 after the first exposure. Delay 2 may be set between 1-800 microseconds.

This time-event sequence will eliminate any rigid body effects due to the pendulum as it swings towards the rod. It also incorporates the Holocamera's ability to electronically lase twice at a separation desired by the operator. This would allow for the examination of the stress wave at times convenient for the study. Since the first exposure is made as the pendulum strikes the rod, the leading fringe obtained is an indication of the distance covered by the wave in the time between the two exposures (Delay 2).

If the Pockels cell were not triggered by the contact of the pendulum and rod, it would then be necessary to record the time between activating the adjustable delay circuit and striking the rod in the actual test. If this time were different to the critical swing time, it would result in the effective time for which the wave has been travelling not being equal to Delay 2. This effective time would then have to be used in subsequent calculation. With the proposed time-event sequence, if the critical swing time is not equal to the actual swing time, three situations can arise:-

1) The pendulum strikes the beam less than 100 microseconds too early or too late. In this case the laser will still fire, albeit without the maximum amount of energy. This would give rise to a

poorer quality hologram, but the interference pattern would still be visible. The disturbance resulting in this interference pattern would have been travelling for a time equal to Delay 2 in the rod.

2) The pendulum strikes more than 100 microseconds too early. The ruby has not charged sufficiently and will not lase.

3) The pendulum strikes more than 100 microseconds too late. The ruby's energy has dropped appreciably and the laser discharges automatically.

It would be possible to know if the test was successful by simply studying the energy trace from the laser on the storage oscilloscope and noting if the typical double pulse trace (Appendix IV) was present.

The proposed time-event sequence required:

1) The release of the pendulum from the same height and with the same initial velocity. Any changes in these initial conditions would have affected the velocity of the pendulum, and hence the critical swing time.

2) The design of a laser firing control circuit to be interposed between the trigger mechanism and the laser.

3) The generation of an electrical signal to activate the laser firing control circuit.

4) The design of a consistent swing pendulum.

The various alternatives examined and the final choices made to meet the above requirements were as follows:-

3.6.3 THE RELEASE OF THE PENDULUM

The restraining of the pendulum by an electromagnet attached to a fixed position on a rigid support should be, and was, very effective. The interruption of the current to the electromagnet ensured the pendulum was released from the same height with zero velocity.

3.6.4 THE LASER FIRING CONTROL CIRCUIT

The circuit diagram is shown in Appendix V. The circuit had three points (BNC Connections) at which it was possible to obtain a 12V signal when required.

a) Direct Out

A 12V signal was available when the trigger device interrupted.

b) Delay Out

A 12V signal was available after a desired time following the interruption of the trigger device.

c) Stop Control

A 12V signal was available when electrical contact was made between the pendulum and the rod.

The "Direct Out" and "Stop Control" output pulses were generated by LM555 general purpose timer integrated circuit chips configured for monostable operation. Both monostable circuits were triggered by a falling edge on pin 2. The duration of the output pulses is given by the relation $PW=1.1RC$, where $R=100k\Omega$ and $C=33\mu F$. Thus the output pulse duration for both circuits was 3.3 seconds.

opening of an electrical circuit.

A well defined instant in the time-event sequence was the release of the pendulum. However, the moment of release cannot be assumed to be identical with (or even consistently related to) the interruption of current, since the latter (and consequent drop in magnetic field) takes a significant amount of time and is affected by many uncontrolled factors. If however, the pendulum bob in its arrested position bridged a pair of contacts, the loss of contact could have reliably been taken to signal the beginning of pendulum motion.

This option was not considered suitable since positioning the pendulum in exactly the same position repetitively between the contacts would prove difficult. In addition the critical swing time is "large" when the pendulum is released from this position, allowing other factors (e.g. temperature) to influence the critical swing time.

2) Interruption of a light beam by the pendulum shortly before the moment of impact.

Two alternatives were considered:-

a) To have the pendulum break a laser beam path between a continuous wave laser and a photocell (similar to Aprahamian's trigger mechanism). A Helium-Neon laser in conjunction with a photodiode was used to investigate this option.

b) To interrupt the optical path of an optical limit switch (MCT81),

by a flag attached to the pendulum.

The optical limit switch should ideally be attached to the rod so as to eliminate the possibility of time variations due to small changes in geometry which are inevitable under repeated impact. Furthermore most metals have an expansion coefficient of about 10^{-5}/K. If the pendulum has a period of 0.5 seconds, a temperature change of 5 K would cause a timing change of about 7 milliseconds. Thus microsecond timing accuracy would require sub-millidegree temperature control. This seemed to be another argument in favour of placing the optical limit switch close to the rod.

It was however hoped that in the establishment of a nondestructive test to determine the Elastic Modulus, it would not be necessary to attach anything to the rod. Therefore the possibility of placing the optical limit switch close to the test rod was investigated.

3.6.6 THE PENDULUM DESIGN

This was an experimental situation in which the final performance was likely to be dominated by mechanical rather than electronic considerations. The swing of the pendulum had to be highly consistent and random variations had to be contained to negligible proportions. Also there could not be a systematic progressive change in timing under repeated impacts (due, for example to creep or ductile deformation).

Two alternative pivots were investigated for the pendulum:-

a) A roller bearing pivot.

b) A knife-edge pivot.

The knife-edge was located inside a groove in brass plates.

3.6.7 EVALUATION OF THE TECHNIQUES TO TRIGGER THE LASER FIRING CONTROL CIRCUIT AND THE PENDULUM DESIGN

As the experimental evaluation for the choice of the trigger and pendulum could not be conducted independently of the other and since it was difficult to decide *a priori* which combination of trigger-pendulum was the best for this experimental situation, a series of tests were conducted using the various possible combinations.

For each combination the critical swing time for a number of releases of the pendulum were recorded (Appendix VI shows some typical times recorded). The timing used a Fluke Digital counter and auxiliary electronics as outlined in section 3.8.4.

The CW-photodiode option, although over short periods of time yielded times with a high degree of precision, drift occurred between one set of readings and another. This was unsatisfactory, as it proved extremely difficult to decide on the required critical swing time and then be assured that when the test was conducted, the critical swing time had not changed sufficiently to render the test useless. The slightest change in the CW-photodiode angle was observed to result in significant changes in the recorded times. This requirement for stability to ensure no changes in the CW-diode angle would prove extremely difficult to meet, as the experimental

rig intrinsically has a moving part i.e. the pendulum. It was possible that some heating of the photodiode was occurring as it was also found that the longer the CW laser was directed towards the photodiode, the greater the drift.

Tests using the optical limit switch with either of the pendulums indicated both increased consistency as well as significantly reduced drift as compared to the times obtained using the CW-photodiode option. For the optical limit switch the knife-edge pivot gave the most consistent times.

It was decided to proceed using an optical limit switch placed close to the rod as the triggering device for the laser firing control circuit (Appendix V) along with the knife-edge pivot pendulum (Fig. 3.9).

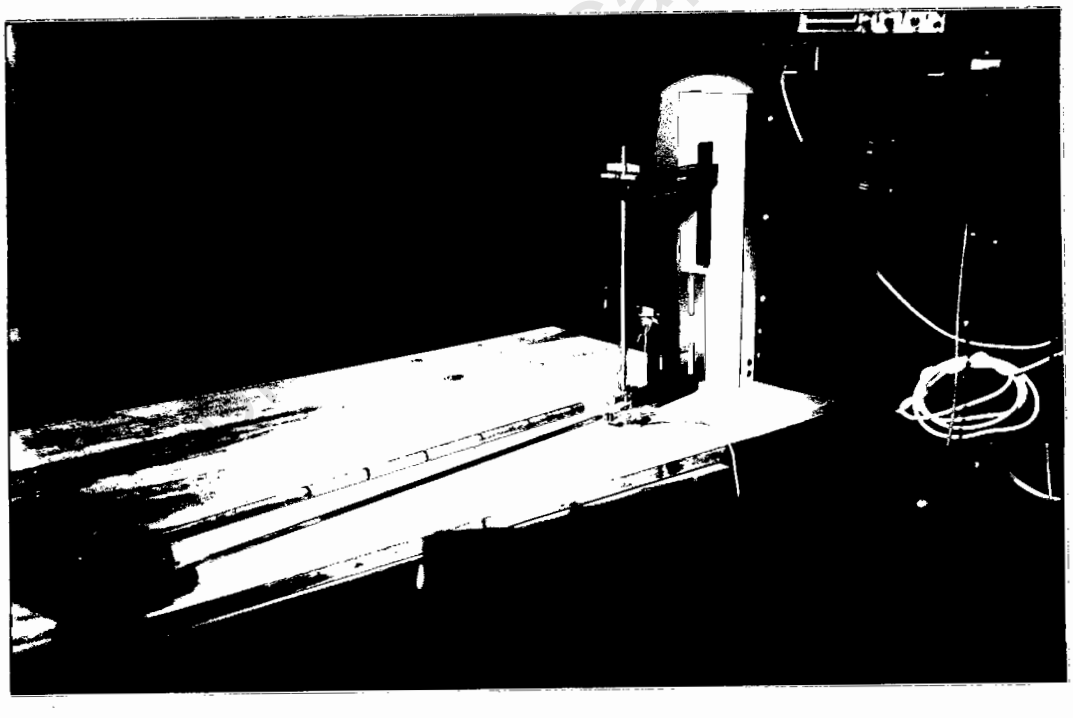

Figure 3.9 Experimental Arrangement

Figure 3.10 is a schematic of the electrical arrangement used to obtain the time-event sequence to make pulsed double-exposure holograms of longitudinal waves propagating in a long rod.

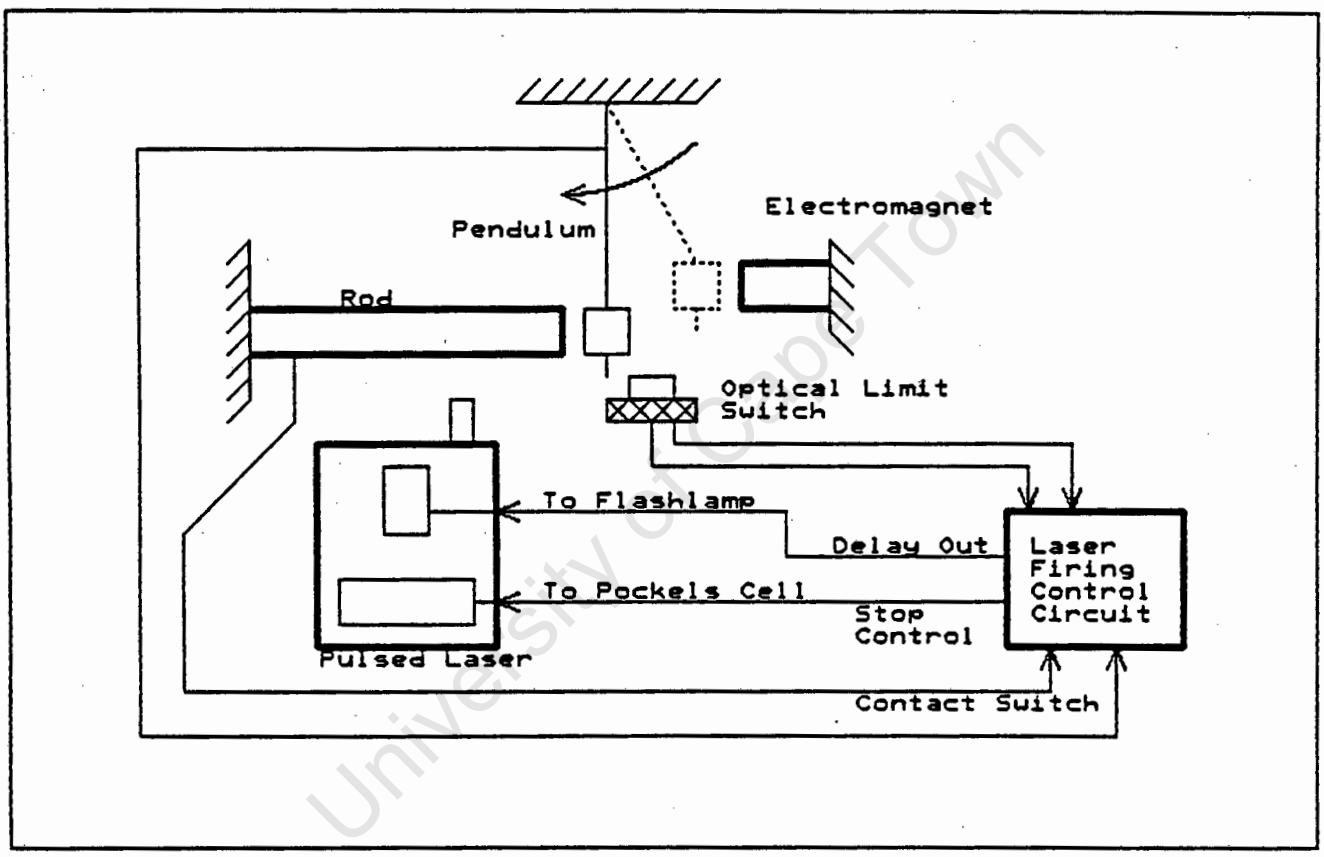

Figure 3.10 Schematic of electrical arrangement for the implementation of the time-event sequence.

When conducting an experimental test the protocol followed with regards to the electronics was as follows:

1. The "Direct Out" was connected to the "a" channel, and the "Stop Control" to the "b" channel of the Fluke Digital Counter.
2. The critical swing times for a number of swings of the pendulum were recorded.
3. After calculating the required Delay Δ_1 (i.e. the difference between the critical swing time and the Delay 1 required by the Holocamera), the "Stop Control" was removed from the Fluke Digital Counter and the "Delay Out" connected to channel "b".
5. The optical limit switch was interrupted by the pendulum, and the delay time observed. The potentiometer was adjusted until the desired delay time was obtained.
6. Steps 1 and 2 were repeated to ensure the critical swing time had not changed.
7 The "Delay Out" was connected to the flashlamp's external trigger and the "Stop Control" to the Pockels cell's external trigger.

Finally, it was not the purpose of this investigation to design and build "the perfect" pendulum, i.e. one whose period was perfectly consistent, but rather to build a pendulum that delivered over a series of tests times which were consistent to within microseconds. As explained previously, the pulsed laser would still operate even if the Pockels cell was not fired exactly at a time equal to Delay 1 after the optical limit switch was interrupted.

3.6.8 PRELIMINARY TEST RESULTS

Preliminary tests indicated the following:-

1. The pendulum/optical limit switch/laser firing control circuit ensured that the pulsed laser fired at the correct instant.
2. An indication was required of the distance of the observed leading fringe from the beginning of the rod.
3. When the rod was parallel to the pulsed ruby laser, the fringes were not localized (i.e. in-plane motion was being observed). Thus it was difficult to determine the exact position of the leading fringe.
4. It was possible that the leading fringe could be "out of view' of the hologram.

Further testing indicated that the problems identified in the preliminary tests could be overcome in the following manner:

1. Black tape placed circumferencially every 10 cm along the rod was sufficient to indicate the distance travelled by the shock wave.
2. By placing the rod at an angle to the laser (i.e. "looking down the rod") it was possible to localize the fringes, and thereby determine the position of the leading fringe.
3. The rod had to be examined piecewise, so as to ensure that there was no leading fringe "out of view" of the hologram. This problem of having to examine piecewise, was greatly reduced by "looking down the rod" since a far greater field of view was available.

3.7 RESULTS

Following the establishment of the test procedure and the modifications indicated by the preliminary tests, Steel and Brass rods of 16 mm diameter and of length 2 m were tested. The delay between the exposures were first set at 50 and then at 100 microseconds (Figs. 3.11 and 3.12 are typical photographs of the reconstructed holograms). The rods were clamped at their ends using a vice and were at fifty degrees to the Holocamera.

A section 90mm (length) x 15.2mm (wide) x 6.15mm (depth) was cut from the steel rod with a mass of 66.17g. The density of the steel was calculated to be 7866 kg/m^2.

From the brass rod a section 90.1mm (length) x 15.2mm (wide) x 6.30mm (depth) was cut with a mass of 74.02g. The density of the brass was calculated to be 8494 kg/m^2.

Appendix VII is a table of the measured distances, the corrected distance (i.e. for the angle of the rod), the calculated velocity and the Elastic Modulus determined by holographic interferometry.

Tests to determine the longitudinal (V_l) and shear wave (Vs) velocities for the two test rods using the 'Velocity measurements of Ultrasonic Wave pulses' technique were conducted at the South African Bureau of Standards (SABS). It was not possible to determine the shear velocity of the brass specimen. Appendix VIII lists the measured wave velocities, typical values for these wave velocities from an acoustic textbook (3.15) and the Elastic Modulus calculated using equation 3.7 with both sets of values. The

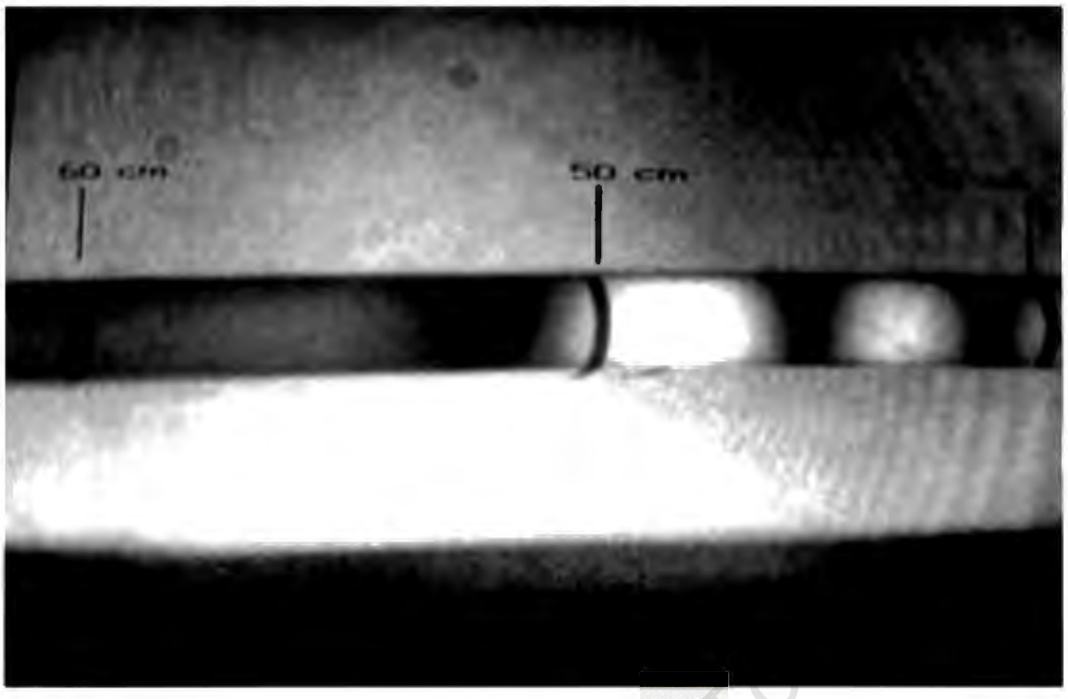

Figure 3.11 Double-exposure holographic interferogram of a propagating longitudinal wave in a steel rod 100 μsec after impact.

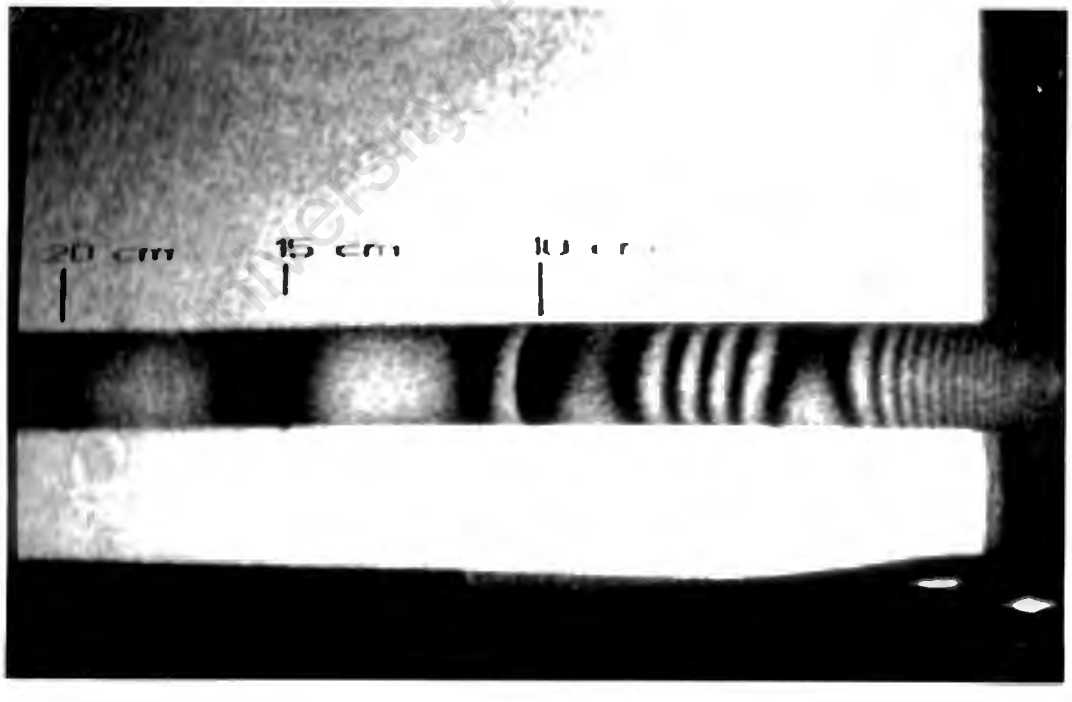

Figure 3.12 Double-exposure holographic interferogram of a propagating longitudinal wave in a brass rod 50 μsec after impact.

standard shear wave velocity was used to calculate the measured Elastic Modulus for the brass specimen.

Table 3.2 lists the Elastic Modulus obtained from i) Holographic Interferometry ii) Ultrasonics iii) an engineering handbook (Shigley) (3.16).

Table 3.2 Elastic Modulus

ELASTIC MODULUS [GPa]			
Material	Holographic Interferometry	Ultrasonics	Shigley
Steel	221.6 215.2	201.5	207
Brass	92.5 106.4	105.8	106

3.8 ANALYSIS AND DISCUSSION OF RESULTS

From Table 3.2 it can be seen that the Elastic Modulus obtained using holographic interferometry compares favourably with those obtained using the ultrasonic technique.

The accuracy to within which the Elastic Modulus was determined was dependent on the accuracy of the measurement of the distance travelled by the leading fringe. From the photographs it is evident that the leading fringe is not a narrow line, but rather blurrs over a section of the rod.

Therefore an accuracy in measurement greater than half a centimeter was extremely difficult to achieve. Even though the pulse of the laser is only 20 nanoseconds, the wave in the steel rod would have travelled 0.1 mm in this time. Assuming $d = m\lambda/2$ this translates into ± 330 fringes. While in the brass the distance travelled would be 0.07 mm which is equivalent to 226 fringes.

An uncertainty in the Elastic Modulus obtained using holographic interferometry can be determined using the following analysis:

$$W_R = \left[\left(\frac{\partial R}{\partial x_1} w_1\right)^2 + \left(\frac{\partial R}{\partial x_2} w_2\right)^2 + \ldots + \left(\frac{\partial R}{\partial x_n} w_n\right)^2\right]^{1/2}$$

where: W_R is the uncertainity in the result

$w_1, w_2, \ldots\ldots w_n$ are the uncertainties in the independent variables

$$E = v^2 \rho$$

$$W_E = [(2v\rho(w_v))^2 + (v^2(w_\rho))^2]^{1/2}$$

For Steel: let $v = 5230$ m/s

$\rho = 7866$ kg/m^3

$w_v = \frac{0.5 \text{ cm}}{100\ \mu\text{sec}} = 50$ m/s

$w_\rho = 20$ kg/m^3

$W_E = 4.15$ Gpa or 2%

For Brass: let $v = 3570$ m/s

$\rho = 8494$ kg/m^3

$w_v = \frac{0.5 \text{ cm}}{100\ \mu\text{sec}} = 50$ m/s

$$w_\rho = 106 \text{ kg/m}^3$$

$$W_E = 3.32 \text{ Gpa or } 3.14\%$$

3.9 CONCLUSIONS

The following conclusions may be drawn from this investigation into the use of holographic interferometry to determine the Elastic Modulus of materials:-

1. The proposed time-event sequence was successfully implemented.
2. The optical limit switch was demonstrated to be a superior means to activate the electronic circuit than the previously used CW-photocell combination.
3. The laser firing control circuit was able to control the test.
4. Once set up the testing was quick and non-destructive. Any changes in critical swing time could easily be corrected by adjusting the variable resistor in the electronic circuit.
5. The ability of the pulsed ruby laser to accurately control the time between the two exposures was fully utilized.
6. The double-exposure holograms obtained could be used to determine the Elastic Modulus of the material being tested.
7. An error analysis indicates that the blurring of the leading fringe does not significantly affect the values obtained for the Elastic Modulus.
8. By setting the test up in an out-of-plane configuration, the fringes were made to localize on the beam, thereby making their observation and subsequent calculations easier to perform.

9. If prior knowledge of the order of magnitude of the acoustic velocity of the material being tested is not available, a long rod must be used and testing must proceed in a piecewise fashion so as to be assured of detecting the leading fringe.

10. Since the Pockels cell are fired by the closing of an electrical circuit incorporating the test piece, the test piece must be conductive. Fortunately, most metals are conductive and therefore suitable as test specimens.

CHAPTER 4

4.1 INTRODUCTION TO POISSON'S RATIO

Experiments demonstrate that when a material is placed in tension, there exists not only an axial strain, but also a lateral strain. Poisson demonstrated that these two strains were proportional to each other within the range of Hooke's Law, and proposed a constant which is expressed as

$$\nu = - \frac{\text{lateral strain}}{\text{axial strain}}$$

Poisson's ratio is used in the design of structures where all dimensional changes resulting from the application of forces need to be taken into account (3.3).

4.2 THE DETERMINATION OF POISSON'S RATIO

The standard test method for determining Poisson's ratio at room temperature is described in ASTM E 132 - 86 (4.1). In summary a test specimen is placed in a tensometer. Two pairs of extensometers are attached to the test specimen. The one pair measures axial strain while the other pair measures transverse strain. The average longitudinal strain, ε_l, and the average transverse strain, ε_t, are plotted against the applied load, P. A straight line is drawn through each set of points, and the slopes, $d\varepsilon_l/dP$ and $d\varepsilon_t/dP$ of these lines are determined. Poisson's ratio is then calculated as follows: $\nu = (d\varepsilon_t/dP)/(d\varepsilon_l/dP)$

The recommended dimensions of the specimen are as follows:-

1. The length of the portion of the specimen that is of constant width be at least five times the width.
2. The length of the specimen between the grips of the testing machine be at least seven times the width.
3. The width itself should be at least equal to the thickness.

4.3 POISSON'S RATIO PREVIOUSLY DETERMINED BY HOLOGRAPHIC INTERFEROMETRY

Cornu (4.2) was amongst the early users of interferometry to study elastic problems. Using an interferometer based on the deflection of light when passing through an air film, Cornu demonstrated that it was possible to determine Poisson's ratio by observing the contour lines of the anticlastic curvature developed by a beam subjected to pure bending.

The anticlastic curvature observed by Cornu had been predicted by Timoshenko (4.3). Timoshenko, in his theory of elasticity gives the deformation of a plate surface occurring under conditions of pure bending (Fig. 4.1) as

$$u = \frac{1}{2R}\left[x^2 - \nu(y^2+d^2)\right] + \text{constant} \qquad (4.1)$$

where R is the radius of curvature of the plate after bending, ν Poisson's ratio of the plate material, $2d$ the plate thickness and x and y the axes of the plate surface.

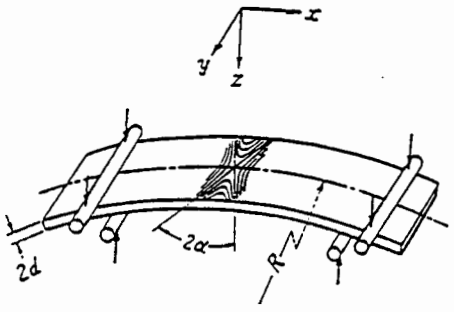

Deformation of a plate by pure bending.

Figure 4.1 (Yamaguchi et al, 1969)

The origin of the co-ordinates is taken at the centroid of the cross-section and the yz-plane in the principle plane of bending. Therefore,the contour lines of the surface displacements are hyperbolas with the asymptotes

$$x^2-\nu y^2 = 0 \tag{4.2}$$

and the smaller angle 2α between them is found from

$$\tan^2\alpha = \nu \tag{4.3}$$

Thus the neutral plane of the beam (that is, the plane in which there is no extension) and the faces of the beam that were originally parallel to the yz-plane are deformed into saddle-shaped, or anticlastic, surfaces (4.4).

The derivation of the formulae assumes a 'thin' strip and deviations may be expected if the strip is too thick (4.5).

Of the first papers to be published following the emergence of holographic interferometry from the principle of holography, one by Yamaguchi et al in

1969 reported on a series of tests, conducted on steel plates, into the "Application of holographic interferometry to the measurement of Poisson's Ratio" (4.6). The motivation for using holographic interferometry was threefold:

1) Its a non-intrusive means to investigate this property, unlike the standard test which uses extensometers.
2) The standard test requires the width of the specimen to be equal to its thickness. In contrast, using holographic interferometry it was possible to use thin test specimens since the anticlastic behaviour of the test specimen was being employed to obtain the Poisson's ratio.
3) While previous interferometric techniques required the material's surface to be polished optically flat, no such requirement existed when using holographic interferometry.

Four-point loading was used to model the pure bending (Fig. 4.2).

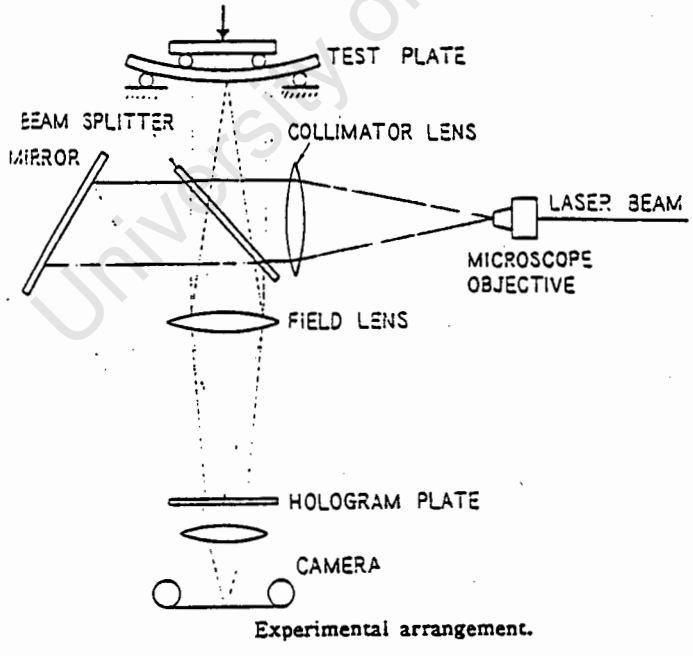

Figure 4.2 (Yamaguchi et al, 1969)

Four test pieces were prepared from a steel plate (Poisson's ratio of 0.292 (3.16)). Their dimensions were 125 mm in length, 3 mm in thickness and 30 mm , 20mm, 15 mm and 10 mm in width. The distance between the loads and that between the supports were 80 mm and 110 mm, respectively.

Using real-time holographic interferometry, about ten interferograms corresponding to different amounts of deflection were taken and analysed for each test piece. The dispersions of the measured angle α were within $\pm$ 0.5° for each test piece. The resultant values of Poisson's ratio against the ratios of the plate width to the distance between the loads are shown in Figure 4.3.

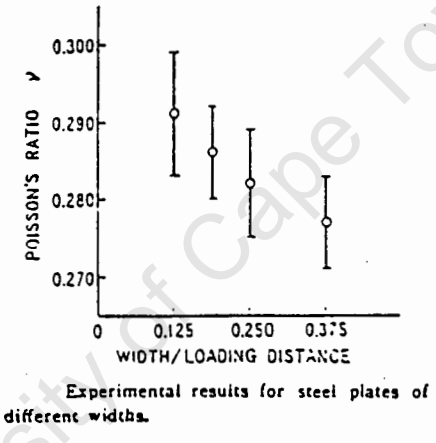

Figure 4.3 (Yamaguchi et al, 1969)

Yamaguchi obtained a smaller value of Poisson's ratio from a wider plate, whose loading and supporting positions were relatively near to the middle. This indicates that the assumption of pure bending, that is, a sufficient distance between loads and the middle of the plate, had not been fully satisfied in his experiment.

In a subsequent investigation Jones et al (4.7), experimentally studied

conditions under which the end effects associated with the four-point bending technique for measuring Poisson's ratio may be neglected. The experiment was performed by investigating strips of the same material with different thicknesses, and width (w) to knife-edge separation (l) ratios (w/l).

Four strips (width 35.5 mm, thickness 2.52 mm, length 130 mm) were cut in the same direction from a strip of mild steel. A value of Poisson's ratio for each specimen using the interferometric technique with identical loading conditions was determined. These values were found to be within the limits of experimental accuracy. This established that any variations in Poisson's ratio found subsequently, could be attributed solely to variations in geometry, and not to differences in the material properties of the specimens. The strips were then machined to different widths (35.2 mm , 30.5 mm, 25.5 mm and 20.2 mm). Values of Poisson's ratio for various combinations of w and l were measured over the range $0.18 < w/l < 0.44$. The thicknesses of the specimens were then reduced using electrochemical shaping, and the measurements were repeated over the same w/l range. The results obtained are shown in Figure 4.4.

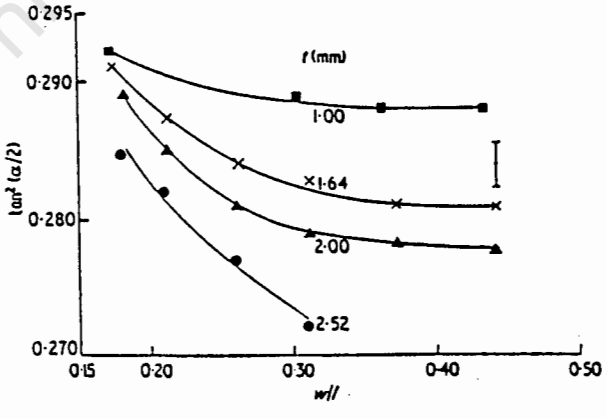

Experimental values of $\tan^2 \frac{1}{2}\alpha$ as a function of specimen and loading geometry

Figure 4.4 (Jones et al, 1969)

It may be concluded that the observed values of Poisson's ratio became less sensitive to specimen and loading geometry as the thickness of the specimen was reduced. Using a criteria that reliable values of Poisson's ratio are only obtained when the thickness is such that the effect of different values of w/l is within experimental error, Jones concluded that only the curve for the 1mm thick test specimen satisfied this criterion with a Poisson's ratio of 0.292.

No previous reports were found in the literature of investigations to dynamically determine Poisson's ratio whilst using holographic interferometry.

4.4 THE DYNAMIC DETERMINATION OF POISSON'S RATIO WHILST USING HOLOGRAPHIC INTERFEROMETRY

Section 2.4.2 presented time-average holographic interferometry and discussed its application to the quantitative analysis of vibrating objects. Typical time-average holograms of a vibrating beam were presented. The anticlastic fringe formed at the anti-nodes due to the anticlastic curvature of the beam was observed to be similar to those obtained when deforming a beam by pure bending (Fig. 4.1).

It seems therefore appropriate in an investigation into the feasibility of using holographic interferometry to determine material properties to explore the possibility of using time-average holograms of resonant vibrating beams to determine Poisson's ratio. From the holograms obtained the angle α of the anticlastic fringe can be measured and the Poisson's ratio calculated.

Another possible approach would be to make a double-exposure hologram of the resonant vibrating beam using the pulsed ruby laser. The first exposure would be made when the beam is in its undisturbed state and the second when it is at its maximum displacement. However, since there is no way to ensure that the second exposure will co-incide with the maximum displacement of the cantilever, the obtained anticlastic fringe would not necessarily be a true representation of the anticlastic behaviour and therefore the values of the Poisson's ratio would be unreliable.

It was decided to proceed using time-average holographic interferometry.

Concurrently with the investigation into the feasibility of using time-average holographic interferometry to determine Poisson's ratio, a study was made into the effect on this ratio due to changes in thickness and width of the test specimens.

4.4.1 EXPERIMENTAL PROTOCOL FOLLOWED TO DETERMINE POISSON'S RATIO BY TIME-AVERAGE HOLOGRAPHIC INTERFEROMETRY

The holographic set-up used to perform the time-average holographic interferometry was the same as that used when recording off-axis transmission holograms (Fig. 2.2). In addition, an acoustic speaker whose frequency and amplitude could be controlled, was placed behind the test beam so as to excite it into its second flexure mode of vibration.

Beams, 125mm long, were cut in the same direction from a strip of mild steel of appropriate thickness. The widths of the beams (Table 4.1) were

chosen so as to keep the same ratios of beam width to thickness for the three thicknesses investigated.

Table 4.1 Thicknesses and widths of beams

THICKNESS [mm]	WIDTH [cm]				
1.0	4.50	5.50	6.50	7.50	8.50
1.5	6.75	8.25	9.75	11.25	12.75
2.0	9.00	11.00	13.00	15.00	17.50

The experimental procedure used was as follows:-

1. The beam was made to act as an upright cantilever by clamping one end into a vise.
2. At first a hologram of the beam in its undisturbed state was obtained, which after developing was replaced it in its original position.
3. The beam was excited and viewed through the hologram with the aid of a video camera on the video monitor.
4. The frequency was adjusted until a single anticlastic fringe appeared indicating that the second mode of vibration had been located. Thereafter the sharpest possible definition was obtained by adjusting the amplitude.
5. After removing the first hologram a time-average hologram was made without any further adjustments being made either to the frequency or amplitude of the acoustic speaker. The frequency was typically of the order of 175 Hz and the exposure time was 4 seconds.
6. After re-setting the acoustic speaker and replacing the real-time hologram steps 3 through 5 were repeated six times.

7. The beam was then removed and replaced with the next beam to be tested.
8. Steps 2 through 7 were then repeated until all the beams had been tested.
9. Using collimated laser light the time-average holograms were reconstructed and via the video camera displayed on the video monitor. Photographs were taken of the images on the video monitor.
10. The photographic negatives were placed in an enlarger and the anticlastic fringe marked off on a piece of paper.
11. The angle 2α was measured using a protractor and the Poisson's ratio (eq. 4.3) calculated.

Care was taken to ensure that the time-average holograms were made at the resonant frequency. In order to minimize distortions during reconstruction and photographing of the time-average holograms, the reconstructing beam was placed at the same angle relative to the hologram as the original reference beam. By placing the anticlastic fringe at the center of the video monitor, distortions due to the curvature of the monitor screen were reduced.

In addition, in order to minimize the error due to the possible distortion of the anticlastic fringe, six time-average holograms were made of each beam.

4.4.2 RESULTS OF USING TIME-AVERAGE HOLOGRAPHIC INTERFEROMETRY TO DETERMINE POISSON'S RATIO

Figure 4.5 is a typical photograph of a time-average hologram obtained.

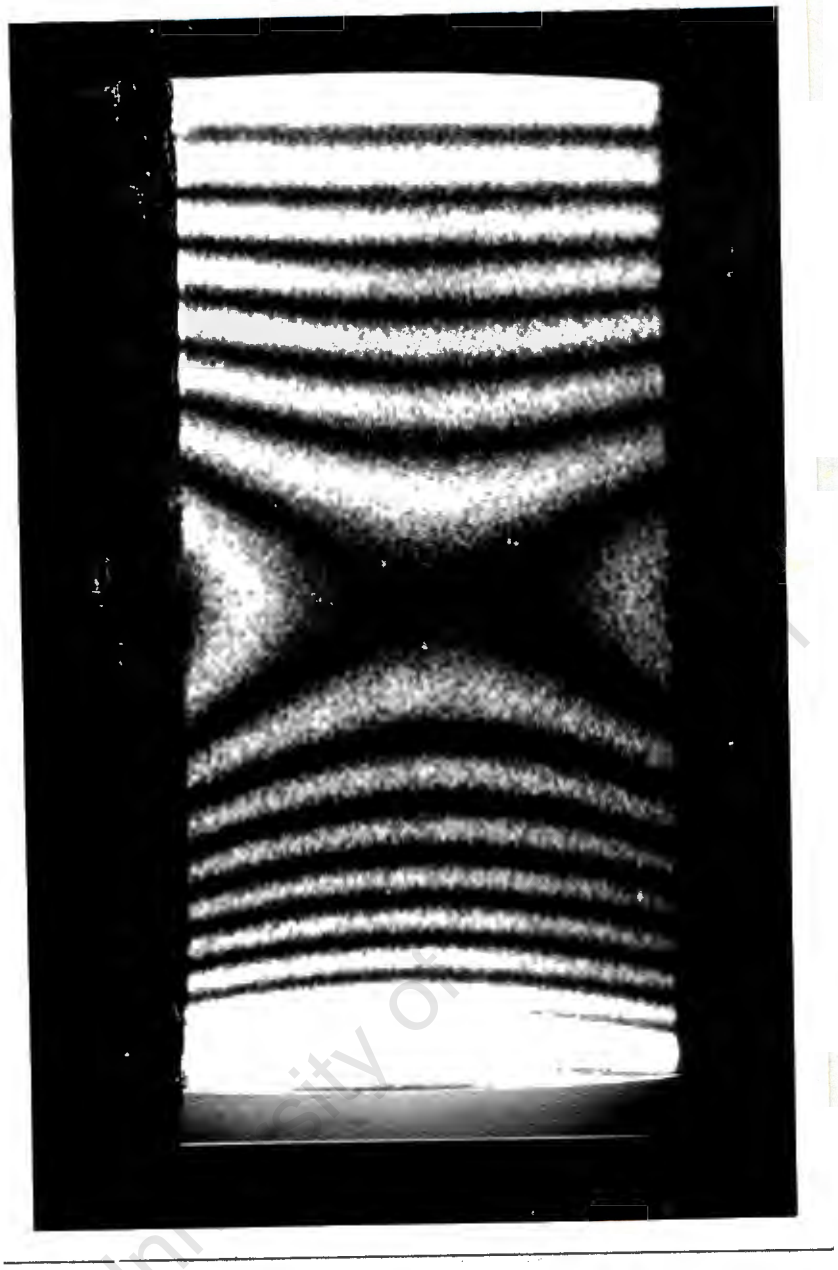

Figure 4.5 Typical time-average hologram of a cantilever beam.

Appendix IX is a table of the results obtained for each beam. The 15 and 17.5 cm wide beams were not tested because the trend in the results had already been established. Appendix X shows graphical representations of these results for beams of thickness 1 mm, 1.5 mm and 2 mm respectively.

The average Poisson's ratio versus the ratio of beam width to thickness

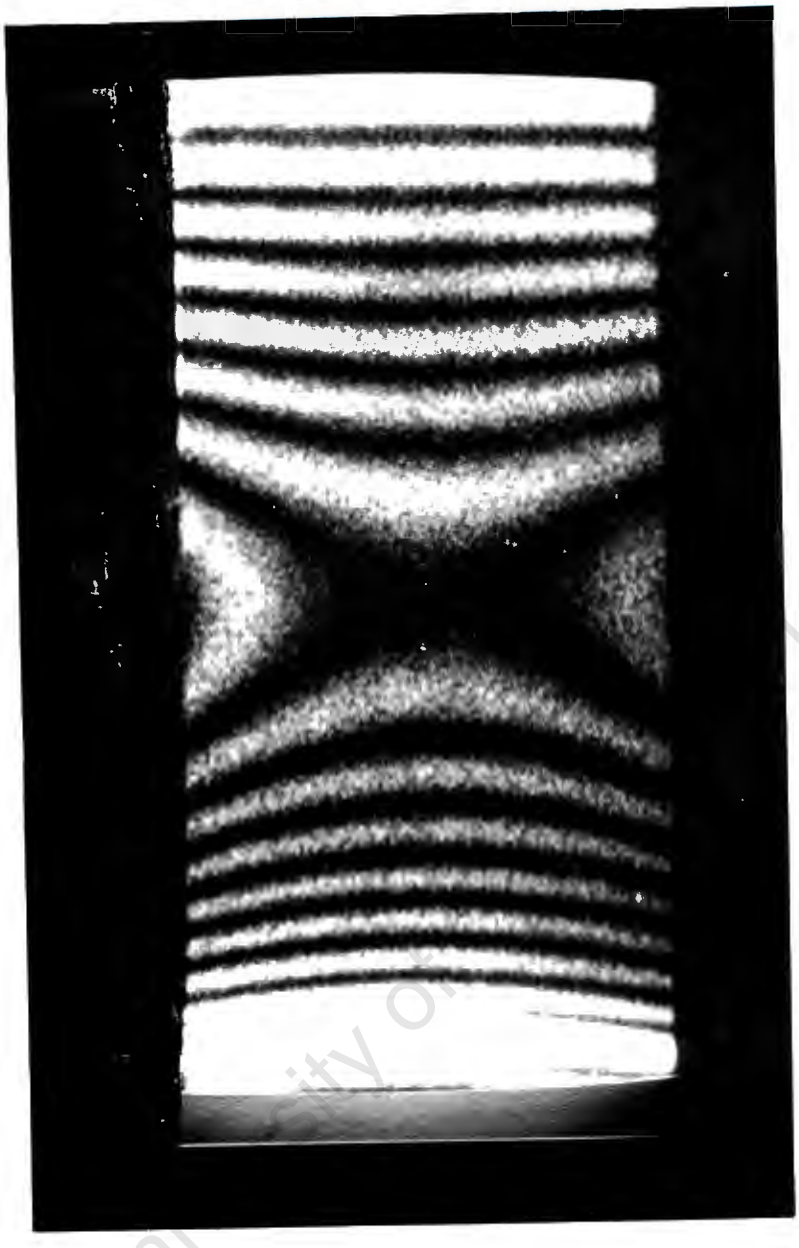

Figure 4.5 Typical time-average hologram of a cantilever beam.

Appendix IX is a table of the results obtained for each beam. The 15 and 17.5 cm wide beams were not tested because the trend in the results had already been established. Appendix X shows graphical representations of these results for beams of thickness 1 mm, 1.5 mm and 2 mm respectively.

The average Poisson's ratio versus the ratio of beam width to thickness

(w/t) is given in Table 4.2 and displayed graphically in Figure 4.6.

Table 4.2 Average Poisson's ratio versus the beam's width to thickness ratio (w/t).

	Beam Width		
(w/t)	1 mm	1.5 mm	2 mm
4.5	0.3307	0.2291	0.1995
5.5	0.2991	0.2167	0.1862
6.5	0.2929	0.1939	0.1834
7.5	0.2942	0.1946	
8.5	0.2924	0.1835	

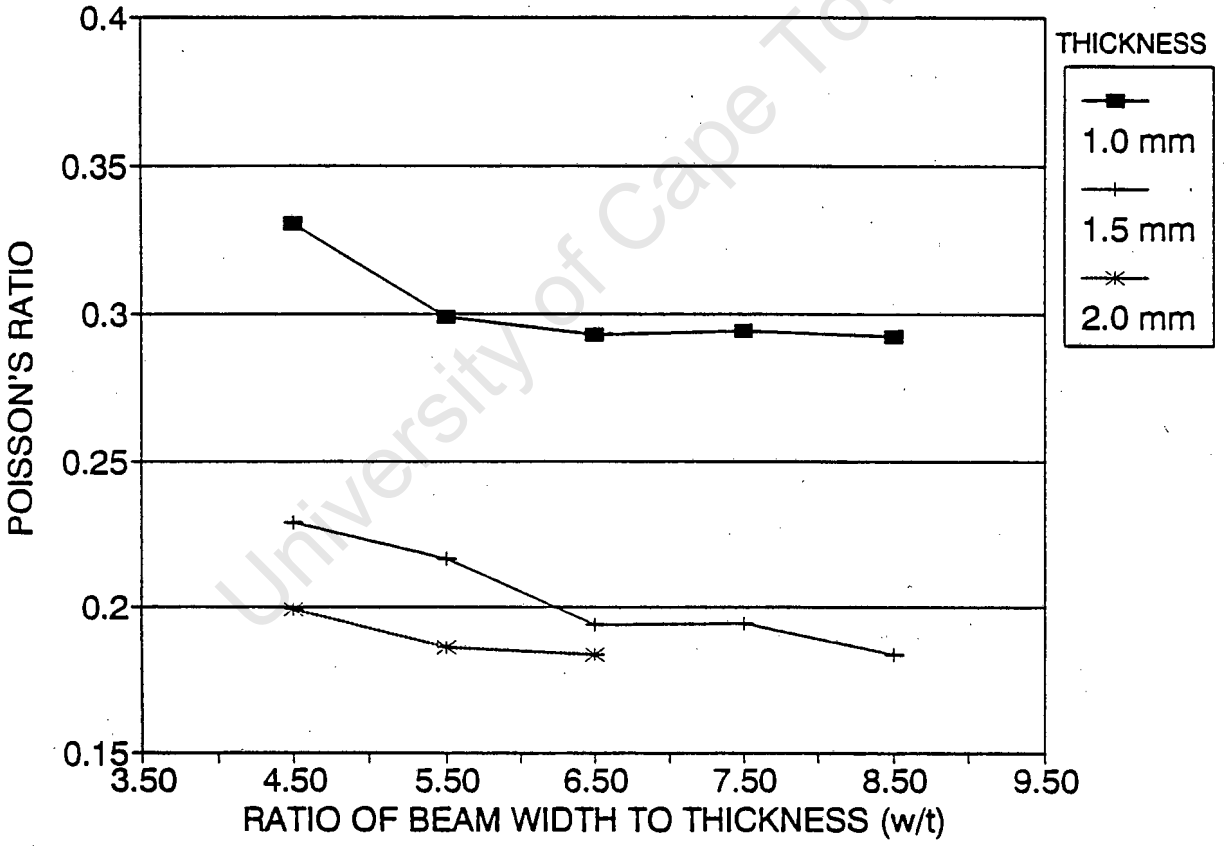

Figure 4.6 Average Poisson's ratio versus the beam's width to thickness ratio (w/t).

4.4.3 ANALYSIS AND DISCUSSION OF RESULTS

An uncertainty analysis was performed on the function used to obtain the Poisson's ratio i.e. $\tan^2\alpha$, to determine its sensitivity to changes in α (Appendix XI is a graph of Poisson's ratio vs α). For the purpose of the analysis the average angle was taken as 28.5 degrees as this is equivalent to a Poisson's ratio of 0.294.

$$W_R = \left[\left(\frac{\partial R}{\partial x_1} w_1\right)^2 + \left(\frac{\partial R}{\partial x_2} w_2\right)^2 + \ldots + \left(\frac{\partial R}{\partial x_n} w_n\right)^2\right]^{1/2}$$

where: W_R is the uncertainity in the result

$w_1, w_2, \ldots\ldots w_n$ are the uncertainties in the independent variables

$$\nu = \tan^2(\alpha)$$

$$W_\nu = 2\tan(\alpha)\sec^2(\alpha)w_\alpha$$

Letting $\alpha = 28.5$ and $w_\alpha = 2$ degrees

$$W_\nu = 0.0488 \text{ or } 16.7\%$$

Letting $\alpha = 28.5$ and $w_\alpha = 4$ degrees

$$W_\nu = 0.0977 \text{ or } 33.3\%$$

Thus a four degree change in α results in a 33.3% uncertainty in the Poisson's ratio. Thus slight distortions in the anticlastic fringe have significant effects on the Poisson's ratio. The lowest value of 0.1674 (Appendix IX) was due to an α of 22.25 degrees, a difference of 6.25 degrees from the optimal value of 28.5 degrees.

The curves presented in Figure 4.6 have the same general shape as those obtained by Jones (Fig. 4.4). Similarly to Jones, as the thickness was reduced the values of Poisson's ratio became less sensitive to specimen geometry. For a particular beam thickness, the lower the aspect ratio (w/t) the higher was the observed Poisson's ratio.

Reliable Poisson's ratios were only obtained for the 1 mm thick beams. The values were essentially insensitive to the aspect ratio (w/t) and yielded an average Poisson's ratio 0.287.

For the 1.5 mm and 2 mm thick beams, the calculated Poisson's ratios are significantly lower. The fall in observed values of dynamic Poisson's ratios, which renders them unreliable, warrants further discussion.

Ashwell in his paper "The anticlastic curvature of rectangular beams and plates" (4.5) states that 'anticlastic curvature can be shown to exist in beams for which w to t are comparable with each other, but if t is small compared with w, i.e. if the beam becomes a flat plate, it is found experimentally that there is no appreciable distortion of the cross-section, and in such cases it is assumed that no anticlastic curvature takes place'. Case (4.8) concluded that the value $w^2/(Rt)$ decides the mode of distortion, and that the change from bending in which anticlastic curvature occurs to bending in which it is very nearly neutralised, will appear as a definite discontinuity, rather than as a gradual change.

Ashwell showed that for large values of $w^2/(Rt)$ (say greater than 100) the

beam is substantially flat except near the edges where they may tend to some constant shape.

In this study although the ratios of w/t where kept the same for the three beam thicknesses, the increase in beam width resulted in significant increases in $w^2/(Rt)$, indicating a reduction in the anticlastic behaviour of the beam. The beams were in fact behaving like plates. While with the 1 mm thick plate it was still possible to detect anticlastic behaviour, the further increase in plate thickness along with an increase in plate width reduced the anticlastic behaviour and thus also the observed Poisson's ratios.

For a particular beam thickness, the narrower beams should display greater anticlastic behaviour (they have a lower $w^2/(Rt)$) This was observed since for a particular beam thickness, the lower the aspect ratio the higher was the Poisson's ratio.

A second investigation was undertaken to determine the feasibility of measuring Poisson's ratios using holographic interferometry.

4.5 POISSON'S RATIO DETERMINED FROM THE MODULUS OF ELASTICITY AND RIGIDITY

Poisson's ratio may be calculated from the Modulus of Elasticity (E) and the Modulus of Rigidity (G) of a material by the following relationship (3.3):

$$\nu = \frac{E - 2G}{2G} \tag{4.4}$$

Since an experimental procedure to determine the Elastic Modulus of a solid rod by holographic interferometry had already been established (Chapter 3), it was necessary to establish a procedure to determine the Modulus of Rigidity of a solid rod by holographic interferometry.

4.5.1 THE MODULUS OF RIGIDITY

For a material which obeys Hooke's Law and is within the elastic range

$$\tau = G\gamma \tag{4.5}$$

where τ is the shear stress , γ the shear strain and G the constant of proportionality known as the Modulus of Rigidity (3.3).

4.5.2 THE EXPERIMENTAL PROTOCOL FOLLOWED TO DETERMINE THE MODULUS OF RIGIDITY BY HOLOGRAPHIC INTERFEROMETRY

The angle of twist (θ) for a solid rod of constant diameter is given by (3.3):

$$\theta = \frac{Tl}{GJ} \tag{4.6}$$

where T = torque

l = length

G = Modulus of Rigidity

J = Polar area moment of inertia

$$= \frac{\pi d^4}{32} \quad ;d \text{ is the diameter of the rod}$$

Based on equation 4.6 a double-exposure holographic interferometric experiment was set up to determine the Modulus of Rigidity of a solid rod.

The one end of the test rod which was freely supported, had a transducer attached to it. The other end was clamped. Figure 4.7 is a schematic of an end view of the long solid rod with the attached transducer.

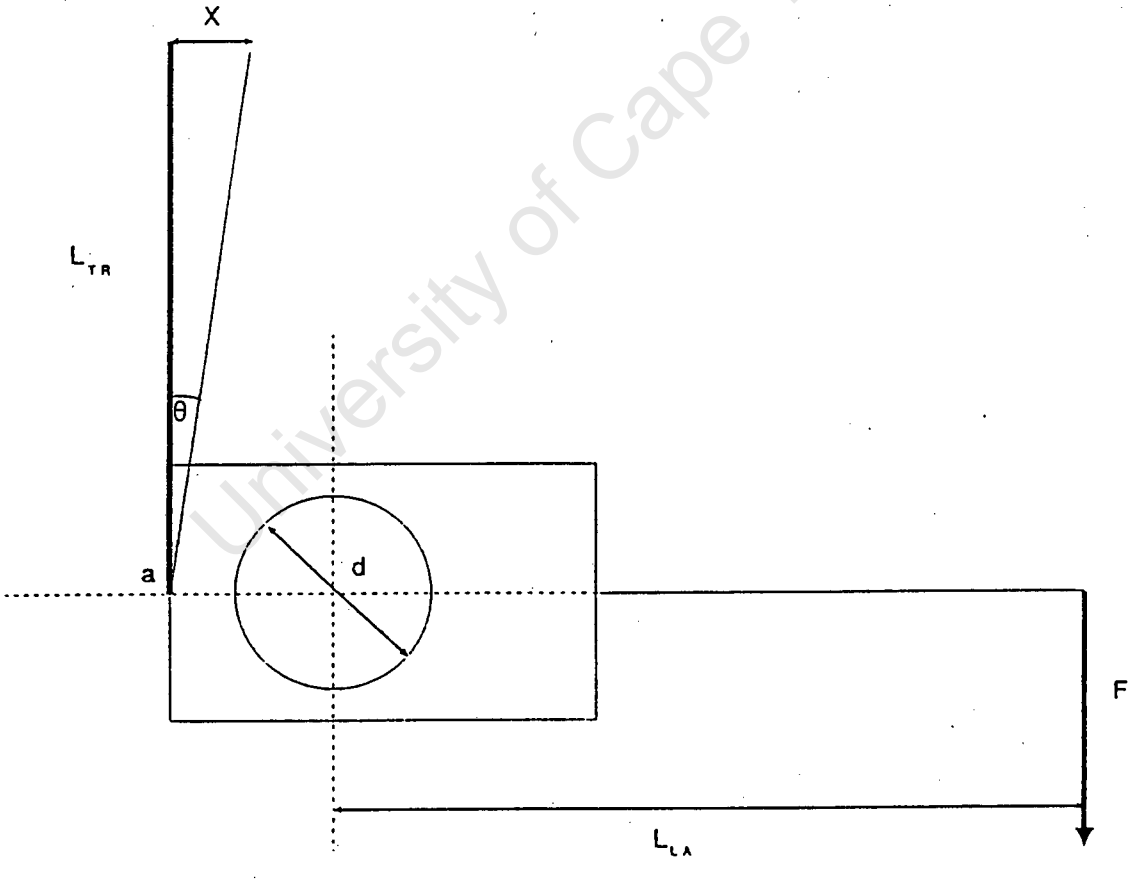

Fig. 4.7 Schematic of end view of solid rod with attached transducer.

As only small angles of twist of the rod were considered, the assumption was made that point 'a' was fixed in space. The implication of this assumption was that the transducer arm was assumed to only experience rotation about a fixed point, and therefore equation 2.8 was used for the quantification of the holographic interferometric fringes on the transducer arm after the rod had been twisted. The following is the derivation of equation 4.13 used to determine the Modulus of Rigidity by holographic interferometry.

From equation 4.6

$$G = \frac{T l_{rod}}{\theta J} \tag{4.7}$$

From the geometry of Figure 4.7:

$$G = \frac{F \times L_{LA} \times l_{rod}}{\theta \frac{\pi d^4}{32}} \tag{4.8}$$

and

$$\sin\theta = \frac{X}{L_{TR}} \tag{4.9}$$

For small θ

$$\theta = \frac{X}{L_{TR}} \tag{4.10}$$

Recalling equation 2.3 with θ and γ equal to zero gives:

$$m = \frac{2X}{\lambda} \tag{4.11}$$

Substituting equation 4.11 into equation 4.10 gives:

$$\theta = \frac{m\lambda}{2L_{TR}} \tag{4.12}$$

Finally, substituting equation 4.12 into equation 4.8 gives:

$$G = \frac{F \times L_{LA} \times l_{rod}}{\frac{m\lambda\pi d^4}{64L_{TR}}} \qquad (4.13)$$

The experimental procedure followed:-

The 16mm diameter steel and brass rods used to determine the Elastic Modulus (Chapter 3) were cut to a length of 92cm. When tested each rod was supported as previously described with the fixed support being provided by a standard drill chuck. At the free end a 2cm section of the rod beyond the transducer lay on a piece of crystal glass acting as a bearing for the vertical support. The effective length of the rod (l_{rod}) was 87.5cm, the force lever arm (L_{LA}) was 8cm and the transducer length (L_{TR}) was 13cm.

The pulsed ruby laser was used to make double-exposure holograms with the first exposure being made with no load on the lever arm of the transducer and the second exposure after the application of the load at the end of the lever arm.

The double-exposure holograms were reconstructed using the Helium-Neon laser and the resulting fringes on the transducer arm were counted.

4.5.3 RESULTS OF USING HOLOGRAPHIC INTERFEROMETRY TO DETERMINE THE MODULUS OF RIGIDITY AND POISSON'S RATIO

The Modulus of Rigidity determined for the steel and brass rods at various loads is presented in tabular and graphical form in Appendix XII.

Excluding the Modulus of Rigidity calculated for the 5 gram load, an average value of 77.5 GPa and 40.7 GPa was determined for the steel and brass rods respectively. Shigley gives a Modulus of Rigidity for steel of 79.3 GPa and for brass of 40.1 GPa.

The following analysis predicts that the difference between the obtained and reported values can be attributed to an uncertainty of less than one fringe in the number of fringes obtained.

Substituting the specific dimensions used into equation 4.13

$$G = \frac{\text{mass x } 43794}{m}$$

$$W_R = \left[\left(\frac{\partial R}{\partial x_1} w_1\right)^2 + \left(\frac{\partial R}{\partial x_2} w_2\right)^2 + \ldots + \left(\frac{\partial R}{\partial x_n} w_n\right)^2\right]^{1/2}$$

where: W_R is the uncertainity in the result

$w_1, w_2, \ldots\ldots w_n$ are the uncertainties in the independent variables

$$W_G = \left[(m^{-1} * 43794 * w_{mass})^2 + (-mass * 43794 * m^{-2} w_m)^2\right]^{1/2}$$

For steel: Let mass = 0.06 Kg; m = 33

w_{mass} = 0.001 Kg; w_m = 1

W_G = 2.75 GPa

For brass: Let mass = 0.06 Kg; m = 63

w_{mass} = 0.001 kg; w_m = 1

W_G = 0.96 GPa

Using equation 4.4 with G=77.5 GPa and E=215.2 GPa (Chapter 3) the Poisson's ratio for steel was calculated to be 0.388 as compared to the value of 0.292 given by Shigley (3.16), a percentage difference of 24.8%.

Using equation 4.4 with G=40.7 GPa and E=106.4 GPa (Chapter 3) the Poisson's ratio for brass was calculated to be 0.307 as compared to the value of 0.324 given by Shigley (3.16), a percentage difference of 5.3%.

Although the values obtained for the Modulus of Elasticity and Rigidity by the holographic interferometric techniques developed compared favourably with values obtained from standard engineering handbooks (e.g. Shigley) and/or from using Ultrasonic techniques, the Poisson's ratios obtained using these values were questionable. The variability is predicted by an uncertainty analysis performed on equation 4.4 which shows it to be extremely sensitive to changes in the Modulus of Elasticity and Rigidity.

Performing an uncertainty analysis on equation 4.4 revealed that:

$$\nu = \frac{E - 2G}{2G}$$

$$W_R = \left[\left(\frac{\partial R}{\partial x_1} w_1\right)^2 + \left(\frac{\partial R}{\partial x_2} w_2\right)^2 + \ldots + \left(\frac{\partial R}{\partial x_n} w_n\right)^2\right]^{1/2}$$

where: W_R is the uncertainity in the result

$w_1, w_2, \ldots\ldots w_n$ are the uncertainties in the independent variables

$$W_\nu = \left[(2G^{-1} w_E)^2 + (-2EG^{-2} w_G)^2\right]^{1/2}$$

For steel: Let E = 207GPa; G = 79.3 GPa

w_E= 10 GPa; w_G= 2 GPa

W_ν= 0.284

For brass: Let E = 106GPa; G = 40.1 GPa

w_E= 3 GPa; w_G= 1 GPa

W_ν = 0.199

4.6 CONCLUSIONS

From the results of the two holographic interferometric experiments performed to obtain Poisson's ratio the following conclusions were drawn:

1. Time-average holographic interferometry may be used to determine Poisson's ratio, provided that care is taken when selecting the test specimens geometry.
2. Using time-average holograms a reliable Poisson's ratio for steel was only obtained for the 1mm thick beam.
3. Inadvertently additional experimental evidence that anticlastic behaviour decreases with the increase in $w^2/(Rt)$ has been provided by time-average holographic interferometry, thereby supporting Ashwell's paper of 1947.
4. An holographic interferometric technique has been developed to determine the Modulus of Rigidity of a solid rod.
4. Acceptable Poisson's ratios could not be calculated from the Modulus of Elasticity and Rigidity determined separately by holographic interferometry for a rod of constant diameter.

CHAPTER 5

5.1 BACKGROUND INFORMATION ABOUT CREEP

At low temperatures the mechanical properties of metallic materials are virtually independent of the rate of straining or duration of the test. At high temperatures this condition is changed and the yield and ultimate tensile stresses are markedly dependent on these factors. The material may plastically deform or 'creep' under the sustained application of loads which would induce only elastic distortions in short-term tests (5.1).

The phenomenon of creep is therefore a source of many problems in design. An engineer requires ways of predicting whether components operating in the creep range will sustain the life required of them. The useful life could be terminated (a) when the deformation becomes excessive, or (b) when rupture occurs. For most practical applications predictive methods must be capable of accounting for complex loadings which vary with time (5.2).

There is thus a need to assess the ability of materials to resist creep, and creep tests are widely used for this purpose (5.3). Very extensive experimental data have and still are being accumulated in the form of creep curves to assist the engineer.

The impetus to investigate the possibility of using holographic interferometry to obtain creep curves arose when during studies on composite materials in the holographic laboratory it was noticed that the fringe order increased, when using real-time holographic interferometry, over a period of time when the material was left under load. Discounting a

change in fringe order due to environmental instabilities over a long period, it was felt that possibly this change in displacement was due to creep and warranted further investigation.

5.2 THE TRADITIONAL TESTS FOR OBTAINING CREEP CURVES

The design engineer uses two criteria in specifying the life of the high-temperature components. Creep test data are used for conditions where small dimensional changes may seriously impair the efficiency or safe operation of the plant. Stress-rupture data are employed in those cases where dimensional stability is less important but where ultimate failure would constitute a hazard.

In both test methods the specimens are usually tested in tension, but compression and flexure tests are sometimes employed. For the tension creep tests, the specimens are similar in shape to those used in the conventional tensile test and are located by screw threads in heat-resisting adaptors linked to the loading mechanism (5.1) (Fig. 5.1). An extensometer is attached to the specimen and the assembly is enclosed in a furnace which maintains a constant temperature over the entire specimen length. The furnace temperature is controlled within specified limits during the test by a thermostatic control system. The specimen is stressed, usually under constant load, and the resulting plastic strain over the gauge length is measured as a function of time, either to a specified strain or until the specimen fractures. Since creep strain is measured regularly during the long test period, a highly sensitive method of measuring the extension is required. This extension has to be measured by mechanically transferring the relative movement of the ends of the

extensometer to a position outside the furnace, where the displacement is determined by optical, mechanical or electrical techniques. In the stress-rupture test, the time at which the load induces rupture of the specimen and the strain at rupture are noted for fixed temperature and load conditions.

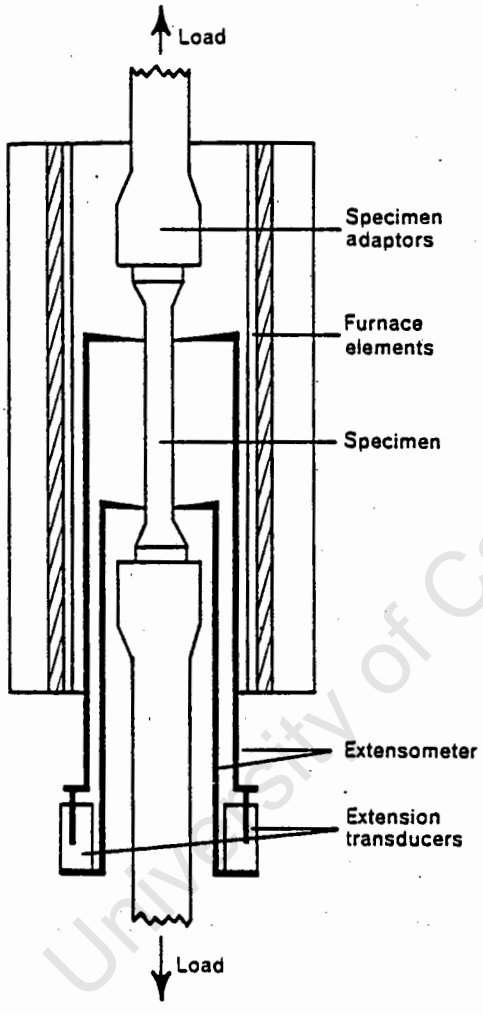

Arrangement of specimen and extensometer for a creep test.

Figure 5.1 (Van Oss, 1970)

A typical set of creep curves, in which the creep strain is plotted as a function of time for specimens tested under different tensile loads, at a fixed temperature, is shown in Figure 5.2.

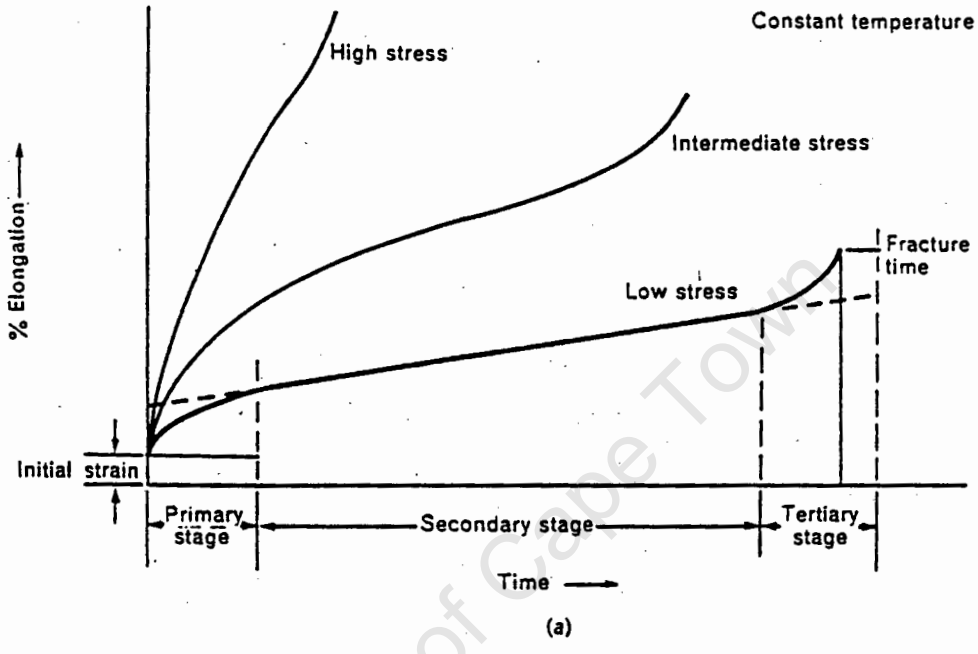

a Creep elongation time curves.

Figure 5.2 (Van Oss, 1970)

The strain is seen to occur in three distinct stages:-

1. The primary stage:-

   The specimen experiences an initial strain on loading, which may be wholly elastic or partly plastic, and then creeps at a decreasing rate.

2. The secondary stage:-

   The creep strain continues at a constant rate and is uniform over the gauge length.

3. The tertiary stage:-

   The creep strain increases with time, due to localized plasticity, until the specimen fractures.

The tensile test at constant temperature remains the dominant test for obtaining creep data, because information obtained from this simple and seemingly artificial state is relatively easy to collect by careful laboratory testing (5.2). Reliable data on the effects of stress variation and multiaxiality and temperature variation are extremely sparse. Clearly if the simple isothermal, constant stress testing is the easiest way of gathering relevant data, then it is desirable that all other effects be related to this test, if it is at all possible.

5.3 EMPIRICAL FORMULAE FOR CREEP CURVES

Since the 1920's numerous investigators have proposed different formulae, some of which are purely empirical while others are based on particular physical considerations, for the experimentally obtained creep curves (5.3).

A tensile specimen under a constant stress will deform with time. This deformation depends on three main parameters, stress, time, and temperature. The most general creep equation is therefore

$$\varepsilon_c = f(\sigma, t, T) \tag{5.1}$$

A useful first approximation is to limit this general function to a commutative law of the form

$$\varepsilon_c = f_1(\sigma) f_2(t) f_3(T) \tag{5.2}$$

The separation of the functions $f_1(\sigma)$ and $f_2(t)$ appears to be generally acceptable for the purpose of calculations on components. Separation of the temperature function $f_3(T)$, is not as easily acceptable as the separation of the stress and time functions. The time and temperature functions are often combined into a single parameter which would not always be consistent with a separate function $f_3(T)$. However, it is possible that an approximation of this kind will be reasonable in may cases, especially when considering a component with thermal gradients (5.2).

5.3.1 THE STRESS FUNCTION

The function $f_1(\sigma)$ has been chosen in many different ways. Some of the most common forms are given below.

Norton (5.4) $$f_1(\sigma) = K\sigma^m \tag{5.3}$$

McVetty (5.5) $$f_1(\sigma) = A \sinh (\sigma/\sigma_o) \tag{5.4}$$

Soderberg (5.6) $$f_1(\sigma) = B \{\exp (\sigma/\sigma_o) - 1\} \tag{5.5}$$

The most commonly used function is the power law attributed to Norton. The reason for its popularity is its simplicity in applications to stress analysis. One of its greatest advantages over the other formulations given is that $f_1(\sigma)$ has the same 'shape' regardless of the magnitude of stress.

This means that under proportional load changes stress distributions are independent of the magnitude of load. On the other hand a hyperbolic sine curve is linear for small stresses and highly non-linear at high stresses.

5.3.2 THE TIME FUNCTION

Many alternative expressions have been suggested for the description of the time dependence of creep under constant stress. Used in the context of their derivation the following time functions can be of practical use

Andrade (5.7)
$$f_2(t) = (1 + bt^{1/3}) \exp(kt) - 1 \cong bt^{1/3} \quad (t \to 0,\ k \to 0) \tag{5.6}$$

Bailey (5.8)
$$f_2(t) = Ft^n \quad (1/3 \leq n \leq 1/2 \text{ usually}) \tag{5.7}$$

McVetty (5.5)
$$f_2(t) = G(1-e^{-qt}) + Ht \tag{5.8}$$

Graham and Walles (5.9)
$$f_2(t) = \sum a_i t^{n_i} \tag{5.9}$$

With regards to the time function Penny states (5.12) 'In practice, the task of describing the time dependence of creep in a complex alloy, displaying a high degree of structural change with high temperature is very difficult, except by extensive curve fitting procedures. At present there is no substitute for the experimentally derived curve. A necessary development must be a rational approach to the basic actions producing the shape of the $f_2(t)$ curve. The function of time must be broken down into parts, each associated with some physical behaviour and these separate parts must then be described if necessary by empirical expressions.'

Equation 5.12 includes the three main parameters that affect creep (viz. stress, time and temperature) in the separable form of equation 5.2. and thus is a useful first approximation to the creep curve.

5.4 HOLOGRAPHIC INTERFEROMETRY APPLIED IN PREVIOUS CREEP STUDIES

Bradford (5.11) investigated the slow recovery that occurs in many natural materials following a disturbance sufficient to stress the material beyond its elastic limit. After the removal of such a stress there is a partial recovery, followed by a much slower recovery of some of the induced strain. Using double-exposure holographic interferometry, experiments were performed using sample pieces of a number of common materials, including wood, compressed fibreboard and metal, which were cut into rectangular shapes (40 x 160 mm) but with thickness dependent on the material. Each specimen was supported horizontally near its ends and loosely restrained against lateral movement. The object field of the holographic arrangement contained two such specimens mounted side by side. They were visible from the recording plane both directly and via an inclined mirror which gave a viewpoint from directly above the specimens. One specimen was disturbed before making the hologram. The other acted as the control.

The experimental procedure followed by Bradford was as follows:- The test sample was disturbed by loading its center for periods from a few seconds to several hours. After the load had been removed, double exposure holograms were made at intervals during the recovery of the material. The two parts of the double exposure were separated by a constant interval of five minutes. Bradford waited fifteen minutes before making the first

exposure. The interference patterns on the reconstructed images thus gave a measure of the rate of change of the samples' dimensions at the time when the double-exposure was made. For example, two hours after unloading, creep was still being detected in the hardboard samples at a rate of about half a fringe per five minutes. Bradford found that the creep recovery effects appeared to follow an exponential decay with a time constant of about half an hour. The analysis used by Bradford is not given in the article.

Bradford's study supported the hypothesis that holographic interferometry could be a useful experimental technique in the study of creep and should be further pursued.

No other studies into creep using holographic interferometry were found in the literature.

5.5 PRELIMINARY TESTS TO OBTAIN CREEP CURVES USING HOLOGRAPHIC INTERFEROMETRY

Conclusions made with regard to the standard test for obtaining creep curves and Bradford's study into the detection of slow changes in materials recovery from a disturbance were:-

1. The standard creep test described in section 5.2, gives rise to in-plane-motion.

   The concept of fringe localization and various schemes proposed to quantify holographic interferometric fringes were presented in

section 2.4. It was shown that out-of-plane motion gives rise to localized fringes which are relatively easier to interpret than fringes due to in-plane-motion. Since the obtaining of creep curves requires the analysis of numerous holograms the creep test should be set up in such a way that would result in out-of-plane motion of the test specimen.

2. Bradford had to wait fifteen minutes before making the first exposure so as to allow the creep recovery to 'slow down'. If he had not waited, conditions of stability required during the exposure of the holographic film would not have been met (i.e. the object surface would have been deforming too "fast"), resulting in blurring of the hologram.

   Using the pulsed ruby laser (the Holocamera) motion of the object surface could be "frozen", allowing for the possibility to investigate the creep behaviour of the test specimen at times closer to the application of the load.

As a consequence of the decision to use the pulsed ruby laser and to load the specimen in an out-of-plane configuration, the following two types of loading situations were investigated in preliminary tests:

1. Four-point bending.

   The advantage of this type of loading is that it results in a constant bending moment over the center portion of the beam.

Appendix XIII lays out a theoretical procedure for the solving of the unknowns in the empirical creep curve formulae using the holographic interferometric fringes resulting from this loading situation. The analysis uses a reference stress creep technique presented by Penny et al (5.12) in "Design for Creep".

The preliminary tests using this loading configuration proved inconclusive, as the fringe count obtained was unreliable due to:-

a. Problems of lack of symmetry caused by loading which resulted in horizontal movement of the beam.

   These problems arose since the loads have to be released from rest at either end of the beam and thereafter the beam has to be free to deflect under the action of these loads, uneffected by any locators which could be used to ensure no horizontal movement of the beam during loading. These problems were not encountered by Bradford since he investigated the creep recovery of materials (i.e. the loads had previously been removed).

b. The appearance of the anticlastic fringe due to the anticlastic curvature of the beam (see Chapter 4 on Poisson's ratio).

   This fringe was not taken into account in the theoretical approach where only vertical fringes are predicted. The anticlastic fringe was usually broad and therefore the number of 'lost' fringes were significant.

It is not clear how Bradford accounted for this fringe in his study, if indeed he did, as it is not mentioned in his article. As no pictures are available of his holograms it is not possible to determine if they arose in his creep recovery study. Possibly the effect of deflection is far greater than the effect of anticlastic behaviour over the five minute period between the two exposures used by Bradford, and therefore the effect of the anticlastic fringe is minimized.

2. A cantilever type loading configuration as shown in Figure 5.3.

Although this loading does not result in constant stress along the beam, it is relatively easy to set up a beam in a cantilever type situation. The load mechanism was arranged so as to effectively apply the force at the end of the cantilever, normal to the surface, by means of a nylon string with a small pan at the end. The nylon string was passed over a pulley so that the mass used to apply the force could be placed onto the small pan (Fig. 5.3).

From preliminary tests using this loading configuration the following was gleaned:

a. Tens of fringes as a result of creep were observed for even relatively small loads (0.5-1.5 Kg). Using loads above this the fringe pattern became too dense and thus the counting of the fringes inaccurate.

b. By using the pulsed ruby laser it was possible to capture the

Figure 5.3 Cantilever

fringe formation closer to the initiation of the creep than Bradford had been able to using the continuous wave laser. Tests indicated that double-exposure holograms with clearly defined fringes (i.e. the motion of the beam had effectively been "frozen" for the duration of the exposure) could be obtained one minute after loading of the cantilever, as compared to the fifteen minutes required by Bradford after unloading his beam.

c. It was possible to place the experiment on a table which did not have any elaborate vibration isolation. Making the exposures fifteen seconds apart with an exposure time of 20 nanoseconds, clear holograms with no rigid body motion on the rig (i.e. the fringes where localized onto the cantilever) were obtained. Fifteen seconds is the minimum time possible for the pulsed ruby laser to fire and recharge when not in internal double pulse mode. In that mode the maximum separation between pulses is 800 μsec which proved to be too fast for this purpose.

Following the preliminary tests it was decided to proceed using pulsed double-exposure holographic interferometry with the test specimen configured in a cantilever type situation. The cantilever was made from lead with dimensions of 147 mm (length) x 30 mm (width) x 6 mm (depth). The decision to use lead took the following into account:

1. Lead has a melting point of 327°C (5.1) and exhibits creep even at room temperature. This is ideal for an investigation using holographic interferometry were it is desirable to conduct studies at ambient conditions to reduce fringe formation from thermal expansions

or the thermal gradients in the specimen.

2. Lead creeps relatively quickly. This allows for the gathering of creep data over a short period of time.
3. Studies were being conducted on the same stock of lead in a tensile test situation elsewhere in the department. Although a creep test using a cantilever with an end load is not a constant creep test, this tensile test data could be a useful measure against which to compare data obtained from the cantilever creep test.

5.6 EXPERIMENTAL PROCEDURE FOLLOWED

The final experimental protocol used was as follows:-

1. The lead beam was clamped in the cantilever rig.
2. The rig was positioned in front of the Holocamera with the θ and γ angles of equation 2.3 set equal to zero.
3. The cantilever was loaded.
4. A minute after loading the first hologram was taken, followed fifteen seconds later by the second exposure.
5. At specific intervals (Appendix XIV) double exposure holograms were made with fifteen seconds delay between the exposures.
6. The making of the double-exposure holograms continued until only two or three fringes were observed in the reconstructed holograms of the cantilever beam. The strain rate was then assumed to have decreased such that the upper range of the primary stage had been reached.
7. The holograms were reconstructed and the fringes counted. A detailed description of the analysis of the fringes is given in the results section that follows.

5.7 RESULTS.

Creep tests were performed on lead beams with dimensions of 147 mm (length) x 30 mm (width) x 6 mm (depth) with loads of 1.5 Kg,1 Kg and 0.5 Kg at ambient conditions.

Figure 5.4 shows a typical double-exposure fringe pattern of a cantilever exhibiting creep behaviour.

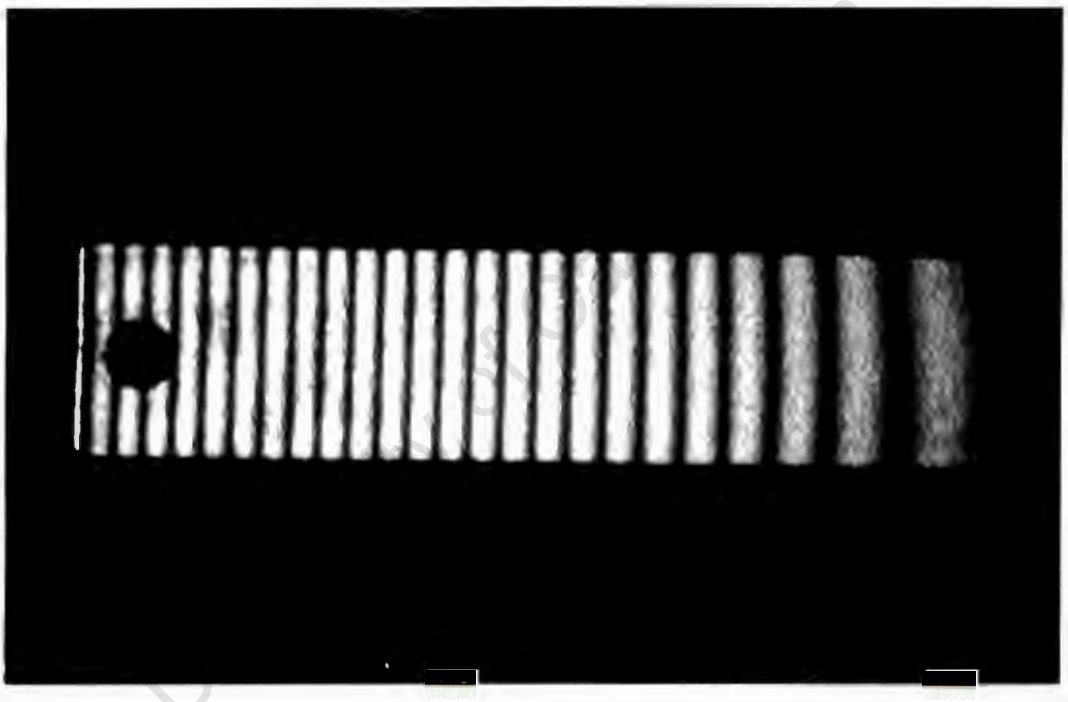

Figure 5.4 Typical double-exposure hologram of a lead cantilever beam displaying creep behaviour.

The times of making the holograms, the fringe order as well as the instantaneous rate of change of fringes associated with each time are given in Appendix XIV. Figures 5.5 and 5.6 are graphs of instantaneous rate of change of fringes versus time on a normal and log scale respectively.

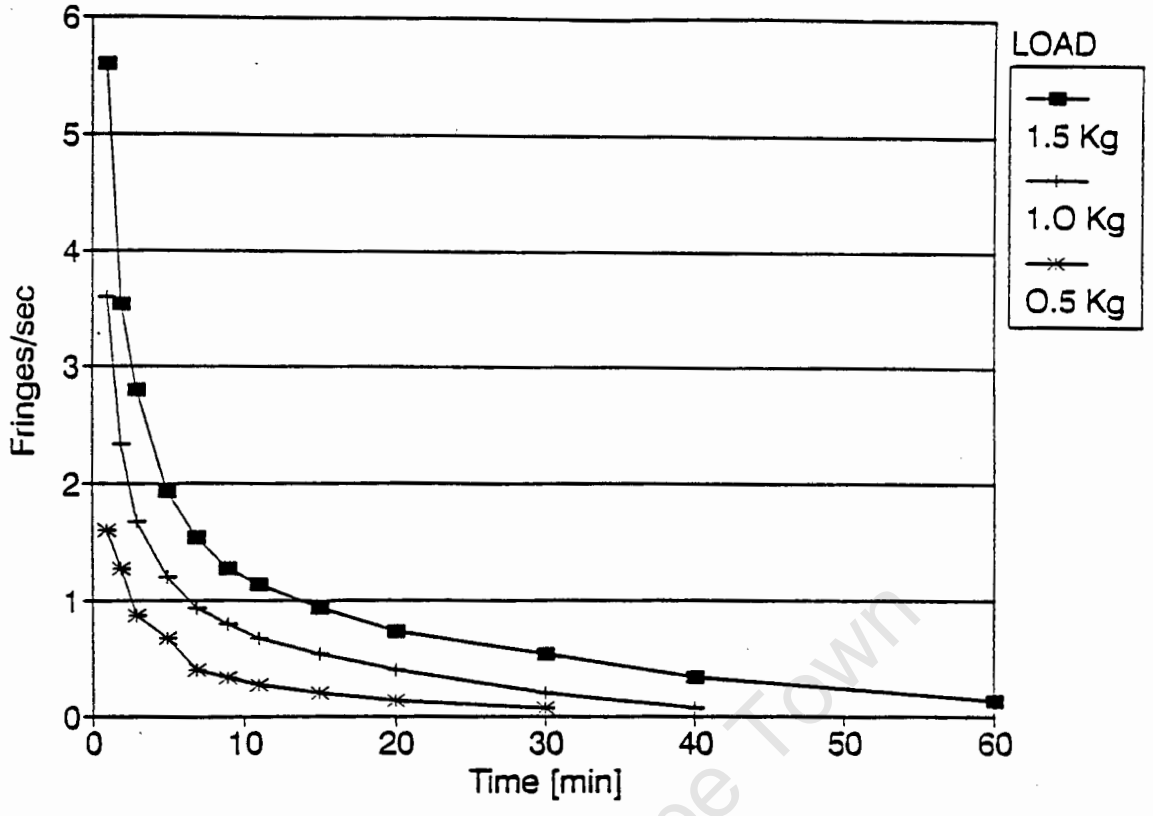

Figure 5.5 Instantaneous rate of change of fringes versus time

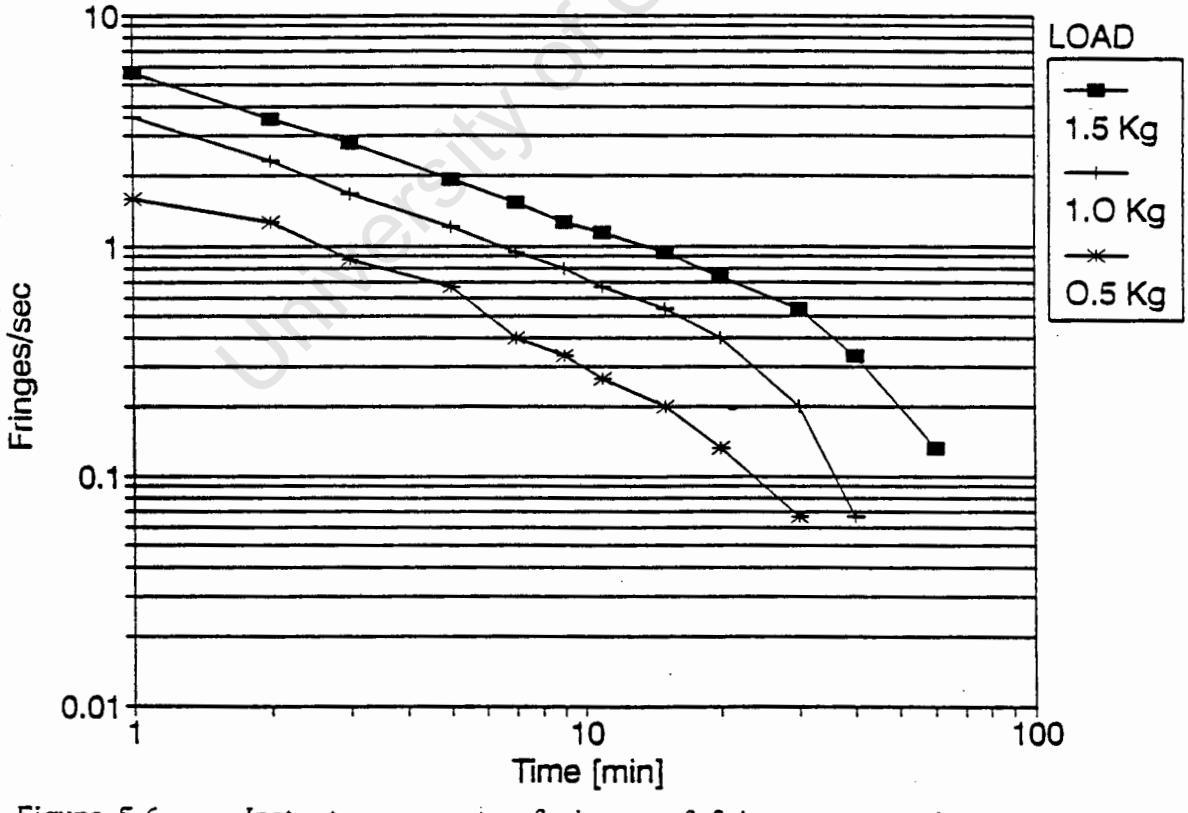

Figure 5.6 Instantaneous rate of change of fringes versus time

From Appendix XIV it may be seen that the intervals increase between the times at which the double-exposure holograms were made. Since the rate of fringe formation was rapid at the beginning, it was crucial to record as much of it as possible. This need was reduced as the rate decreased, evidenced by the lessening number of fringes observed between subsequent double-exposure holograms.

5.8 ANALYSIS AND DISCUSSION OF RESULTS

The straight line obtained when plotting the rate of change of fringes versus time on a log-log scale (Fig. 5.6) is consistent with that which is obtained when a power law function is plotted on a log-log scale. This was encouraging since as may be recalled, Bailey (5.8) (eq. 5.7) proposed a time function of the power kind.

A numerical integration type procedure was performed. The instantaneous rate of change of fringes obtained at a test time and that obtained at the next test time were averaged. This average instantaneous rate of change of fringes multiplied by the time between the test times gave the total number of fringes that would have been counted had the separation between the two exposures been equal to this time. The accumulated fringe total at each test time was then calculated. The values obtained are shown in Appendix XV.

A best-fit power law function was fitted to the accumulated fringe total versus time values shown in Appendix XIV using a curve fitting program available for the HP-28s calculator. As zero is an invalid value for a power law function, values were only entered from the first non-zero value

in Appendix XIV. The functions obtained are shown in Table 5.1.

Table 5.1 Best-fit time functions for creep of lead cantilever beam.

LOAD [Kg]	POWER LAW	CORRELATION
0.5	$72t^{0.664}$	0.93
1.0	$147t^{0.652}$	0.95
1.5	$238t^{0.645}$	0.95

The correlation between the experimental results and the best-fit power functions was good. The range of the index from 0.645-0.664 compares favourably with the average value obtained in the laboratory under tensile load conditions of 0.66 (5.13).

The exponents of the power law functions decrease with an increase in load, whilst the amplitude constants increase with increased load. Thus the power law functions indicate that the higher the load, the greater was the creep deformation prior to the secondary stage of creep being reached. In addition, since the time constant (τ) which is the inverse of the exponent, increases with increased load, the higher the load the longer it took to reach the secondary stage of creep. This is consistent with the typical creep curves of Figure 5.2 obtained using the standard creep test. The best-fit curves are shown in Figure 5.7.

It was not possible to relate the amplitude constant to the stress function

component of the separable creep function proposed as a first approximation to the creep curve (eq. 5.2), since this was not a constant stress test.

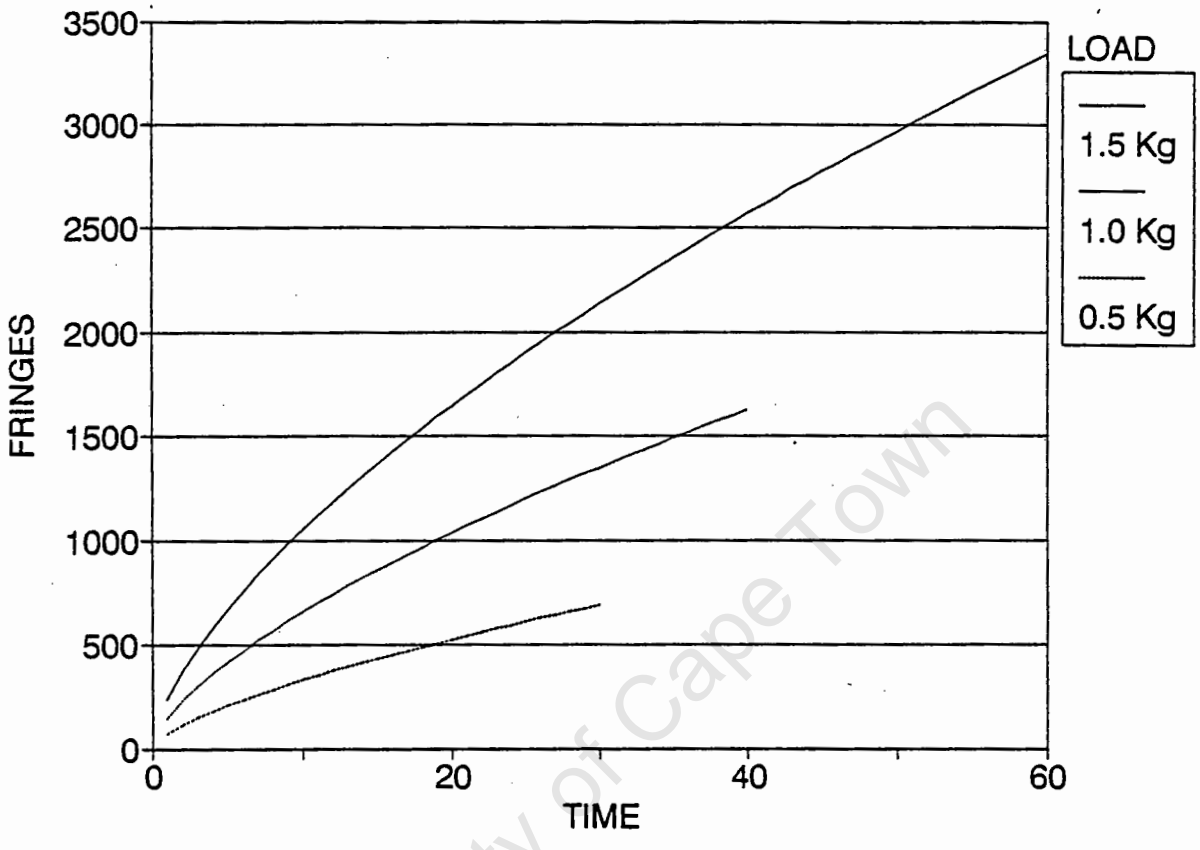

Figure 5.7 Best-fit time function curves for creep of lead cantilever beam.

5.9 CONCLUSIONS

Based on the study into the feasibility of using holographic interferometry as an experimental technique in creep studies, the following conclusions

were made:-

1. A creep study using holographic interferometry was undertaken for the first time with encouraging results.
2. It was possible to determine the exponent of the time function during the primary creep stages. The experimentally determined exponent of 0.64-0.665 compares favourably with the average tensile determined value of 0.66.
3. Short-time data have been used to obtain information usually determined only after many hours of testing.
4. Using pulsed ruby holographic interferometry, it was possible to get closer to the time of loading than would have been possible if continuous wave lasers had been used.
5. It was shown that for the purpose of holographically determining the time function during the primary stage of creep, a cantilever type set-up may be used. This type of set-up was easier to construct and load than that required in a four-point load test.
6. This experimental procedure does not allow for the determination of the constants of the stress function.

RECOMMENDATIONS

This investigation has provided further experimental evidence of the applicability of holographic interferometry as a non-intrusive means to investigate mechanical properties and behaviour of materials.

It was shown that with a holographic laboratory equipped with both a continuous wave and pulsed laser and associated optical equipment a diverse range of material properties and behaviours could be investigated.

With reference to the specific properties or behaviour of materials investigated, the following recommendations are made:-

1) Elastic Modulus

Although the error analysis indicated that the effect of the blurring of the leading fringe was not significant, further research is required to investigate possible techniques to reduce this occurrence and thereby obtain sharper holograms. The holographic interferometric determination of the Elastic Modulus for specimen geometries other than long solid rods could also be investigated.

2) Poisson's ratio

Geometrical aspects of the material being investigated affect the feasibility of using holographic interferometry to investigate this property. Further testing of materials is required so as to determine bounds on these geometrical constraints for a given material.

3) Modulus of Rigidity

The holographic interferometric technique used to determine this material property required the attachment of a transducer to the test specimen. Additional methods should be investigated to obtain this material property which do not require such an attachment. One such method could use the relationship between the Modulus of Rigidity and the transverse velocity of a shock wave in a material.

4) Creep

Pulsed laser holographic interferometry can play a valuable role in creep studies and further research should be undertaken in this regard. Aspects that could be investigated may include the determination of the stress function constants and obtaining creep curves for different temperatures. The extension of the experimental procedure to the secondary and tertiary stages of creep may also be investigated.

LIST OF REFERENCES

2.1 Gabor, D, 'A New Microscopic Principle,' *Nature*, 161 (1948), 771.

2.2 Gabor, D, 'Microscopy by Reconstructed Wavefronts,' *Proceedings of the Royal Society of London*, A197 (1949), 454.

2.3 Leith, E N and Upatnieks, J, 'Reconstructed Wavefronts and Communication Theory,' *Journal of the Optical Society of America*, 52 (1962), 1123-1130.

2.4. Leith, E N and Upatnieks, J, 'Wavefront Reconstruction with Continuous-tone Objects,' *Journal of the Optical Society of America*, 53 (1963), 1377-1381.

2.5 Leith, E N and Upatnieks, J , 'Wavefront Reconstruction with Diffused Illumination and Three-dimensional Objects,' *Journal of the Optical Society of America*, 54 (1964), 1295-1301.

2.6 Denisyuk, Y N, 'On the Reproduction of the Optical Properties of an Object by Wavefield of its Scattered Radiation,' *Optics and Spectroscopy*,'15 (1963), 297-284.

2.7 Walters, J P, 'Holography,' in Holographic Nondestructive Testing, ed. R K Erf, New York :Academic Press, 1974, 5-58.

2.8. Smith H M, Principles of Holography, New York: John Wiley & Sons, 1969, 118.

2.9 Pitlak, R T and Page, R, 'Pulsed Lasers for Holographic Interferometry,' *Optical Engineering*, 24(4) (1985), 639-644.

2.10 Gagosz, R M, 'Pulsed Holography,' in Holographic Nondestructive Testing, ed. R K Erf, New York :Academic Press, 1974, 62-84.

2.11 Stetson, K and Powell, R, 'Interferometric Vibration Analysis by Wavefront Reconstruction,' *Journal of the Optical Society of America*, 55 (1965), 1593-1598.

2.12 Haines, K A and Hildebrand, B P, 'Surface-deformation Measurement using the Wavefront Reconstruction Technique,' *Applied Optics*, 5 (1966), 595-602.

2.13 Briers, J D,'Review: The Interpretation of Holographic Interferograms,' *Optical and Quantum Electronics*, 8 (1976), 469-501.

2.14 Aleksandrov and Bonch-Bruevich, 'Investigation of Surface Strains by the Hologram Technique', *Soviet Physics: Technical Physics*, 12, (1967), 258 -265.

2.15 Ennos, 'Measurement of In-plane Surface Strains by Hologram Interferometry', *Journal of Physics E*, (1968), 731-734.

2.16 Walters, J P, 'Interferometric Holography,' in Holographic Nondestructive Testing, ed. R K Erf, New York :Academic Press, 1974, 87-103.

2.17 Pryputniewicz, R J, 'Time-Average Holography in Vibration Analysis,' *Optical Engineering*, 24(5) (1985), 843-848.

2.18 Gryzagoridis, J,Findeis, D and Pearce, H T, 'Pulsed Ruby Holography in Vibration Studies,' *R & D Journal*, 7(1) (1991), 32-34.

3.1 Standard Test Method for Young's Modulus, Tangent Modulus, and Chord Modulus - ASTM E 111-82

3.2 Wolfenden, A, Harmouche, M R, Blessing, G V, Chen, Y T, Terranova, P, Dayal, V, Kinra, V K, Lemmens, J W, Phillips, R R, Smith, J S, Mahmoodi, P and Wann, R J, 'Dynamic Young's Modulus Measurements in Metallic Materials: Results of an Interlaboratory Testing Program,' *Journal of Testing and Evaluation*, 17(1) (1989), 2-13.

3.3 Shigley J E, Mechanical Engineering Design, 1st metric ed., New york:McGraw-Hill Book Company, 1986, 36-65.

3.4 Kolsky H, Stress Waves in Solids, New York:Dover Publications, 1963, 41-43.

3.5 Rosinger, H E and Ritchie, I G, 'A Critical Assessment of theCantilever Beam Method for the Determination of Dynamic Young's Modulus,' *Journal of Testing and Evaluation*, 2(3) (1974), 131-138.

3.6 Kinra, V K and Dayal, V, 'A New Technique for Ultrasonic NDE of Thin Specimens,' *Experimental Mechanics*, 28(9) (1988), 288-297.

3.7 Aprahamian, R, Evensen, D A, Mixson, J S and Wright, J E, 'Application of Pulsed Holographic Interferometry to the Measurement of Propagating Transverse Waves in Beams,' *Experimental Mechanics*, 11(7) (1971), 309-314.

3.8 Aprahamian, R, Evensen, D A, Mixson, J S and Jacoby J L, 'Holographic Study of Propagating Transverse Waves in Plates,' *Experimental Mechanics*, 11(8) (1971), 357-362.

3.9 Holloway, D C and Fourney, W L, 'An Investigation of Ground Motions from Blasting through the use of Holographic Interferometry. ' in *Proceedings 18th U.S Symposium on Rock Mechanics* (Keystone, Colorado, June 1977).

3.10 Holloway, D C , Fourney, W L and Patacca, A M, 'Application of Holographic Interferometry to a Study of Wave Propagation in Rock,' *Experimental Mechanics*, 17(8) (1977), 281-289.

3.11 Birch, F, 'Velocity of Compressional Waves in Rock to 10 Bars,' *Journal of Geophysical Research*, 65(4), Part I, (1960), 1083-1102.

3.12 Carlsson, T E, Bjarnholt, G, Abramson, N and Holloway, D C, 'Holographic Interferometry Applied to a Study of Ground Vibrations Produced from Blasting,' *Optical Engineering*, 27(11) (1988), 923-927.

3.13 Gagosz, R M, 'Pulsed Holography,' in Holographic Nondestructive Testing, ed. R K Erf, New York :Academic Press, 1974, 62-84.

3.14 Holocamera - Manufactures Manual

3.15 Kinsler, L E and Frey,A R, Fundamentals of Acoustics, 2nd ed., New York: John Wiley & Son, 1950

3.16 Shigley J E, Mechanical Engineering Design, 1st metric ed., New York:McGraw-Hill Book Company, 1986, 647.

4.1 Standard Test Method for Poisson's Ratio at Room Temperature - ASTM E 132 - 86

4.2 Cornu, A, *C. R. Acad. Sci.*, 69 (1969), 333.

4.3 Timoshenko, S and Goodier, J N, Theory of Elasticity, 2nd ed., New York: McGraw-Hill Book Company, 1951, 250.

4.4 Sokolnikoff, I S, Mathematical Theory of Elasticity, 2nd ed., New York: McGraw-Hill Book Company, 1956, 102.

4.5 Ashwell, D G, 'The Anticlastic Curvature of Rectangular Beams and Plates,' *Journal of the Royal Aeronautical Society*, 54 (1950), 708-715.

4.6 Yamaguchi, I and Saito, H, 'Application of Holographic Interferometry to the Measurement of Poisson's ratio,' *Japanese Journal of Applied Physics*, 8(6) (1969), 768-771.

4.7 Jones, R and Bijl, D, 'A Holographic Interferometric study of the End

Effects associated with the Four-point Bending Technique for Measuring Poisson's ratio,' *Journal of Physics E*,(1974), 357-358.

4.8 Case, J, Strength of Materials, Arnold, 3rd ed., 1938, 546-554.

5.1 Van Oss, J F, Materials and Technology, London:Longman Group, Volume III, 1970, 56-58.

5.2 Penny, R K and Marriott, D L, Design for Creep, London:Mcgraw-Hill Book Company, 1971, 1-11.

5.3 Rabotnov, Y N, Creep Problems in Structural Members, Amsterdam, North-Holland Publishing Company, 1969, 176-180.

5.4 Norton, F H, The Creep of Steels at High Temperatures, McGraw-Hill, 1929

5.5 McVetty, P G, 'Creep of Metals at Elevated Temperatures-the Hyperbolic sine Relation between Stress and Strain Rate', *Transactions of American Society of Mechanical Engineers*, 65, 1943

5.6 Soderberg, C R, 'The Interpretation of Creep Tests for Machine Design', *Transactions of American Society of Mechanical Engineers*, 58, 1936

5.7 Andrade, E N da C, 'The Viscous Flow in Metals and Allied Phenomena', *Proceedings of Royal Society*, 84, 1910

5.8 Bailey, R W, 'The Utilization of Creep Test Data in Engineering Design', *Proceedings of Royal Institute of Mechanical Engineers*, 131, 1935

5.9 Graham, A and Walles, K F A, 'Relations between Long and Short Time Properties of a Commercial Alloy', *Journal of Iron and Steel Institute*, 179, 1955

5.10 Dorn, J E, 'Some Fundamental Experiments on High Temperature Creep', *Journal of Mechanical Physical Solids*, 3, 1955

5.11 Bradford, W R, 'Holographic measuring techniques,' in Engineering uses of holography, *Proceedings of Symposium Strathclyde* ,1968, eds. E R Robertson and J M Harvey, Cambridge University Press, 1970, 57-70.

5.12 Penny, R K and Marriott, D L, Design for Creep, London:Mcgraw-Hill Book Company, 1971, 122-133.

5.13 Lawrie, P R, 'Creep of Component using Model Material', unpublished, University of Cape Town, 1990

COMPONENT LAYOUT FOR HLS-2 HOLOCAMERA

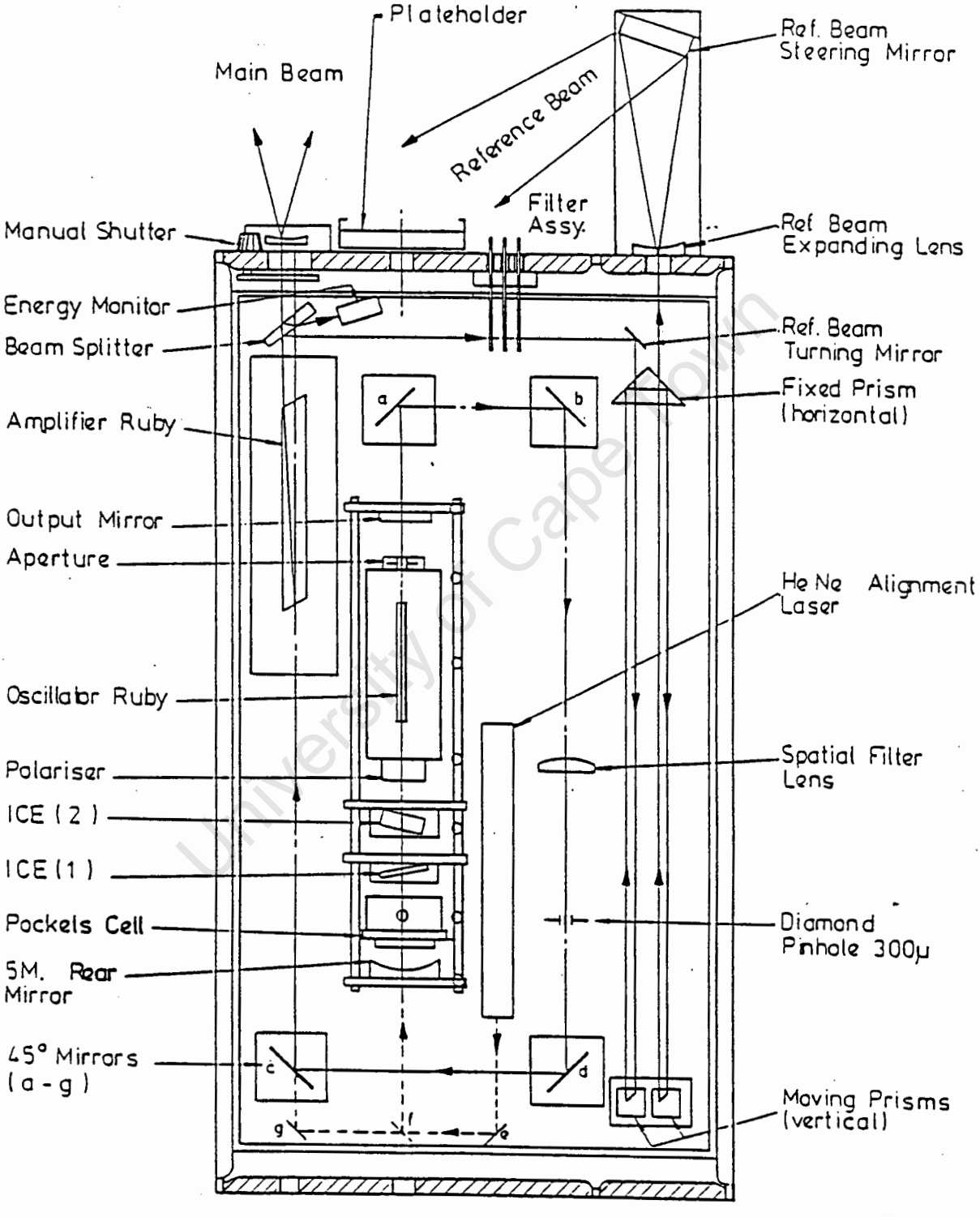

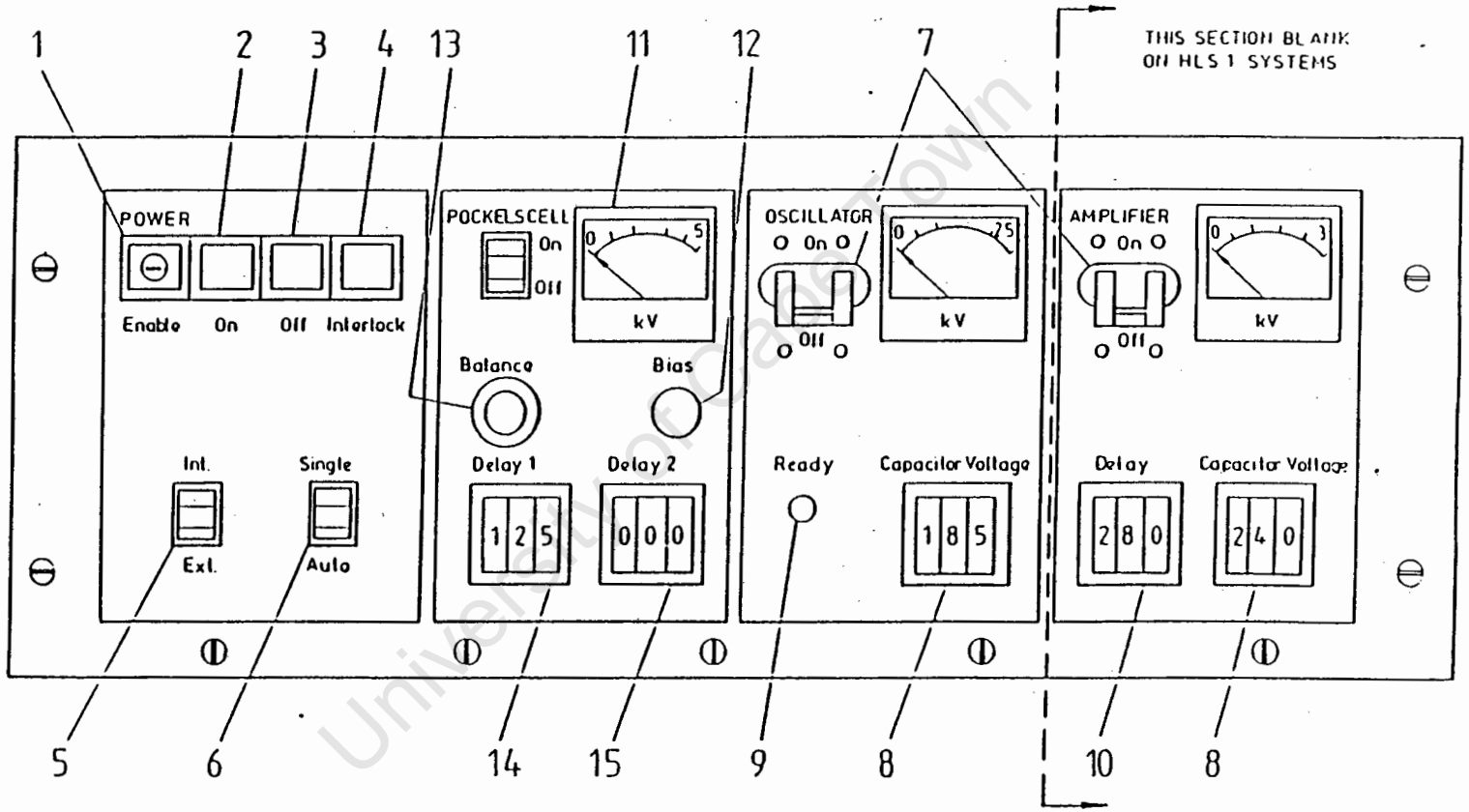

THE H.L.S. POWER SUPPLY CONTROL UNIT

APPENDIX III

CONTROL UNIT SETTINGS

Pulse Interval uS	DELAY 1	DELAY 2	OSC CAPACITOR VOLTAGE KV	AMP DELAY	AMP CAPACITOR VOLTAGE KV	BALANCE
Single Pulse	125	000	165	200	280	max
1	110	001	175	200	275	*1.9
10	110	010	175	200	275	*1.9
100	105	100	165	200	265	*3.2
200	097	200	165	200	270	*5.0
400	*093	400	165	160	270	max
600	*087	600	175	210	280	max
800	*082	800	185	240	290	max

* Adjust these settings to maintain equal double pulses

APPENDIX IV

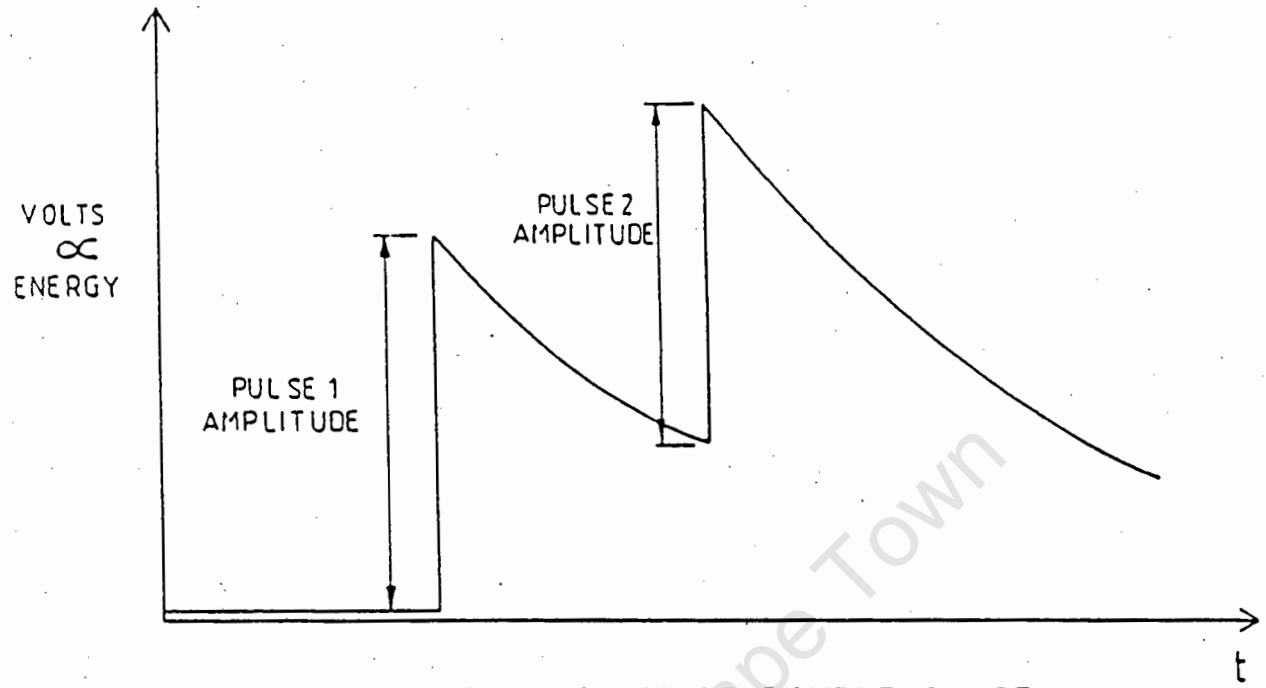

C.R.O. DISPLAY OF DOUBLE PULSE LASER OUTPUT

APPENDIX V

LASER FIRING CONTROL CIRCUIT

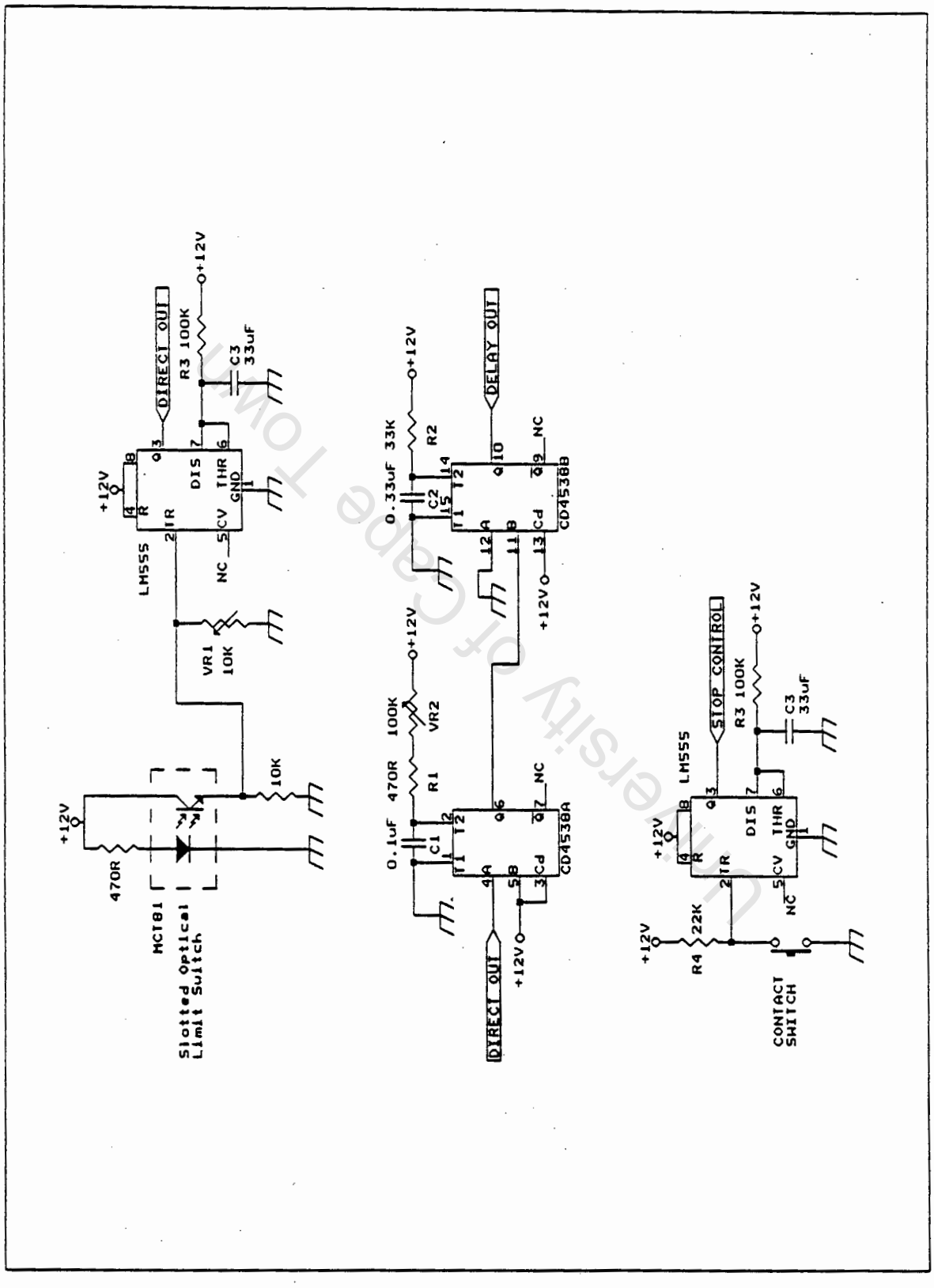

Typical Critical Swing Times (milliseconds)				
Optical Device	Optical Limit Switch		Photocell	
Pendulum with	Knife-Egde	Roller-Bearing	Knife-Egde	Roller-Bearing
1	4.6552	3.8715	4.2913	3.5240
2	4.6481	3.8613	4.2650	3.5382
3	4.6479	3.8810	4.3215	3.5452
4	4.6510	3.8249	4.2876	3.5447
5	4.6541	3.9217	4.2692	3.5158
6	4.6522	3.8626	4.2710	3.5454
7	4.6547	3.8676	4.1453	3.5537
8	4.6495	3.8753	4.3217	3.5651
9	4.6543	3.8568	4.3414	3.5217
10	4.6621	3.8627	4.2846	3.8508
11	4.6552	3.8682	4.2662	3.5962
12	4.6571	3.8295	4.2387	3.6043
13	4.6585	3.9135	4.2836	3.5905
14	4.6557	3.8312	4.2788	3.6084
15	4.6555	3.8867	4.3243	3.5967
16	4.6559	3.8251	4.3670	3.5897
17	4.6558	3.8492	4.2770	3.5724
18	4.6614	3.8641	4.2813	3.5851
19	4.6644	3.8772	4.2552	3.5777
20	4.6591	3.8578	4.2687	3.5547

APPENDIX VII

Elastic Modulus (Holographic Interferometry)						
Material	Time (sec)	Density (kg/m ^ 3)	Measured Distance (m)	Corrected Distance (m)	Velocity (m/s)	Elastic Modulus (GPa)
Steel	50 100	7866 7866	0.26 0.515	0.265 0.523	5307 5230	221.6 215.2
Brass	50 100	8494 8494	0.16 0.335	0.175 0.354	3300 3540	92.5 106.4

APPENDIX VIII

Elastic Modulus (Ultrasonics)							
Material	Density (kg/m ^ 3)	Longitudinal Measured (m/s)	Velocity Standard (m/s)	Transverse Measured (m/s)	Velocity Standard (m/s)	Elastic Measured (GPa)	Modulus Standard (GPa)
Steel	7866	6150	6100	3105	3100	201.5	200.6
Brass	8494	5170	4700	N/A	2110	105.8	104

Poisson's Ratio determined using Time-Average Holographic Interferometry

1 mm Thick Steel Beam			1.5 mm Thick Steel Beam			2 mm Thick Steel Beam		
Width [mm]	Angle [Degrees]	Poisson's Ratio	Width [mm]	Angle [Degrees]	Poisson's Ratio	Width [mm]	Angle [Degrees]	Poisson's Ratio
4.5	31.00	0.3610	6.75	23.50	0.1891	9	25.50	0.2275
4.5	29.50	0.3201	6.75	24.00	0.1982	9	24.00	0.1982
4.5	29.25	0.3136	6.75	27.50	0.2710	9	23.00	0.1802
4.5	31.00	0.3610	6.75	26.00	0.2379	9	23.50	0.1891
4.5	30.00	0.3333	6.75	24.50	0.2077	9	23.25	0.1846
4.5	28.50	0.2948	6.75	27.50	0.2710	9	25.00	0.2174
5.5	30.25	0.3401	8.25	25.50	0.2275	11	22.50	0.1716
5.5	29.00	0.3073	8.25	24.00	0.1982	11	24.00	0.1982
5.5	27.00	0.2596	8.25	23.00	0.1802	11	23.50	0.1891
5.5	27.00	0.2596	8.25	24.50	0.2077	11	24.00	0.1982
5.5	30.00	0.3333	8.25	26.00	0.2379	11	23.00	0.1802
5.5	28.50	0.2948	8.25	26.50	0.2486	11	23.00	0.1802
6.5	28.50	0.2948	9.75	24.50	0.2077	13	22.50	0.1716
6.5	28.50	0.2948	9.75	23.50	0.1891	13	24.00	0.1982
6.5	28.50	0.2948	9.75	25.00	0.2174	13	22.25	0.1674
6.5	29.00	0.3073	9.75	23.00	0.1802	13	23.50	0.1891
6.5	27.50	0.2710	9.75	23.50	0.1891	13	22.75	0.1758
6.5	28.50	0.2948	9.75	23.00	0.1802	13	24.00	0.1982
7.5	28.00	0.2827	11.25	24.00	0.1982			
7.5	29.25	0.3136	11.25	23.75	0.1936			
7.5	29.50	0.3201	11.25	23.50	0.1891			
7.5	28.75	0.3010	11.25	25.00	0.2174			
7.5	27.50	0.2710	11.25	23.50	0.1891			
7.5	27.75	0.2768	11.25	23.00	0.1802			
8.5	28.50	0.2948	12.75	23.00	0.1802			
8.5	29.00	0.3073	12.75	22.50	0.1716			
8.5	27.75	0.2768	12.75	24.00	0.1982			
8.5	30.00	0.3333	12.75	22.50	0.1716			
8.5	27.50	0.2710	12.75	22.50	0.1716			
8.5	27.50	0.2710	12.75	24.50	0.2077			

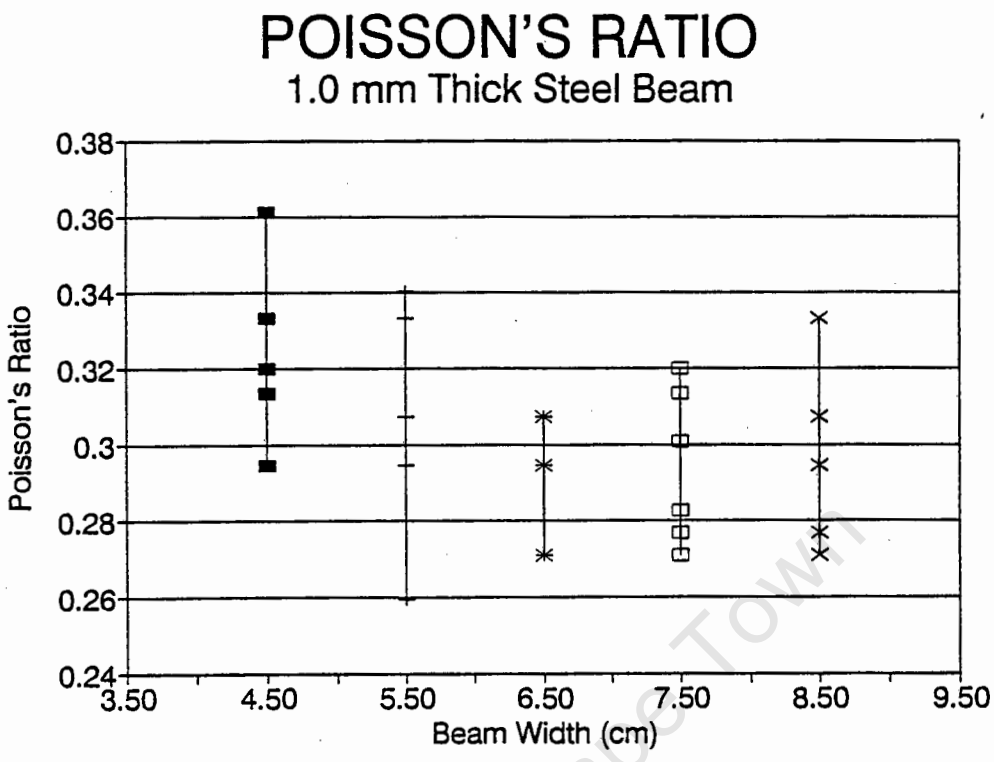

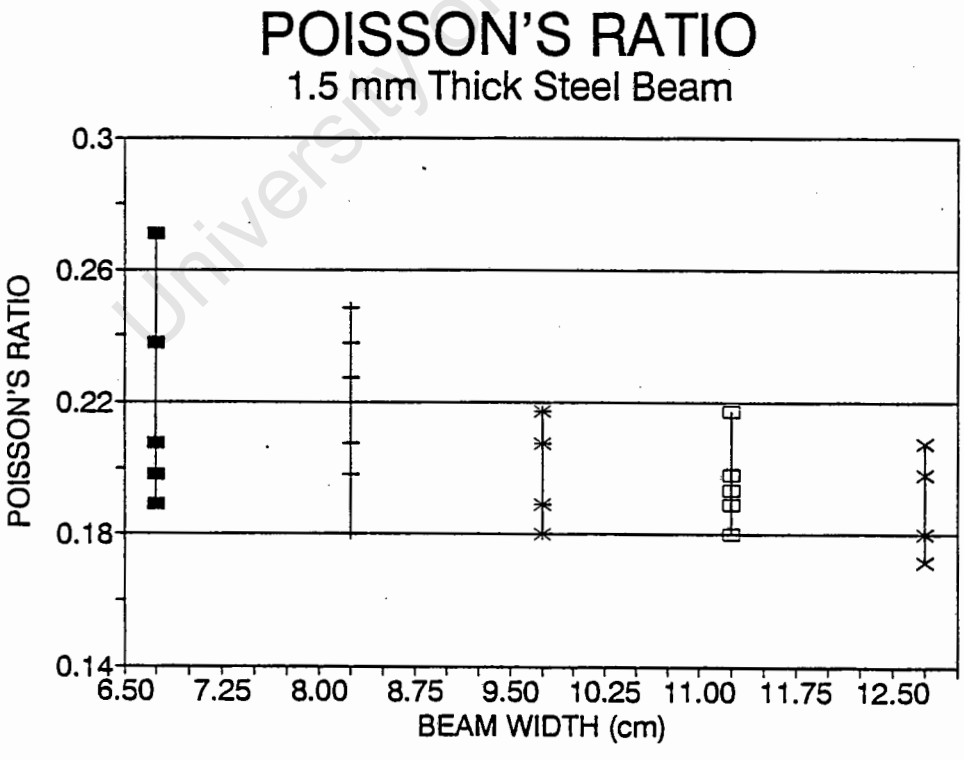

POISSON'S RATIO

2.0 mm Thick Steel Beam

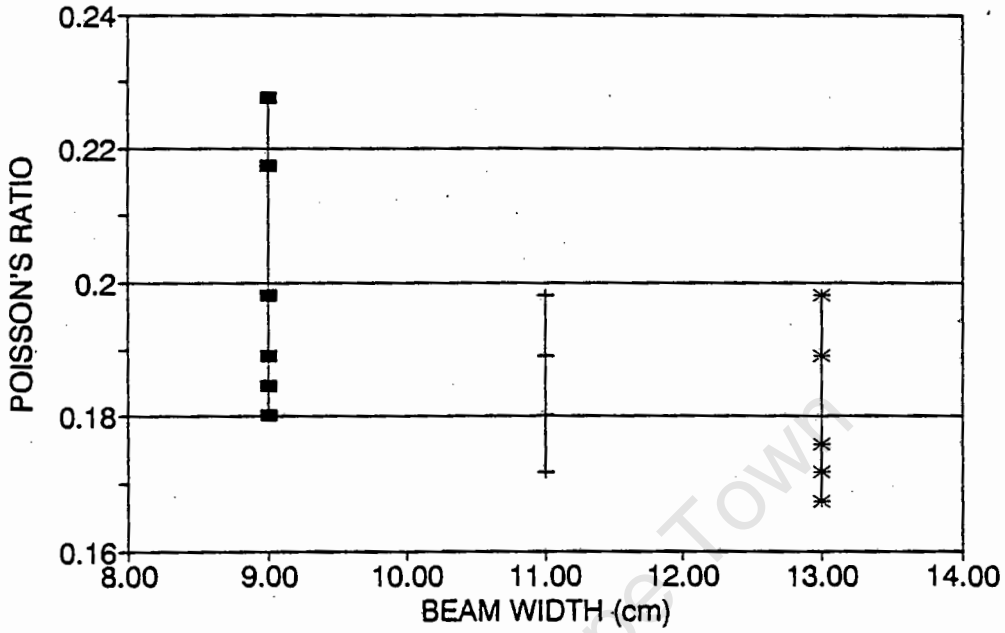

APPENDIX XI

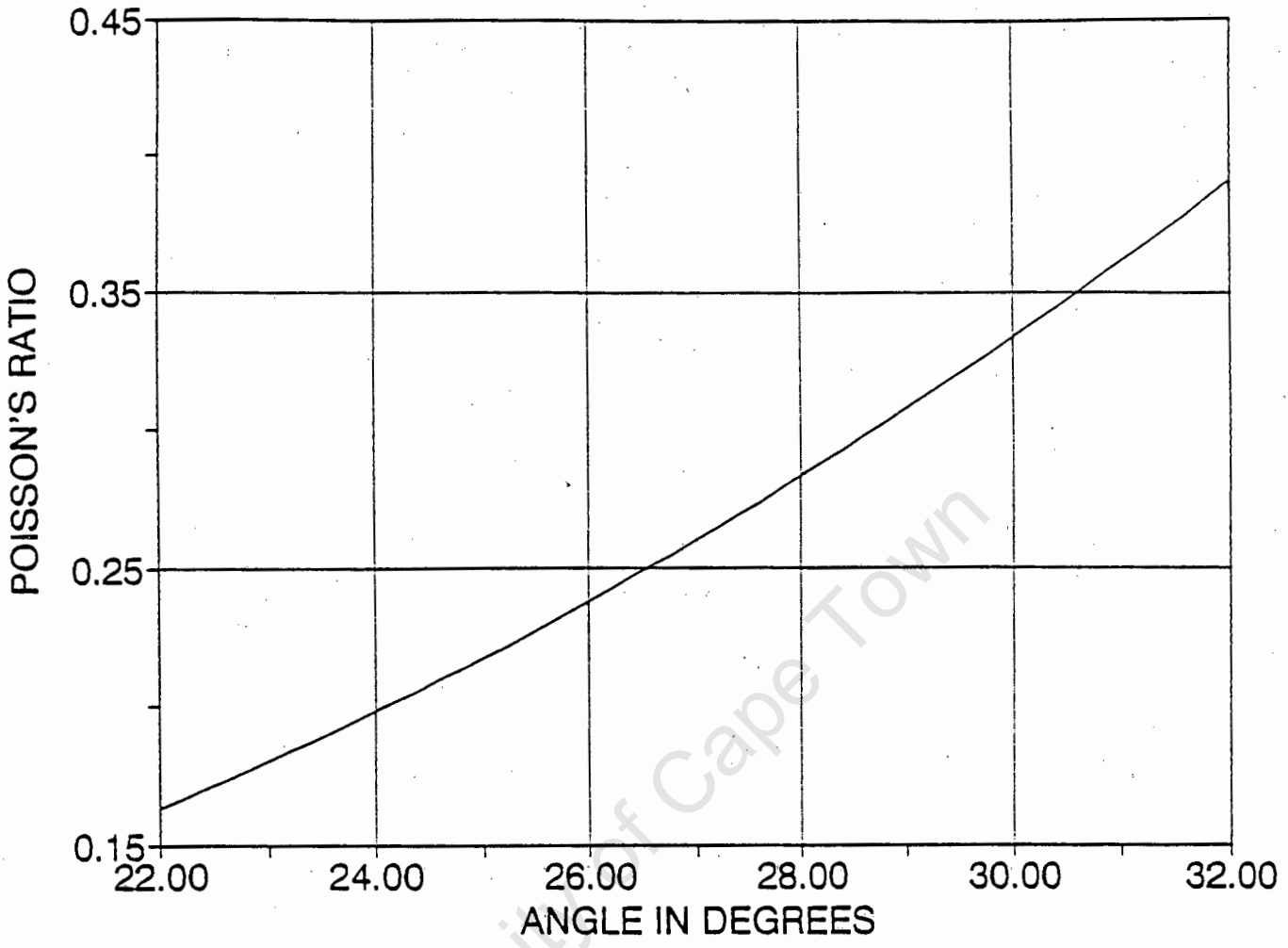

MODULUS OF RIGIDITY VS LOAD

BRASS

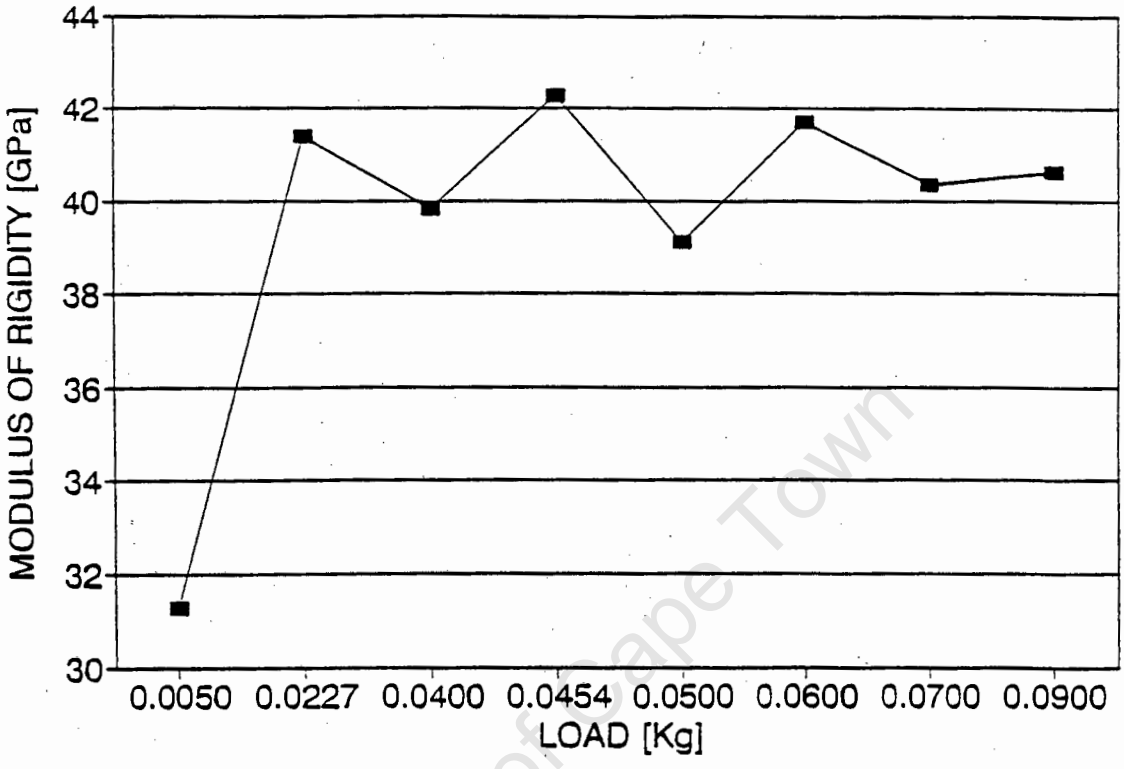

APPENDIX XIII

The reference stress method applied to the creep of a beam under four-point loading.

Cross section of beam

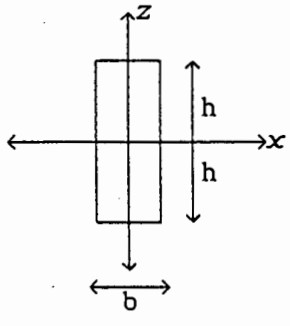

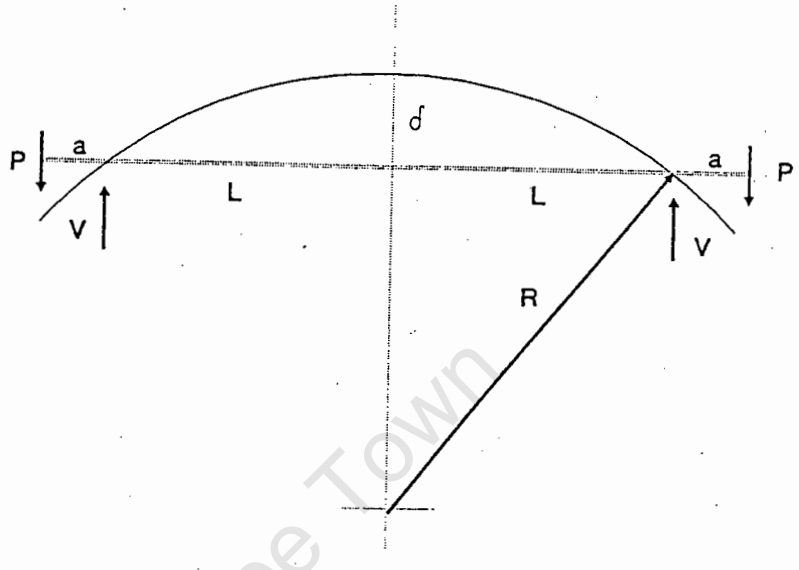

The constant bending moment M between the supports (V) is equal to Pa.

From the geometry of the four-point loading

$$L^2 = 2\delta R \qquad \text{(i)}$$

Therefore

$$\delta = \frac{L^2}{2R} \qquad \text{(ii)}$$

The rate of curvature is

$$\dot{K} = \frac{\dot{\varepsilon}_{ref}}{z} \qquad \text{(iii)}$$

where $\dot{\varepsilon}_{ref}$ is the reference strain rate given by

$$\dot{\varepsilon}_{ref} = (M/bh^2)^m \, f(t) \qquad \text{(iv)}$$

Since $K = 1/R$ equation (ii) may be written

$$\dot{\delta} = \frac{L^2 \dot{K}}{2} \qquad (v)$$

Substituting equation (iii) into equation (v) and noting that for the reference stress, $z = \frac{2}{3}h$

$$\dot{\delta} = \frac{L}{2}^2 * \frac{3}{2h} * \dot{\varepsilon}_{ref} \qquad (vi)$$

Which by substituting equation (iv) into equation (vi) gives

$$\dot{\delta} = \frac{3L^2}{4h} (M/bd^2)^m f(t) \qquad (vii)$$

Writing equation 2.3 as

$$\dot{\delta} = \frac{N\lambda}{2} \qquad (viii)$$

Equating equations (vii) and (vii) and solving for N

$$N = \frac{3L^2}{2h\lambda} (M/bd^2)^m f(t) \qquad (ix)$$

Thus from a double-exposure hologram of a beam experiencing creep under four-point loading, if the time function is known it is possible to solve for the exponent of the stress function or alternatively, if the exponent of the stress function is known it is possible to solve for the time function.

APPENDIX XIV

Creep Of Lead Cantilever Beam Measured By Holographic Interferometry						
Load (kg)	0.5		1.0		1.5	
Time (min)	Fringes	Fr/sec	Fringes	Fr/sec	Fringes	Fr/sec
1	24	1.60	54	3.60	84	5.60
2	19	1.27	35	2.33	53	3.53
3	13	0.87	25	1.67	42	2.80
5	10	0.67	18	1.20	29	1.93
7	6	0.40	14	0.93	23	1.53
9	5	0.33	12	0.80	19	1.27
11	4	0.27	10	0.67	17	1.13
15	3	0.20	8	0.53	14	0.93
20	2	0.13	6	0.40	11	0.73
30	1	0.07	3	0.20	8	0.53
40			1	0.07	5	0.33
60					1	0.07

Creep of Lead Cantilver Beam Measured By Holographic Interferometry under 1.5 Kg Load				
Time (min)	Fringes	Fr/sec	Avg. Fringes for period	Total Fringes
1	84	5.60	0	0
2	53	3.53	274	274
3	42	2.80	190	464
5	29	1.93	284	748
7	23	1.53	208	956
9	19	1.27	168	1124
11	17	1.13	144	1268
15	14	0.93	248	1516
20	11	0.73	250	1766
30	8	0.53	380	2146
40	5	0.33	260	2406
60	1	0.07	240	2646

Creep of Lead Cantilver Beam Measured By Holographic Interferometry under 1.0 Kg Load				
Time (min)	Fringes	Fr/sec	Avg. Fringes for period	Total Fringes
1	54	3.60	0	0
2	35	2.33	178	178
3	25	1.67	120	298
5	18	1.20	172	470
7	14	0.93	128	598
9	12	0.80	104	702
11	10	0.67	88	790
15	8	0.53	144	934
20	6	0.40	140	1074
30	3	0.20	180	1254
40	1	0.07	80	1334

Creep of Lead Cantilver Beam Measured By Holographic Interferometry under 0.5 Kg Load				
Time (min)	Fringes	Fr/sec	Avg. Fringes for period	Total Fringes
1	24	1.60	0	0
2	19	1.27	86	86
3	13	0.87	64	150
5	10	0.67	92	242
7	6	0.40	64	306
9	5	0.33	44	350
11	4	0.27	36	386
15	3	0.20	56	442
20	2	0.13	50	492
30	1	0.07	60	552